Linking hippocampal sequences and spatial representations

Yuk Hoi Yiu

Graduate School of
Systemic Neurosciences

LMU Munich

Supervisor:

Prof. Dr. Christian Leibold

Theoretical Systems Neuroscience

Institut für Biologie III, Bernstein Center Freiburg

Albert-Ludwigs-Universität Freiburg

Germany

First Reviewer: Prof. Dr. Christian Leibold

Second Reviewer: Dr. Caroline Geisler

Date of Submission: October 16, 2023

Date of Defense: February 26, 2024

Abstract

In the rodent hippocampus, spatial pathways are represented by the sequential activation of multiple place cells, each corresponding to a specific location. This activation pattern, referred to as theta sequences, occurs at theta frequencies (4–12 Hz) and reflects a one-dimensional (1D) trajectory. Akin to drawing a line on a paper surface, the spatial pathway conveyed by a theta sequence may assume arbitrary shapes within a 2D space. The precise way theta sequences propagate within the 2D topology spanned by place cells and the nature of the spatial pathways they represent remain unclear.

In the first manuscript, we investigated the firing order of theta sequences as the animal traverses their respective place fields. By analyzing the place cell activities while the rats were free foraging in a 2D open space, we found that some place cells mirrored the temporal order of the locations visited by the animal, while others exhibited a fixed firing order independent of the running trajectory. This finding leads to our proposition that theta sequences result from the interaction between extrinsically and intrinsically driven mechanisms, with firing orders coordinated by extra-hippocampal sensorimotor input and intra-hippocampal network connectivity, respectively.

In the second manuscript, we proposed a theoretical framework to account for the observed heterogeneity of theta sequences. We simulated a spiking neural network of place cells within the cornus ammonia 3 (CA3) and dentate gyrus (DG) layers. Extrinsic sequences arise from short-term plasticity mechanisms among CA3 place cells and propagate in the direction of movement. In contrast, intrinsic sequences propagate in a fixed temporal order along the CA3 place cells connected by unidirectional projections via the DG layer. Our simulations demonstrated that this two-layer network enabled the concurrent propagation of extrinsic and intrinsic sequences, reproducing the experimental findings of two temporal orders of theta sequences.

In conclusion, this thesis reveals the phenomenon wherein 1D theta sequences propagate within a 2D space along multiple 1D manifolds, namely the running trajectory and the spatial paths determined by intra-hippocampal connectivity patterns. The intrinsic sequences extend beyond the animal's actual positions, offering a non-local representation of space, and potentially support spatial memory through their stable temporal patterns.

Contents

1 Introduction

1.1 The hippocampus

1.1.1 The hippocampus and episodic memory

The hippocampus is located in the medial temporal lobe. The name "hippocampus" originated from its shape resembling a seahorse. The memory function of the hippocampus garnered attention following the study of patient H.M., who underwent surgery to remove the medial temporal lobe including a large part of the hippocampus, to control his epileptic seizures (Scoville and Milner, 1957). After the surgery, he suffered from severe anterograde amnesia as he could not acquire new memories from recent events, and moderate temporally graded retrograde amnesia, since he was able to recall the memories of his early life but not the memories shortly before the surgery. However, his other cognitive functions, such as general intelligence, working memories and sensory perception, remained unaffected. The inability to remember new events, and his memory being more degraded in the recent than the remote past, suggest a functional role of the hippocampus in memory consolidation since an interruption of the consolidation process would result in a failure of recalling those memories still in the progress of consolidation but spare those already consolidated.

Although the brain areas removed in patient H.M. included not only the hippocampus but also the surrounding regions—such as amygdala and entorhinal cortex—further studies in the following decades have confirmed the association between the hippocampus and memory function. Studies have demonstrated that (see Squire et al. (2015) for review) lesions in the hippocampus lead to both anterograde and temporally graded retrograde amnesia in rodents (Morris et al., 1982, Moser and Moser, 1998, Clark et al., 2002), primates (Zola-Morgan and Squire, 1990) and humans (Squire and Alvarez, 1995). Furthermore, increased neuronal activity in the human hippocampus correlates with memory encoding and retrieval behaviors (Addis et al., 2004, Greicius et al., 2003). Researchers, therefore, hypothesized that the hippocampus is crucial for memory processes, including memory acquisition, consolidation, and retrieval.

1.1.2 The trisynaptic circuit

Our understanding of the memory functions of the hippocampus has improved through the study of its anatomy and functional connectivity (Figure 1A). The hippocampal formation consists of the dentate gyrus (DG), cornus ammonis 3 (CA3), CA1, and subiculum regions. The entorhinal cortex (EC) layer II primarily inputs to the hippocampal formation via the perforant path; this pathway delivers sensorimotor inputs (e.g., visual, vestibular, or proprioceptive from perception and self-motions during spatial navigation) from neocortical regions to the hippocampus. The hippocampus, including DG, CA3, and

1

CA1, propagates information through both feed-forward and recurrent network structures (see Figure 1B). Eventually, the information is projected back to the deep layer V and VI of the EC and cortical areas. This pathway, known as the trisynaptic circuit, involves connections from the EC layer II to DG (first synapses via the perforant path), DG to CA3 (second synapses via mossy fibers), and CA3 to CA1 (third synapses via Schaffer collaterals) and serves as an information processing unit for the sensorimotor inputs from the neocortex. The perforant path from the EC layer II also branches off and projects directly to CA3 (Steward, 1976). In parallel, the EC layer III also forms synaptic projections to the CA1 area, known as temporoammonic pathway (Witter et al., 1988, 2000), allowing the EC inputs to reach CA1 directly, skipping DG and CA3.

Intracellular recordings have demonstrated synaptic plasticity, such as long-term potentiation and depression, in the hippocampus, including the perforant path (Bliss and Lømo, 1973, Lømo, 2003), mossy fibers (Alger and Teyler, 1976, Zalutsky and Nicoll, 1990, Weisskopf et al., 1993), Schaffer collaterals (Schwartzkroin and Wester, 1975, Alger and Teyler, 1976), and the temporoammonic path (Dvorak-Carbone and Schuman, 1999, Remondes and Schuman, 2003, Aksoy-Aksel and Manahan-Vaughan, 2013). Therefore, the hippocampus is capable of experience-dependent changes that may subserve memory functions. For instance, the CA3's auto-associative network structure enables pattern completion, which allows partial inputs to trigger previously remembered complete patterns stored in synaptic strengths (Jensen et al., 1996, Bennett et al., 1994). The DG network, on the other hand, facilitates pattern separation, which differentiates similar memory items with different contexts through competitive learning and inhibitory feedback connections (Leutgeb et al., 2007, Myers and Scharfman, 2009a, 2011, Guzman et al., 2021). Notably, lesion studies and pharmacological blocking along the trisynaptic circuit have demonstrated various types of memory dysfunctions in remembering spatial locations (Morris et al., 1982), object identification (Zola-Morgan and Squire, 1990), fear conditioning (Kim and Fanselow, 1992, Anagnostaras et al., 1999), and socially acquired memories (Winocur, 1990).

1.1.3 Selectivity to different sensorimotor stimuli

One manifestation of memory is the emergence of selective neuronal activity. A well-known example is the "Jennifer Aniston neuron" (Quiroga et al., 2005). In their study, electrodes were implanted into the medial temporal lobes of eight human patients to record neuronal activities. The subjects were presented with various pictures of individuals and objects. They found that some neurons exhibited high firing selectivity towards specific types of pictures. For instance, a neuron in the left posterior hippocampus responded exclusively to photos of the celebrity Jennifer Aniston, regardless of different costumes, backgrounds, expressions, and viewing angles. However, when presented with photos of other individuals, landmarks, or objects, this neuron remained inactive. Interestingly,
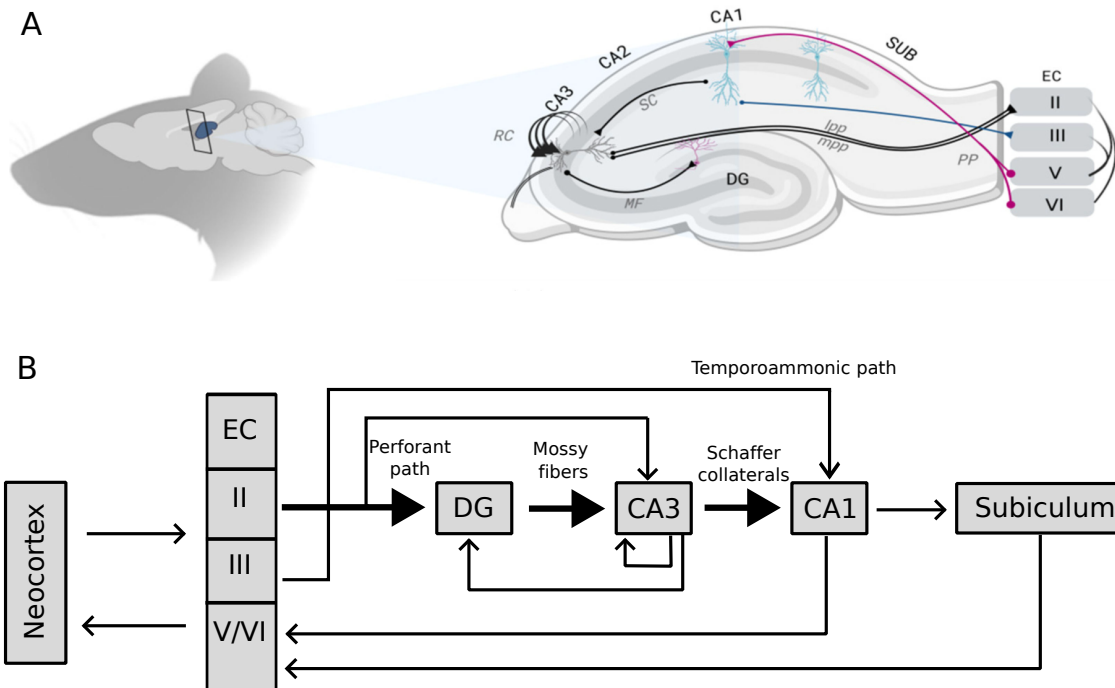
Figure 1: (A) Locations of the hippocampus and different subregions. Figure adapted from Roux et al. (2021) with permission under Creative Commons Attribution (CC BY) 4.0 license: https://creativecommons.org/licenses/by/4.0/. MF: Mossy fibers. RC: Recurrent collaterals. SC: Schaffer collaterals. PP: Perforant path. lpp: Lateral perforant path. mpp: Medial perforant path. (B) Schematic illustrations of neural pathways in the hippocampus according to Amaral and Witter (1989) and Andersen et al. (2006). The hippocampal formation (DG, CA3, CA1, subiculum) receives cortical input via the superficial layers II and III of the EC and projects the output back to the neocortex via the deep layers V/VI of the EC. CA3 forms recurrent connections with itself and back-projections to the DG (Scharfman, 2016). Thick arrows denote the trisynaptic circuit (PP, MF, and SC).

these neurons also responded to letter strings of the name of the preferred celebrity, photos of the characters played by that celebrity in movies and even the sound of the spoken name (Quian Quiroga et al., 2009). The high selectivity to the identity of a stimulus, and the invariance to the change in stimulus features irrelevant to the identity and sensory modalities, signify a recognition of the abstract identity of the stimulus. The stimulus is, hence, represented by neuronal activity, which is often considered a form of memory since the stimulus information is encoded in a neural substrate and available to be further retrieved and processed by other neurons.

The "Jennifer Aniston cell" is just an example of selective activity in the hippocampus. Decades of research have shown that pyramidal cells in CA1 and CA3, and granule cells in DG exhibit tuning curves of firing rates in response to a wide variety of stimuli. Place cells (O'Keefe, 1976), for example, only generate action potentials when an animal visits a specific location in an environment, remaining inactive in other locations. Time cells (Eichenbaum, 2014), on the other hand, fire exclusively at specific moments when a behavioral task reaches a particular time interval. Other stimuli include odors (Shahbaba et al., 2022a) and sounds (Aronov et al., 2017). In the primate hippocampus, selective activities extend even to stimuli with complex features like faces and objects (Fried et al., 1997, Sliwa et al., 2016), as well as abstract cognitive information such as reward values (Knudsen and Wallis, 2021). The wide range of selective activities suggests that the hippocampus serves a more general memory function rather than being limited to specific types of stimuli like places and odors. It is worth emphasizing that the selective activity or tuning curve of a neuron is a correlational measure. This means that the information of the stimulus is encoded or represented by neuronal activity, without necessarily implying that the neuronal activity is causally responsible for the conscious mental recall or utilization of the stimulus information.

1.2 Roles of the hippocampus in spatial navigation

The hippocampus plays a vital role in memory function across various sensorimotor modalities, but neuroscientists have shown particular interest in studying the spatial memory represented by the hippocampus. One reason is that spatial memory is critical to daily activities, such as foraging for food, exploring unfamiliar territories, or remembering object locations. Since the emergence of mobile animals, navigation has been essential for survival and adaptive behavior. Furthermore, spatial memory gives a measurable behavioral output. The ability of a rodent to remember a space can be measured by its performance to navigate in a maze. In contrast, other memory types, such as episodic memory, are more challenging to measure due to their mental and internal nature. The explicit behavioral output of spatial memory thus allows simpler experimentation. As spatial memory is one aspect of the overarching general memory functions of the hippocampus, the study of it could also provide implications on the underlying mechanisms of memory as a whole.

In the present thesis, we primarily focus on the rodent hippocampus due to the accessibility of its experimental data. Additionally, the structural similarities between the rodent and human brain, as both are mammals, can also provide valuable insights into fundamental aspects of human memory function.

1.2.1 Place cells: positional tuning and spatial memories

The crucial role of the hippocampus in spatial memory was demonstrated by Morris et al. (1982). In their experiment, rats navigated a water maze without visual or olfactory cues to find a fixed hidden platform. Rats with intact spatial learning abilities remembered the platform's location and improved their performance over multiple trials. However, rats with complete damage to the dorsal and ventral hippocampus took significantly longer to reach the goal than the control group. Despite showing improvement over time, the performance of the lesion group never surpassed that of the best-performing normal rats trained to search for a random platform. This finding indicates the essential role of the rodent hippocampus in spatial memory.

The neuronal activity that represents spatial memory was first identified by O'Keefe and Dostrovsky (1971). They discovered that pyramidal cells in the CA regions of the hippocampus only discharge action potentials when the animal is in a specific location of the environment and remains inactive when the animal is outside of that region. These cells are called place cells, and the regions with the elevated firing activity are referred to as place fields (Figure 2A). Since place cell activity correlates with the animal's position, it is believed to represent the spatial environment. This gave rise to the concept of a cognitive map, where neural activity supports the mental representation of space, including the identities of locations and their relationships. Place cells are considered the fundamental building blocks of the cognitive map as their firing patterns encode positional information essential for navigation.

Notably, hippocampal pyramidal cells only develop location-specific firing after the animals become familiar with the environment, typically requiring more than 4–5 minutes of exploration time (Bittner et al., 2017, Frank et al., 2004) or several laps of track traversal (Dong et al., 2021). Hence, the formation of place fields is a result of experience-dependent changes in neural activity induced by learning or memory processes. Furthermore, place cells also encode locations that are significant for the animals. Studies have shown concentrated firing activity of hippocampal pyramidal cells in regions associated with reward (Hollup et al., 2001), preferred grooming locations (Pfeiffer, 2022), and locations of objects and landmarks (Deshmukh and Knierim, 2013). This demonstrates that the representation of spatial memory in the hippocampus is often influenced by visual salience and contextual factors such as motivational aspects of tasks.
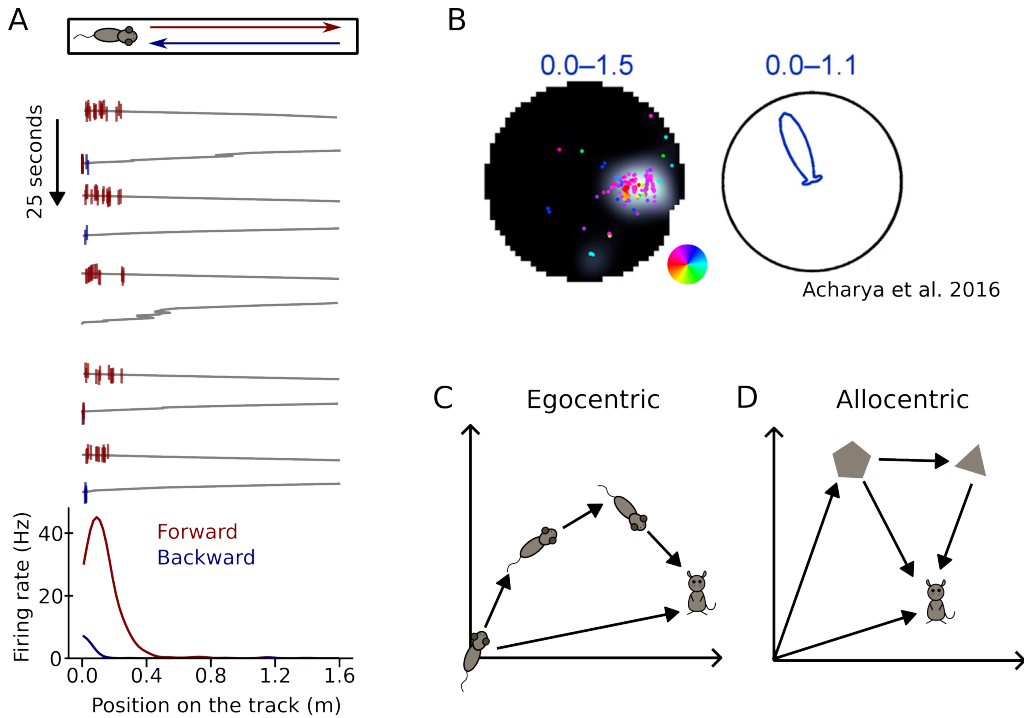
Figure 2: (A) Place fields on a linear track. Top: Schematic illustration of the behavioral task, where the rat runs back and forth along a 1.6m linear track for a reward. Middle: Recorded spikes of a CA1 pyramidal cell as vertically jittered ticks overlaid on the animal's trajectory (gray line). Red and blue colors indicate the forward and backward instantaneous heading direction at the spike times. Bottom: Average firing rate of the neuron as a function of the animal's position on the track. The place cell is active only for the positions between 0 m and 0.4 m and exhibits directional selectivity preferring forward heading direction. An open dataset (available at https://crcns.org/data-sets/hc/hc-11/about-hc-11) provided by Grosmark and Buzsáki (2016) and Grosmark et al. (2016) was used. (B) Positional and directional firing rate map of a CA1 pyramidal neuron in a 2D space reported by Acharya et al. (2016). Left: Firing rate is depicted as the grayscale heatmap. Numbers on top denote the range of the firing rate in Hz. Spikes are plotted as dots colored according to the instantaneous heading direction following the color wheel. Note the position specificity and the preferred heading direction of the firing activity. Right: Polar plot of the firing rate as a function of heading orientation. Figure reused with permission of the rights holder, Elsevier. (C) Navigation by egocentric representation of space. The current position estimate is computed by integrating the previous positions and heading directions provided by self-motion cues such as vestibular input. (D) Allocentric representation of spatial map. A spatial map is constructed based on the relationship between landmark features. Self-position is thus determined by the landmark positions as observed by the animal. This spatial representation relies on external visual cues rather than self-motion cues.

1.2.2 Directional tuning of place cells

In terms of spatial memory, the activity of place cells is selective not only to positions, but also to the heading direction of the animals. The first discovery was by McNaughton et al. (1983), where they found that in a radial 8-arm maze, some pyramidal cells in the hippocampus exhibited a higher firing rate for inbound trajectories but lower than outbound ones, or vice versa. Subsequent studies further demonstrated the directional selectivity of place cells in linear mazes (Figure 2A) and 2D space (Figure 2B) in CA1, CA3 and DG regions (Muller et al., 1994, Markus et al., 1995, Cacucci, 2004, Mankin et al., 2019, Acharya et al., 2016, Stefanini et al., 2020).

The selectivity to directionality, however, varies across different task demands. Markus et al. (1995) found that the proportion of place fields with significant directional tuning (10%) in 2D open space is much less than those in linear and radial mazes (80%). The directional selectivity of place cell thus depends on how open the spatial environment is and how stereotypical the animal's movement trajectory is. A further study by Acharya et al. (2016) demonstrated that narrowing the width of a visual bar on the wall was enough to increase the sharpness of the directional tuning curve of place cells, despite the environment enclosure remaining the same. The above studies showed that the degree of directional selectivity in place cell firing is influenced by how much the directional information is demanded by the behavioral tasks and available from the sensory cues.

How the hippocampal place cells become selective to heading direction is still unclear. According to the neural pathways (Figure 1B), directional modulation of hippocampal place cells presumably inherits from the upstream activity of head-direction cells in the medial EC and the postsubiculum (Taube et al., 1990a,b, Bett et al., 2013). Head-direction cells are different from place cells. Their firing rate only depends on the head direction but not the animal's location. These cells are prevalent in the postsubiculum as well as in the MEC, where they exist across all layers (Giocomo et al., 2014). The head-direction signal in these regions likely originates from both vestibular and visual systems (for reviews, see Yoder and Taube (2014), Munn and Giocomo (2020)). Lesions in the vestibular system have been shown to disrupt the directional tuning in the head-direction cells in postsubiculum (Stackman and Herbert, 2002), and manipulation of visual cues was able to predict the change in directional tuning (Goodridge et al., 1998, Acharya et al., 2016). However, both types of inputs could compensate for the behavioral deficit arising from the absence of one another (Hüfner et al., 2011, Wallace et al., 2002, Stackman and Herbert, 2002), indicating that the either vestibular or visual inputs can be flexibly utilized depending on their availability.

1.2.3 Navigation by path integration and the allocentric cognitive map

The neural representations of positions and head directions serve as crucial spatial metrics for spatial navigation. One method of navigation that utilizes these metrics is path integration (Figure 2C, also called dead reckoning), where animals internally update their current position relative to a starting point by integrating past locations and heading directions over time. This kind of navigation is egocentric, meaning that the spatial metrics are referenced to the animal itself and self-motion cues such as vestibular inputs are used to update position estimates. Previous study has shown that rats are able to navigate in the dark when only self-motion cues are available (Wallace et al., 2002), demonstrating their ability to utilize path integration for spatial navigation.

On the other hand, navigation also involves an allocentric representation (Figure 2D), which relies on spatial relationships like distances and orientations between visual landmarks, objects, and pathways to create a global map of the environment (Buzsáki and Moser, 2013). Animals determine their position on the spatial map by comparing their orientation and distance to landmarks. Since the spatial map is constructed using external visual cues, self-motion cues are no longer necessary for estimating self-location. Past studies have provided supportive evidence for such allocentric representation. For example, Stackman and Herbert (2002) showed that visual cues providing allocentric references of space became necessary for the rats to complete the spatial navigation task, after their vestibular system was lesioned. Other studies demonstrated that changes in visual cues can control the locations of place fields (Muller and Kubie, 1987, Knierim et al., 1995), suggesting that neural representations of space carry information related to allocentric references. Furthermore, recent research identified "landmark vector cells" in the hippocampus (Deshmukh and Knierim, 2013), which fire specifically when the animal is at a certain distance and orientation to a landmark, providing evidence of a relational representation between landmarks and objects in the hippocampus.

Both egocentric and allocentric navigation require the spatial metrics provided by the position and head-direction signals for calculating the self-position and constructing a spatial map of the environment. The neural representation of position and head directions in the hippocampus is thus a potential candidate for supporting the navigation behaviors. Targeted activation of place cells has been shown to bias the behavior to the associated location (Robinson et al., 2020), indicating the causal role of hippocampal place representation in spatial navigation. The exact mechanism of how spatial representations support navigation behaviors is, however, still unclear and an ongoing area of research.

1.3 Theta rhythm and the temporal code

In the hippocampus, large groups of neurons participate in synchronized firing activity at theta-band frequency (6–12Hz), which can be observed in the electroencephalogram and

electrophysiological recordings as a rhythmic signal. The theta oscillation power waxes and wanes depending on the behavioral state of the animal. It becomes stronger when the animal actively explores an environment or engages in locomotion, and becomes weaker when the animal is immobile or sleeping. The firing activity of place cells is also modulated by the theta oscillation and phase-locked to the theta oscillation on average (Fox et al., 1986).

One primary functional role of the theta oscillation is to support the temporal code. Unlike the rate code, in which the neurons encode the spatial memories via their firing rate, place cells also encode information via the precise spike timings of their action potentials. The spike times are organized by theta oscillation and can encode the animal's position as well as relational memories. Indeed, past studies have shown that disruption of the theta rhythm could severely affect spatial navigation performance (Mitchell et al., 1982). It is worth noting that some of the experiments employed targeted pharmacological blocking (Bolding et al., 2020) and cooling (Petersen and Buzsáki, 2020) of the medial septum and were able to disrupt the theta rhythm while leaving firing fields of place cells intact. They demonstrated that a mere rate code without the theta temporal code is insufficient for spatial navigation. In this chapter, we discuss the spatial representation in the hippocampal theta temporal code and the origin of the theta rhythm.

1.3.1 Phase precession and theta sequences in 1D

One prominent reflection of the theta temporal code is phase precession. O'Keefe and Recce (1993) discovered that the spike timing of place cells relative to the background theta oscillation could indicate the animal's location within the place field (see Figure 3A). During their experiment, they recorded hippocampus activity using tetrodes while the animal ran on a linear track. The local field potential (LFP), resulting from the synchronized firing of nearby neurons around the recording site, exhibited a theta rhythm at 7–12Hz.

As the animal entered a place field, the associated place cell began firing. Initially, the timing of the action potential was in the late phase of the theta oscillatory cycle, but it progressively advanced with each cycle as the animal moved across the field. Finally, as the animal exited the place field, the spike occurred in the early theta phase. As a result, the spike phase of a place cell precesses in every theta cycle and negatively correlates with the distance travelled within the place field (Figure 3B), encoding the positional information via the theta temporal code.

Phase precession is a phenomenon observed in single-cell activity. However, the theta temporal code can also be observed at the population level. When the animal sequentially traverses multiple overlapping and neighboring place fields, each cell undergoes phase precession, but the spike phases of different cells are separated by a phase lag. This
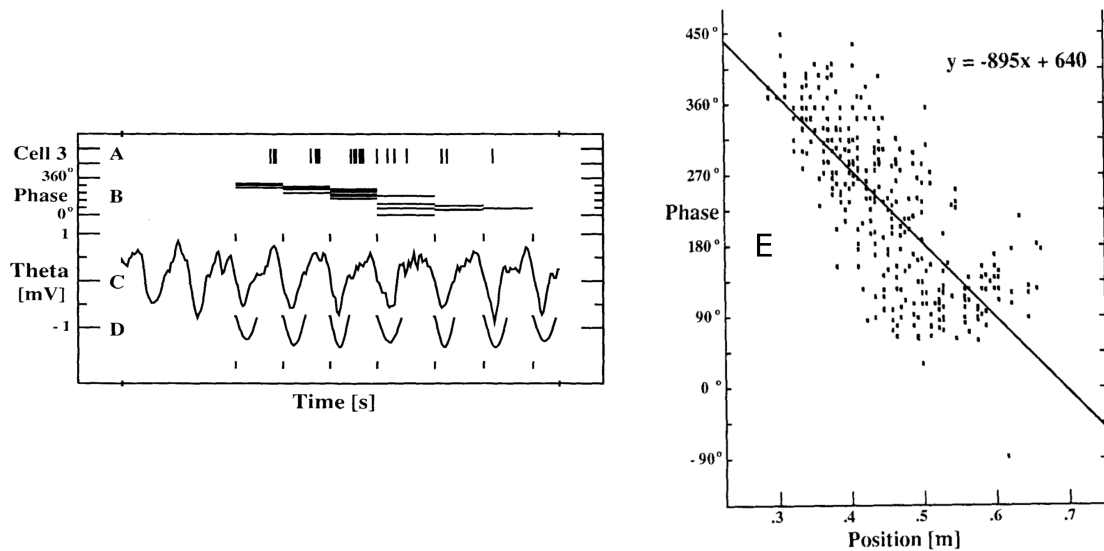
Figure 3: Figure adapted from O'Keefe and Recce (1993) demonstrating phase precession of a CA3 place cell on a linear track. (A) Recording of action potentials of the place cell. (B) Theta phases at the spike times. The spike phase starts from the later portion of the theta cycle at about 360 degrees and progressively advances (or decreases) through each subsequent theta cycle as the rat moves within the place field. (C) Theta activity of the local field potential (LFP) recorded by tetrodes. Vertical ticks mark the beginning of a theta cycle. (D) Identification of the beginning of the theta cycle via a template matching algorithm. (E) Phase-position relationship of all the spikes from a different place cell. Each spike is plotted with its spike phase against the animal's position at the time of the spike occurrence. Phase precession is discernible through the negative correlation between the spike phase and animal positions within the place field. Parameters of the linear regression fit are provided on top. Figure was reused with permission of the rights holder, John Wiley and Sons.

phenomenon, known as theta sequences, has been observed in experiments where the activation of the next cell follows a phase delay after the previous cell, forming a firing sequence of multiple place cells within a theta cycle (Figure 4A and 4B).

The theta sequences can be examined by the cross-correlation between a pair of place cells, which describe the probability that one cell would fire a spike after the spike of another cell, as a function of the time lag. The theta sequence was first discovered by Skaggs et al. (1996) through cross-correlation methods, and subsequently confirmed by other studies (Dragoi and Buzsáki, 2006, Foster and Wilson, 2007, Feng et al., 2015). Figure 4C shows the cross-correlation functions between a place cell with the three other place cells with progressively farther place fields. At behavioral timescale, spike probability peaks at 100ms, 200ms and 300ms, corresponding to the behavioral times required for the animal to travel to the place field centers in this example. However, within the window of the theta cycle (about ±100 ms), correlation already peaks at 10ms, 20ms and 30ms, indicating that the sequences of places are reflected by the spike sequences ten times faster than the behavioral experiences. This leads to the idea of sequence compression (Skaggs et al., 1996, Dragoi and Buzsáki, 2006), where behavioral sequences at a longer timescale are encoded by spike sequences coordinated by theta rhythm at a much shorter timescale. The spatial representation of theta sequences thus also "sweeps ahead" of the animal as place cells representing the prospective locations fire even before the animal actually reaches their place field centers.

One of the functional benefits of sequence compression is the facilitation of associative learning via long-term synaptic plasticity. A theta sequence compresses multiple behavioral experiences into a theta cycle, which is approximately the induction time window (below ±20 − 40 ms) of spike-time-dependent plasticity (Bi and Poo, 1998) in the hippocampus, facilitating binding of memory events and learning of their temporal order. Such possibilities have been confirmed by various theoretical models (Jensen et al., 1996, Scarpetta and Marinaro, 2005, Shen et al., 2008, Sato and Yamaguchi, 2009, George et al., 2023). Sequence learning encompasses not only spatial memories but also non-spatial stimuli such as odors in rodents (Allen et al., 2016, Shahbaba et al., 2022b) and object identities in human (Heusser et al., 2016), leading to the notion that the hippocampus supports the relational memory in general or even episodic memory, where a sequence of events is re-experienced by recalling memories in the correct temporal order.

1.3.2 Theta sequences and phase precession in 2D

Most studies concerning the temporal code in theta rhythm focus on 1D linear tracks. However, naturalistic navigation often requires spatial memories of a 2D or 3D environment. One fundamental issue is that the theta sequence is propagated from one place cell to another, inherently making the sequence propagation 1D. In a 1D linear track, the
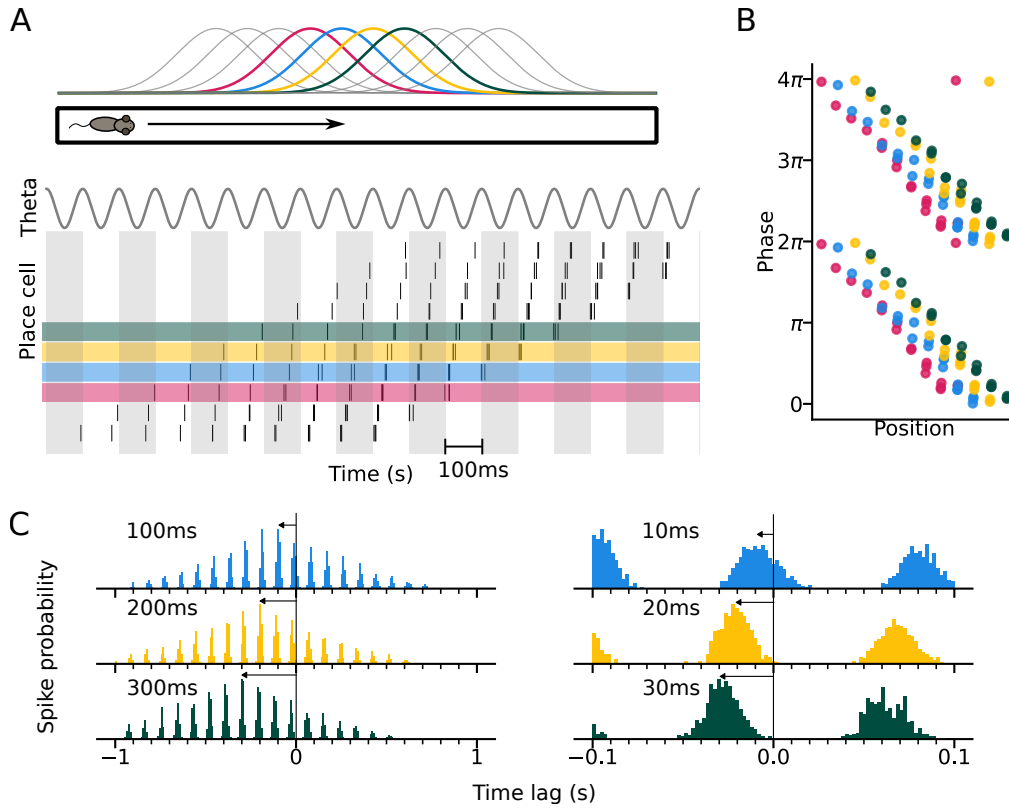
Figure 4: Schematic illustration of theta sequences in a 1D environment. (A) Top: A rat traverses a series of place fields along a linear track. Bottom: Theta activity with 100ms period and raster plot of spikes from the place cell population. Four example place cells are shaded with the same colors as the place fields. Place cells fire sequentially within each theta cycle as the rat moves through them. (B) Phase precessions of the four example cells, each separated by a phase shift. (C) Cross-correlation indicating the spike probability versus the time lags from the red cell to all other three cells (from top to bottom rows). Left: Cross-correlations at the behavioral timescale. Peak time lags indicate the time it takes for the animal to move from the center of the red place field to the blue, yellow, and green field centers in 100 ms, 200 ms, and 300 ms, respectively. Right: Cross-correlations at the theta timescale. Peak time lags are 10ms, 20ms, and 30ms, respectively, in the theta sequences, demonstrating a ten-fold temporal compression of behavioral sequences into the theta spike sequences.

activity propagation necessarily follows the movement trajectory. In a 2D environment, space is represented by 2D place fields distributed across the environment and sequence propagation is no longer restricted to align with the movement trajectory due to the spatial topology, allowing it to vary in the propagation direction. It is, therefore, unclear how activity can be propagated among the place cells spanning a 2D topology and, consequently, how the spike phase precesses when the animal approaches a place field from different directions.

The question was addressed by Skaggs et al. (1996), who also examined the spike phase of place cells in a 2D space. They found that place cells tended to fire in the later part of theta cycle when the rat entered the place field and in the early part of theta cycle when the rat exited the field. However, the question remains whether spike phases still advance progressively with traveled distance, as seen in 1D tracks. A more detailed investigation by Huxter et al. (2008) demonstrated that phase precession occurs in a 2D place field regardless of the travel direction (Figure 5A-B). Specifically, they devised a measure called the "directional rate zone" (DRZ) as a positional variable that is invariant to the angle of place field traversal (Figure 5C). The DRZ is negative when the animal is heading towards the peak of the rate map, and positive when the animal is heading away, with the magnitude of the DRZ normalized to the values of the firing rate map (0 at the maximum firing rate and 1 at zero firing rate). They found that the negative correlation between the DRZ and spike phase still exists regardless of the approach direction, demonstrating the presence of phase precession in a 2D environment (Figure 5D-E).

Furthermore, Huxter et al. (2008) also investigated the theta sequence in 2D space (Figure 6A). They found that the peak time lag of the cross-correlation between two place cells flipped signs when the rat encountered the place fields in the opposite temporal order. It indicates that whichever place cell is activated first, its spike would precede the spike of the next place cell in the firing sequence. A theta sequence thus propagates in the same direction as the running direction and flips its firing order when the running direction is reversed (Figure 6B-C).

The findings of Huxter et al. (2008) confirm that, at least in the investigated CA1 region of the hippocampus, the temporal code in theta rhythm exists in 2D space. The theta sequence propagates along place cells in the same order as sampled by the running movement and thus encodes the running trajectory. As a result, single-cell phase precession is preserved in different directions of approach.

1.3.3 Origin of theta oscillations

The medial septum (MS) has long been considered the putative source of the theta rhythm in the brain, with previous studies indicating that lesions in the MS region disrupt theta oscillations in the hippocampus (Mitchell et al., 1982, Yoder and Pang, 2005). Notably,
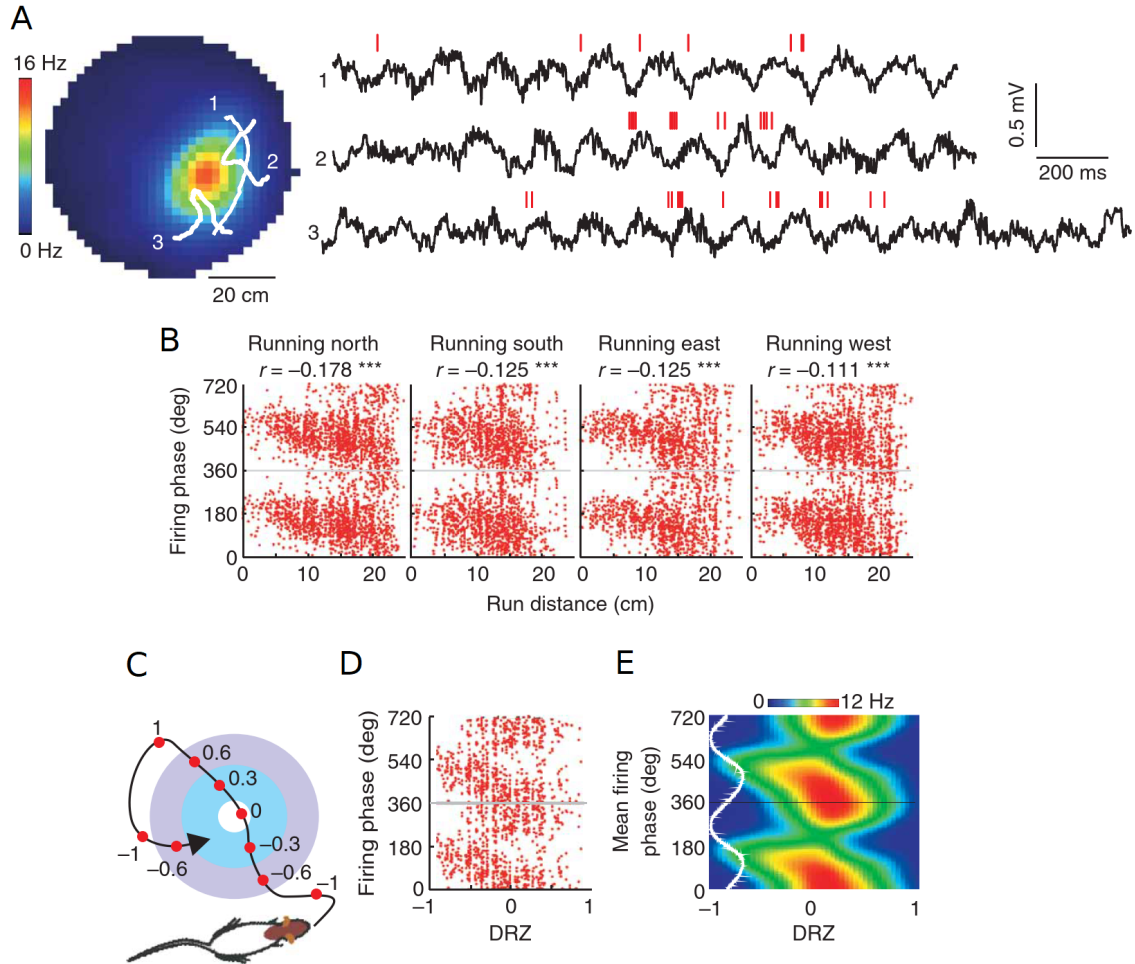
Figure 5: Figure adapted from Huxter et al. (2008), demonstrating phase precession in a 2D space. (A) Left: Three trajectories overlaid on a firing map of a place cell. Right: Spike timings of place cells relative to theta oscillations along the three running trajectories. Spike phase advances in each theta cycle. (B) Phase-distance relationship of the place cell in (A) in four running directions. r denotes the Pearson's correlation coefficient. (C) Calculation of the directional rate zone (DRZ). |DRZ|=0 when the animal is at the field peak location and |DRZ|=1 when the firing rate is zero. DRZ is positive when the animal moves toward the field center and negative when it moves away. (D) Phase-DRZ relationship displays phase precession across all running directions. (E) Phase-DRZ relation plot color-coded by the mean firing rate of all place cells from all rats in Huxter et al. (2008). Figure reused with permission of the rights holder, Springer Nature.

14
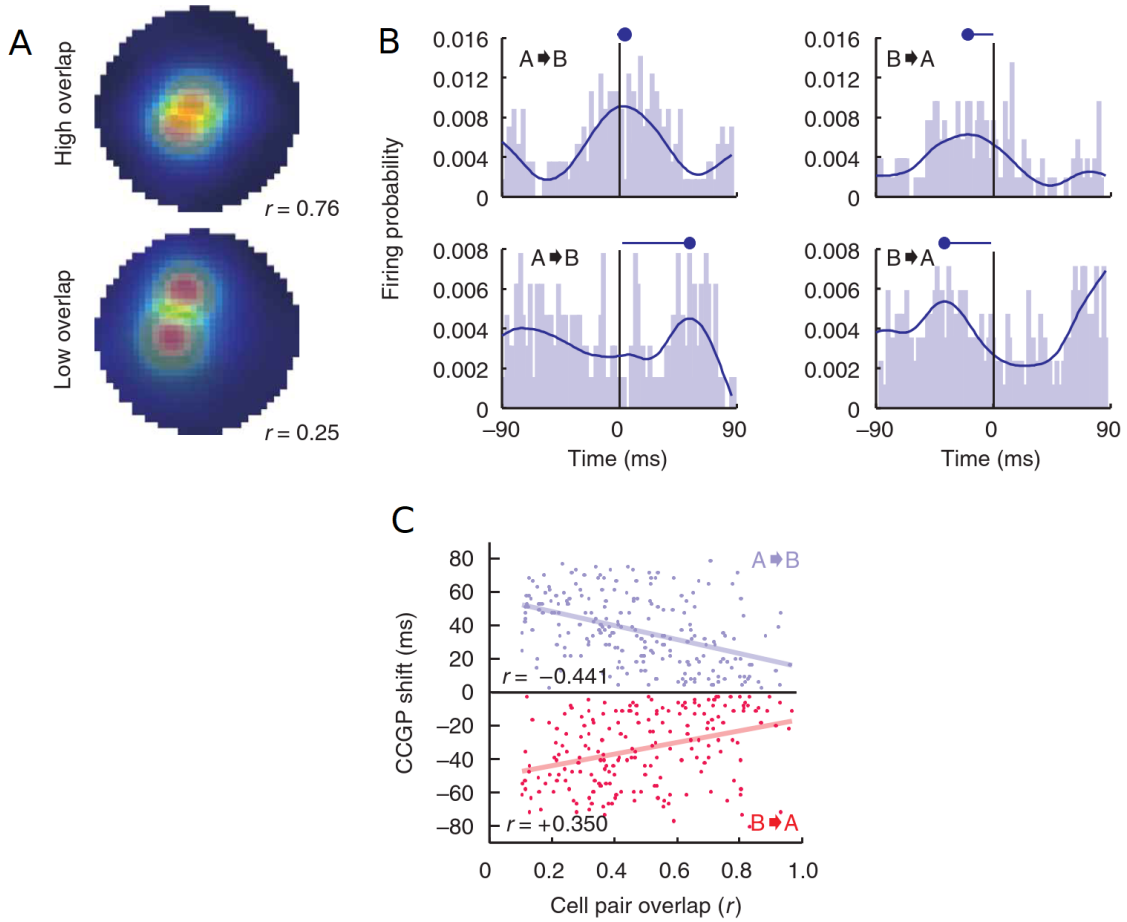
Figure 6: Figure adapted from Huxter et al. (2008), demonstrating the dependence of theta correlations on the running trajectory. (A) Two place fields with high and low overlap. r indicates spatial correlation of the firing rates over the spatial bins. (B) Cross-correlation of spike trains between a pair of place cells with high overlap (top) and low overlap (bottom) for trajectories running from field A to B (left) and from B to A (right). The time shift, determined by the peak firing probability, varies with the amount of overlap. The sign of the time shift depends on the trajectory direction (A to B or B to A). (C) Time shifts versus spatial overlap of the place field pairs. Like the 1D case in Skaggs et al. (1996) and Figure 4, time shift increases as the place fields become farther apart. Figure reused with permission of the rights holder, Springer Nature.

Bland et al. (1999) reported that the transition of the hippocampus from an irregular firing state to a synchronized theta state was preceded by the activation of theta-firing neurons within the MS, suggesting that the MS neurons may play a pivotal role in initiating the theta oscillation within the hippocampus.

Further investigation has narrowed down the source of theta rhythm to pace-making neurons within the MS, which can spontaneously generate periodic firing patterns at theta frequencies (Sotty et al., 2003, Morris et al., 2004, Varga et al., 2008). These pacemaker cells are characterized by hyperpolarization-activated cyclic nucleotide-gated (HCN) channels, which are permeable to sodium and potassium ions and can be activated by hyperpolarization at -50mV (Benarroch, 2013). Consequently, the hyperpolarization following an action potential would activate the HCN channels and trigger depolarization again, producing periodic firing.

Notably, the GABAergic neurons in the MS were shown to possess HCN channels and demonstrate rhythmic activity at the theta frequency (Varga et al., 2008). These GABAergic cells project synapses to hippocampal CA1 interneurons, which, in turn, project to CA1 pyramidal cells, thereby establishing a pathway for theta rhythmic modulation of the hippocampus (Toth et al., 1993, Tóth et al., 1997). Such septal projections were also found to terminate in DG, CA3 and the subiculum (Crutcher et al., 1981) and could similarly modulate the theta rhythms in these areas. Importantly, experimental studies have demonstrated the functional significance of these MS-Hippocampus connections. Pharmacological blockade of HCN ion channels within the MS has been shown to diminish theta power in the hippocampus (Xu et al., 2004). Also, temporal analysis has revealed that MS GABAergic neurons with HCN channels precede hippocampal CA1 interneurons by approximately 30ms and the (LFP) by about 80ms (Hangya et al., 2009), further supporting the notion of an MS-hippocampus pathway of rhythmic synchronization. Therefore, converging lines of evidence demonstrate that the synchronized activity at theta frequency in the hippocampus is coordinated by the pacemaker cells of the MS.

However, the exclusive role of MS in theta rhythm generation has historically been challenged by evidence suggesting that the intrinsic circuits in the hippocampus can produce rhythmic activity independently. Early *in vitro* studies (Konopacki et al., 1987, Bland et al., 1988) demonstrated that cells in isolated hippocampal slices can spontaneously fire at theta frequencies, highlighting the pace-making capabilities of the hippocampus's intrinsic circuits. However, these studies relied on the induction of theta rhythm through carbachol, a cholinergic agent, thereby necessitating external cholinergic activation to stimulate the pace-making circuits.

A similar *in vitro* study by Goutagny et al. (2009), which utilized an improved slicing preparation that preserved more intrinsic circuits, revealed that spontaneous rhythmic

firing in the hippocampus could occur without cholinergic activation or afferent inputs. This finding suggests that isolated hippocampal circuits can initiate and maintain theta oscillations autonomously. Furthermore, the study identified a coupling mechanism between the CA1 interneurons and pyramidal cells responsible for rhythmic firing. This coupling involves interneurons receiving excitatory postsynaptic potentials (EPSPs) from pyramidal cells and reciprocally providing inhibitory postsynaptic potentials (IPSPs), leading to rebound spikes in pyramidal cells and maintaining periodic firing. Theoretical models further support the notion that this coupling can result in self-sustained rhythmic firing patterns (Santos et al., 2021). An optogenetic study by Amilhon et al. (2015) showed that interneurons in CA1 expressing parvalbumin (PV) were able to control the theta rhythm generation at 8 Hz. Additionally, computational simulations incorporating realistic hippocampal models have revealed that theta rhythms can spontaneously emerge within the CA1 region without external oscillatory modulation and identified the PV interneurons are the primary contributors (Bezaire et al., 2016). Collectively, these studies support the notion of intrinsic generation of theta rhythmic activity in the hippocampus as opposed to the necessary external modulation from the MS.

While the involvement of the MS and the hippocampus itself in the theta rhythm generation is evident, either of these structures might not exclusively account for the origin of theta oscillation (for reviews, see Buzsáki (2002), Colgin (2013)). Several other brain areas have been revealed to contribute to the theta rhythm generation, including the brain stem-diencephalon system (Vertes et al., 2004) and the EC (Montoya and Sainsbury, 1985, Gu and Yakel, 2017). Moreover, the systemic theta phase shift along the septo-temporal axis of the brain (Lubenov and Siapas, 2009, Patel et al., 2012) has also led to the proposition of multiple intrinsic theta oscillators (Colgin, 2013). In conclusion, the origin of theta rhythm in the hippocampus appears to involve a heterogeneous interplay among generators, potentially encompassing the MS, intrinsic hippocampal circuits, and other brain regions, collectively contributing to synchronized firing patterns at the theta frequency. Further research is needed to fully comprehend the intricate interplay among these generators and their contributions to theta oscillations in the brain.

1.4 Computational models of the theta temporal code

The mechanism underlying the theta temporal code for space is still an ongoing area of research. Neuroscientists have proposed theoretical models to account for the phenomena of theta sequences and phase precession. The present thesis categorizes the computational models into two families: intrinsic and extrinsic.

In intrinsic models, theta correlation depends solely on intra-hippocampal connectivity. A simple example would be a unidirectional projection from one place cell to another, which can create a short time latency between their spikes and, consequently, a phase

lag in cross-correlation. The unidirectional projection implies that the sign of the theta correlation does not change in response to extra-hippocampal sensorimotor inputs such as running trajectory. In such cases, the sign of theta correlation remains the same even when the running direction is reversed.

Conversely, in extrinsic models, theta correlation depends on the extra-hippocampal sensorimotor input. The sequence order of place cell activity should mirror the order in which their place fields are traversed. As a result, the theta correlation represents the temporal order of the trajectory and flips signs when the trajectory is reversed, as observed in Huxter et al. (2008).

In this section, we discuss how these two families of models can explain the theta temporal code and their strengths and weaknesses.

1.4.1 The intrinsic family

One representative model within the intrinsic family is Tsodyks et al. (1996). In their theoretical framework, place cells unidirectionally project to the cells that represent the next locations along the trajectory (Figure 7A). The activity of the place cell at the current position of the animal causes the place cell at the next position to fire with a time delay, which further activates the next connected place cell. The chain effect generates a spike sequence of multiple place cells (Figure 7B top). Importantly, all place cells receive global theta oscillatory inhibitory modulation, which resets the population activity in every theta cycle and confines the spike timings into the theta timescale. A crucial component in the model is the asymmetry of synaptic connections. Place cells project synapses in a unidirectional manner to their counterparts, thereby preventing a bidirectional propagation of place cell activity. Consequently, the temporal order of the spike sequence is determined by the intra-hippocampal network connectivity.

The intrinsic models, therefore, heavily rely on the assumption of asymmetric connectivity. Past modelling work by Wallenstein and Hasselmo (1997) and Scarpetta and Marinaro (2005) showed that this asymmetric connectivity pattern could be acquired through past experience. Specifically, they applied a causal Hebbian-like synaptic learning rule which strengthens the connection from a pre-synaptic place cell to a post-synaptic place cell if the former fires a spike before the latter. As a result, when place cells are activated sequentially by a running trajectory, asymmetric connections reflecting the activation order of these place cells are formed. Spike sequences can thus be coordinated by the asymmetric connectivity after spatial experience. A similar model by Jensen et al. (1996) showed that such sequence learning can be extended to remember a sequence of activation patterns of neurons in general, not just place cells. This demonstrates that the capacity of the theta sequence mechanism to encode the temporal order of multiple memory items. Apart from learning, the asymmetric pattern could also arise from pre-existing synaptic

connections among hippocampal neurons, which can already contribute to the temporal correlation between their firing activities even prior to behavioral experiences (Dragoi and Tonegawa, 2011, 2013).

However, the fundamental assumption of asymmetric connectivity poses a major challenge of the model, as it fails to account for phase precession during backward travel against the unidirectional projections (Cei et al., 2014). In such cases, the theta sequence would propagate backward, and the theta correlation would not flip sign in response to movement reversal (for illustration, see Figure 7B). Hence, the intrinsic model is unable to explain the dependence of theta correlations on the behavioral trajectory, as observed in Huxter et al. (2008) (also see Figure 6).

1.4.2   The extrinsic family

In contrast to intrinsic models, the theta correlation in extrinsic models is determined by the temporal information from the extra-hippocampal input, specifically the sensorimotor input current from the EC during spatial navigation. Thus, the theta correlation is able to represent the trajectory and reproduce the trajectory dependence observed in Huxter et al. (2008). One notable example is Romani and Tsodyks (2015). In their theoretical framework, place cells are recurrently connected with symmetrical synaptic strengths but undergo a mechanism called short-term depression (STD) (Tsodyks and Markram, 1997). The STD limits the resource of neurotransmitters at the synapses, such that they could be depleted by the sustained activity of the pre-synaptic neuron. As the animal traverses a sequence of place fields, the place cells with field centers behind the animal are left with depleted synapses and receive reduced recurrent input compared to those ahead of the animal (Figure 7C). This creates a temporarily asymmetrical connectivity that is stronger in the direction of travel and propagates the sequential activity of place cells forward. The depleted synaptic resource will recover after the pre-synaptic neuron stops firing, with a time constant between 200 and 800ms (Tsodyks and Markram, 1997). This period is approximately the time required for rodents to cross a place field in most experimental enclosures. Thus, the theta sequence can be initiated again when the same place field is visited thereafter. Although the spike sequence is still produced by recurrent connections, the temporal order of the sequence is determined by the animal's movement (Figure 7D).

Several other models exist within the extrinsic family. Similar to STD, spike timings in theta oscillation can also be coordinated by short-term facilitation (STF) (Thurley et al., 2008). STF progressively amplifies the sensorimotor input received by the place cells ahead of the animal compared to those behind it, creating a similar sequential activity.

Beyond the mechanisms of short-term plasticity, phase precession can also arise by leveraging the negative correlation between the amount of depolarization by spatial input and the spike latency of a neuron. Increasing depolarization causes the membrane potential to
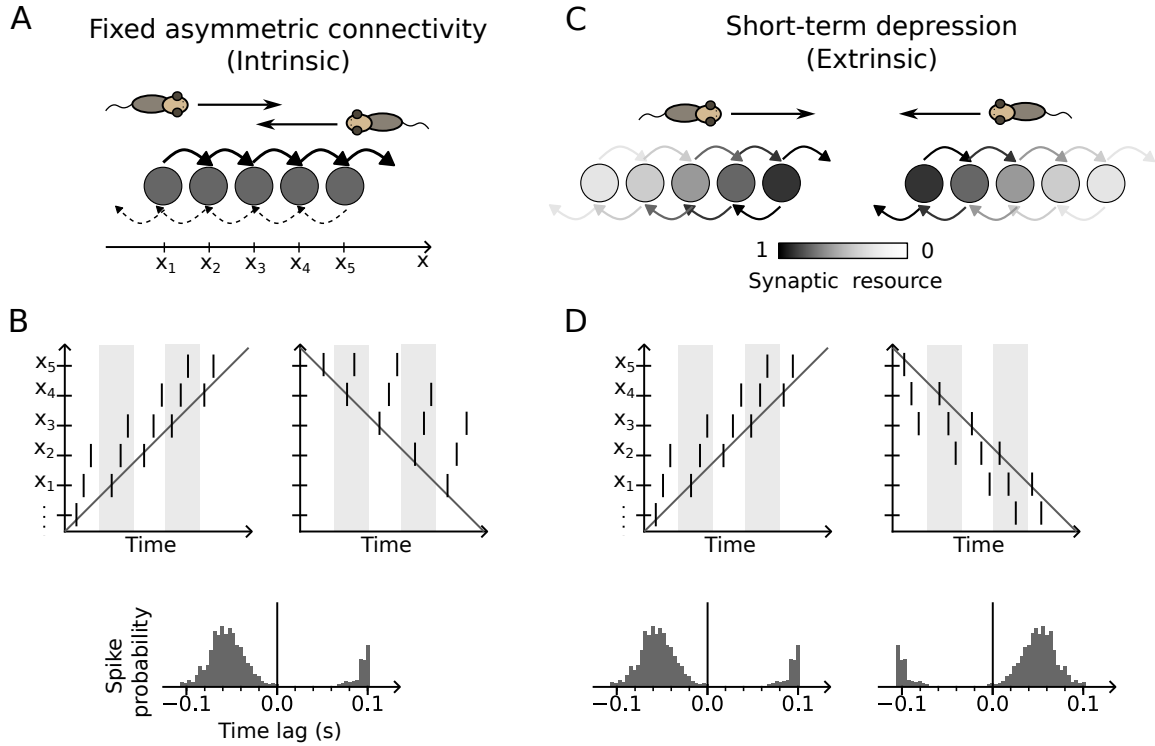
Figure 7: Schematic illustrations of the theta sequence generation mechanisms in the intrinsic and extrinsic models. (A) Theta sequences generation by the intrinsic network connectivity with asymmetrical projections to the neighboring place cells, as originally proposed by Tsodyks et al. (1996). Place cells project more strongly to their rightward neighbors than to their leftward neighbors. x_i indicates the center locations of the place fields. (B) Spike raster plot of place cells (at location x_1 to x_5) when the animal moves forward along the stronger direction of the asymmetry (left panel) and backward against it (right panel). The model fails to account for phase precession during backward travel. The solid gray line marks the running trajectory. Bottom: Cross-correlation between a pair of place cells remains unchanged in both directions. The peak time lag is always negative (the left cell fires before the right cell), even when the animal travels from right to left. (C) Theta sequence generation by short-term depression mechanism proposed by Romani and Tsodyks (2015). The synaptic resource (grayscale color) of the place cells behind the movement is depleted, thereby generating spike sequence in the forward-moving direction. (D) The theta sequence is movement-dependent and propagates forward in the direction of travel. Theta correlation changes signs when the running direction is reversed.

surpass the firing threshold progressively earlier, thereby inducing precessing spike phases. However, as the spatial input diminishes, additional mechanisms are required to suppress the progressive increase of spike phases in the later part of place field. Harris et al. (2002) employed adaptation dynamics that prohibits spiking activity in the decreasing part of the spatial input. In addition, Mehta et al. (2002) directly employed an asymmetrical increasing ramp of spatial input, without a decreasing part of the spatial input, to generate phase precession.

The extrinsic models coordinate spike timings via the temporal order of sensorimotor input, which is fundamentally different from the intrinsic family where spike timings are coordinated by recurrent connectivity. The trajectory-dependent theta temporal code thus does not necessitate recurrent connectivity as demonstrated by the recurrence-free models that utilize STF and asymmetry of spatial input.

1.5 Contributions of intrinsic circuitry to the temporal code

While the extrinsic models excel in accounting for the dependence of theta temporal code on trajectories, the study by Huxter et al. (2008) primarily focused on the CA1 region but not CA3 region. The CA1 region is a primarily feed-forward network structure while the CA3 has more recurrent projections. As discussed in the previous section about intrinsic models, theta sequences could be coordinated by recurrent connectivity between place cells. This implies that the intra-hippocampal network connectivity should play a larger role in the theta temporal code in the CA3 region and consequently, their theta temporal code would be more consistent with the intrinsic models. However, a detailed investigation into the theta temporal code in CA3 in comparison to CA1 has been lacking. Moreover, the feedback projections linking CA3-DG and the phenomenon of hippocampal replays during sharp-wave ripples (SWRs) also point towards potential contributions to the temporal code from intra-hippocampal connectivity. Therefore, this section discusses the rationales behind the intrinsically driven theta temporal code within the CA3 region.

1.5.1 Recurrent networks in the CA3 region

One anatomical difference between CA1 and CA3 is their network structures. In CA3, pyramidal cells not only project axons to CA1 via Schaffer's collaterals but also establish connections with other pyramidal cells within the same CA3 region (Amaral and Witter, 1989, Ishizuka et al., 1990, Andersen et al., 2006). Roughly 30 to 70% of synapses from CA3 pyramidal cells terminate within the same CA3 region (Le Duigou et al., 2014, Li et al., 1994), forming a large recurrent and auto-associative network. In contrast, CA1 region is a mostly feed-forward structure. It receives the major input from the upstream pyramidal cells in CA3 and EC layer II regions, mainly projecting to the subiculum region, EC layer V and VI, and exhibiting comparatively fewer recurrent projections to themselves

(Amaral and Witter, 1989, Andersen et al., 2006).

Furthermore, CA3 pyramidal cells form not only recurrent projections to themselves, but also backward projections to the DG. The CA3 neurons innervate mossy cells in the DG hilus, which subsequently project to DG granule cells, and, in turn, to the CA3 pyramidal cells via mossy fibers (Scharfman, 1994, 1995, 2007, 2016). Although the pathway is indirect and involves inhibitory interneurons, it has been shown that activity of CA3 can be reverberated to themselves via DG area (Penttonen et al., 1998), allowing DG activity to participate in CA3 place cell computation. In fact, this CA3-DG recurrence has been suggested to support the retrieval of hetero-associative memories (Lisman et al., 2005), pattern separation of contextually similar memories (Myers and Scharfman, 2009b, 2011), and prospective firing activity of CA3 place cells (Sasaki et al., 2018), indicating that the back-projection pathway is functional for information processing.

The feedback projections within CA3 and the CA3-DG network can render the CA3 theta temporal code less dependent on the external sensorimotor drive and more on the intra-hippocampal connectivity. Hence, the experimental observation of trajectory-dependence in CA1 theta correlations by Huxter et al. (2008) might not be transferable to the CA3 region and would warrant further investigation.

1.5.2 Hippocampal replay and preplay

Other than theta timescale, sequential activity of place cells also occurs during SWRs which are high-frequency (100–250Hz) oscillations observed in LFP. These oscillations typically appear as brief periods of high-amplitude deflections lasting for 100-200ms in each event. SWRs can be generated by rapid bursts of spike sequences from place cells, which often reactivate the spatial locations previously visited by the animal, giving rise to the term "replay" (see Figure 8 for the illustration). The replay sequences are associated with the performance of spatial learning (Girardeau et al., 2009, Ego-Stengel and Wilson, 2009, Carr et al., 2011), are thought to enhance memory consolidation, as the temporal correlation between neurons can reinforced by synaptic plasticity through repeated sequential reactivation. Unlike theta sequences, which occur only when the animal is actively running , the replay sequences exclusively occur during sleep (Wilson and McNaughton, 1994, Skaggs and McNaughton, 1996, Lee and Wilson, 2002), or awake but immobile periods (Foster and Wilson, 2006, Karlsson and Frank, 2009, Diba and Buzsáki, 2007, Silva et al., 2015, Carr et al., 2011).

The temporal order of replay sequence is often considered to arise from the intrinsic network connectivity. This is because the replay sequence emerges during stationary states, even though the place cell sequence represents a trajectory extending beyond the animal's current stationary position. Therefore, the sequence order is not organized by external sensorimotor inputs during online locomotive behaviors. Instead, it rather reflects

correlations originating from intrinsic network dynamics, as the sequence order resembles the past behavioral experiences, which could be encoded in the network connectivity. Notably, the more frequently place cells are co-activated in theta cycles during running, the stronger their correlations are in the replay sequences during sleep, indicating a Hebbian-like learning rule underlying the acquisition of replay sequences (O'Neill et al., 2008). Blocking NMDA receptors also prevents the replay sequences from encoding new spatial sequences (Silva et al., 2015). These studies support the hypothesis that replay sequences are coordinated by intrinsic network connectivity through learning.
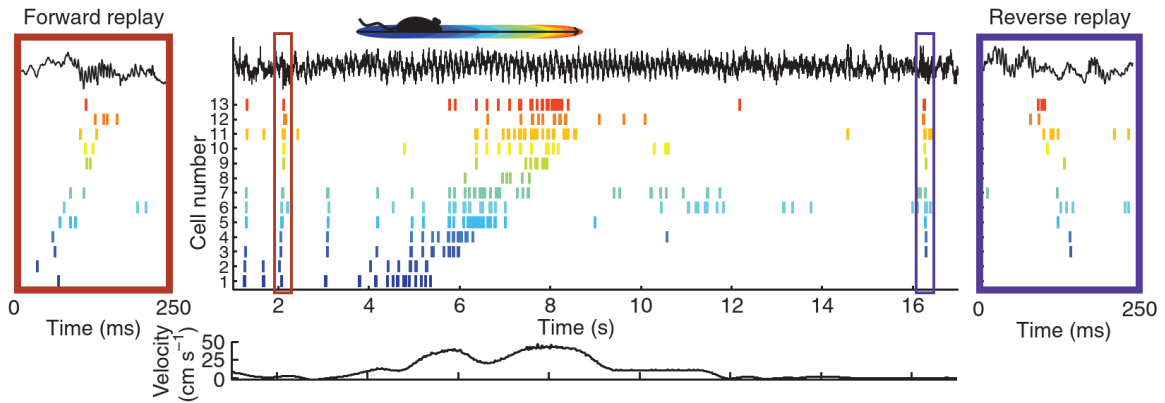

Figure 8: Figure by Carr et al. (2011), adapted from Diba and Buzsáki (2007), illustrating hippocampal replay. Middle: Raster plot showing the spike times of 13 place cells (color-coded) on the linear track as their place fields were sequentially traversed by the animal. The LFP recorded in CA1 is shown on top of the spike raster. The left and right insets illustrate the magnified windows of a forward and reverse replay sequence within their SWRs, respectively. Note that both types of replays occur during immobile periods as indicated by the low velocities. Figure reused with permission of the rights holder, Springer Nature.

Another similar phenomenon is hippocampal preplay Dragoi and Tonegawa (2011, 2013). In contrast to replay, preplay activates neuron sequences in SWRs even before the animal explores a novel environment. These neurons later develop spatial tuning and become place cells that represent the environment. Retroactively decoding the preplay sequences using the place cells reveals spatially plausible trajectories. This discovery implies that new behavioral experiences can be mapped onto pre-existing temporal sequences, presumably generated by intrinsic network connectivity, removing the need to re-learn a new sequence structure of memory. It emphasizes the role of intrinsic network connectivity in coordinating temporal coding.

Both hippocampal replay and preplay phenomena suggest that intrinsic network dynamics could contribute to the coordination of sequence activity. Thus, it is worth investigating whether a similar intrinsic mechanism, such as theta oscillations, can contribute to the temporal code at a longer time scale.

23

1.6   Summary

As discussed in previous sections, the CA3 region is well poised to generate sequential activity reflective of intrinsic network dynamics, rather than the sensorimotor input, due to the feedback projections with itself and the DG. Despite the evidence that the theta sequence in CA1 represents the online running trajectory (Huxter et al., 2008), a direct comparison of theta temporal code between CA3 and CA1 remains unexplored. Therefore, we were motivated to investigate whether the theta temporal code in the CA3 region would still exhibit the same degree of dependence on sensorimotor input.

In the first publication "Directional Tuning of Phase Precession Properties in the Hippocampus", we analyzed the electrophysiological data from the rat hippocampus during a free-foraging task in a 2D space. We assessed the contribution of intrinsic network circuits to theta temporal code, by systemically quantifying the properties of phase precession and theta correlation as a function of running direction. According to the predictions from Tsodyks et al. (1996) model (Figure 7), a more intrinsically driven theta correlation would remain invariant to trajectory reversal, and the phase precession should vary in different running angles (Figure 9). With these indicators, we were able to gauge the influence of intrinsic network dynamics and sensorimotor input on the theta temporal code. We demonstrated that theta sequences were comprised of both extrinsically and intrinsically driven correlations, with the latter being more pronounced in the CA3 place cell population. Thus, the theta temporal code is coordinated by both intrinsic network dynamics and sensorimotor input.
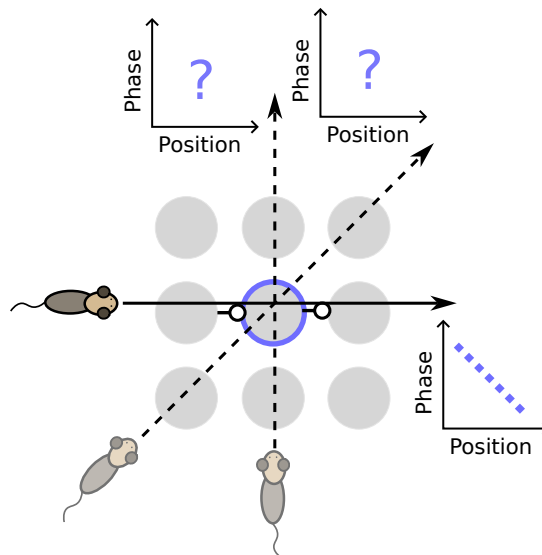

Figure 9: Phase precession of a single place cell (shown in blue) driven by intrinsic network dynamics through unidirectional (rightward) projections. However, it remains unclear how the phase-position relationship varies with the running direction in a space represented by a 2D topology of place cells.

In the second manuscript "A theory of hippocampal theta correlations accounting for
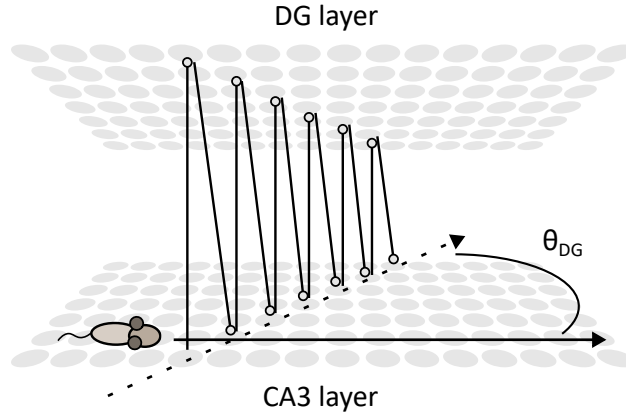
Figure 10: The network model of CA3 and DG place cells. The extrinsic sequence is generated by the running trajectory via STD mechanisms within CA3 place cells. The intrinsic sequence is produced by unidirectional feedback projections via the DG layer. Temporal sequences thus propagate along the two 1D manifolds in a 2D space, namely the trajectory and the spatial pathway represented by the CA3-DG projections.

extrinsic and intrinsic sequences", we followed the notion of the heterogeneous nature of theta correlations and proposed a spiking neural network model that can account for the extrinsically and intrinsically driven theta correlations. The spike sequences that induce these two types of correlations are termed extrinsic and intrinsic sequences. In more detail, the model consists of two layers of place cells - CA3 and DG. Extrinsic sequences arise from the STD mechanism within the CA3 layer, while intrinsic sequences are organized by unidirectional feedback projections between CA3 and DG. The layer separation allows for the simultaneous propagation of both types of sequences. Working in concert, they generate theta correlations and phase precession that align quantitatively with experimental findings. Furthermore, the extrinsic sequence follows the movement trajectory, while the intrinsic sequence propagates along the unidirectional projection pattern, which can to spatially deviate from the trajectory (Figure 10). Consequently, the theta time code becomes capable of representing a 2D space through spike sequences along multiple distinct 1D manifolds.

Conventionally, the theta sequence was solely considered extrinsic, representing the running trajectory. The present thesis reveals an additional dimension of spatial encoding within the theta temporal code characterized by intrinsic network dynamics and demonstrates that multiple 1D theta sequences can represent 2D space.".

2 Manuscripts

2.1   Manuscript I - Directional Tuning of Phase Precession Properties in the Hippocampus

Directional Tuning of Phase Precession Properties in the Hippocampus

Yuk-Hoi Yiu, Jill K. Leutgeb, and Christian Leibold (2022)

Author Contributions

Y.-H.Y., J.K.L., and C.L. designed research; C.L. conceived the project and supervised the research; J.K.L. provided data; **Y.-H.Y.** and C.L. performed research; **Y.-H.Y.** implemented data analysis; **Y.-H.Y.**, J.K.L., and C.L. wrote the manuscript.

Systems/Circuits

Directional Tuning of Phase Precession Properties in the Hippocampus

Yuk-Hoi Yiu,[1,2,3] **Jill K. Leutgeb,**[4] and ⬤ **Christian Leibold**[1,2]

[1]Fakultät für Biologie, Bernstein Center Freiburg, Albert-Ludwigs-Universität Freiburg, 79104 Freiburg, Germany, [2]Department Biology II, Ludwig-Maximilians-Universität München, 82152 Martinsried, Germany, [3]Graduate School of Systemic Neurosciences, Ludwig-Maximilians-Universität München, 82152 Martinsried, Germany, and [4]Neurobiology Section and Center for Neural Circuits and Behavior, University of California, San Diego, La Jolla, California 92093

Running direction in the hippocampus is encoded by rate modulations of place field activity but also by spike timing correlations known as theta sequences. Whether directional rate codes and the directionality of place field correlations are related, however, has so far not been explored, and therefore the nature of how directional information is encoded in the cornu ammonis remains unresolved. Here, using a previously published dataset that contains the spike activity of rat hippocampal place cells in the CA1, CA2, and CA3 subregions during free foraging of male Long-Evans rats in a 2D environment, we found that rate and spike timing codes are related. Opposite to a preferred firing rate direction of a place field, spikes are more likely to undergo theta phase precession and, hence, more strongly affect paired correlations. Furthermore, we identified a subset of field pairs whose theta correlations are intrinsic in that they maintain the same firing order when the running direction is reversed. Both effects are associated with differences in theta phase distributions and are more prominent in CA3 than in CA1. We thus hypothesize that intrinsic spiking is most prominent when the directionally modulated sensory-motor drive of hippocampal firing rates is minimal, suggesting that extrinsic and intrinsic sequences contribute to phase precession as two distinct mechanisms.

Key words: Directional sensitivity; hippocampus; phase precession; place cells; sequences; theta rhythm

---

Significance Statement

Hippocampal theta sequences, on the one hand, are thought to reflect the running trajectory of an animal, connecting past and future locations. On the other hand, sequences have been proposed to reflect the rich, recursive hippocampal connectivity, related to memories of previous trajectories or even to experience-independent prestructure. Such intrinsic sequences are inherently one dimensional and cannot be easily reconciled with running trajectories in two dimensions as place fields can be approached on multiple one-dimensional paths. In this article, we dissect phase precession along different directions in all hippocampal subareas and find that CA3 in particular shows a high level of direction-independent correlations that are inconsistent with the notion of representing running trajectories. These intrinsic correlations are associated with later spike phases.

Introduction

Hippocampal place cells establish a neuronal representation of space by exhibiting elevated firing rates at only few

locations in an environment called place fields (O'Keefe and Dostrovsky, 1971). Place field firing is thought to underlie the capacity of an animal to navigate in space and to form spatial memories (Morris et al., 1982; Moser et al., 1993; Nakazawa et al., 2002). Place field firing also includes a temporal code associated with the theta oscillation (4–12 Hz) of the local field potential (O'Keefe and Recce, 1993): As a rat passes through a place field, the spikes phase precess, that is, they occur at successively earlier theta phases thereby encoding the relative location of the animal within a place field (O'Keefe and Recce, 1993; Harris et al., 2002). Phase precession is generally thought to implement a compression of behavioral sequences to the theta time scale so that in a 100 ms time window, spikes of multiple place cells are elicited in the same order as the activation of the associated place fields along the trajectory of the animal

over the time scale of seconds (Melamed et al., 2004; Dragoi and Buzsáki, 2006; Foster and Wilson, 2007; Jaramillo and Kempter, 2017).

In one-dimensional mazes, the trajectory of an animal can be uniquely mapped to a sequence of place fields; thus, spike sequences on the theta time scale (Foster and Wilson, 2007) can be easily interpreted as reflecting memories of previous locations or planning of future actions (Feng et al., 2015). In two-dimensional environments, place fields can be entered from multiple directions, and hence place cells generally take part in encoding multiple trajectories. Thus, place cells could either be linked to multiple sequences, or place field sequences could be directional. In the former case, sequential structure would be imposed by sensory-motor (extrinsic) inputs, whereas the latter case would render sequences of intrinsic origin supported by recurrent circuits or associative loops. Previous reports revealed that pair correlation lags of place fields in the CA1 subregion depend on running direction (Huxter et al., 2008) and thus support the extrinsic hypothesis, but similar analyses for the CA2 and CA3 subregions, which differ substantially in their cytoarchitecture, plasticity, and protein chemistry, are missing.

In addition to sequence order, directional information is also available to the entorhinal-hippocampal circuits from head direction cells of the postsubiculum (Taube et al., 1990a,b) and the medial entorhinal cortex (Sargolini et al., 2006; Giocomo et al., 2014) and, to a limited extent, from within the cornu ammonis itself (Leutgeb et al., 2000). These inputs might explain observed directionality of some place fields (Leutgeb et al., 2004; Acharya et al., 2016; Mankin et al., 2019); however, it is unclear to which extent this rate directionality is related to directionality of theta sequences.

Past studies have shown that compared with the CA1 region, place cells in CA3 demonstrate a more persistent and consistent activity pattern over an extended period of time (Mankin et al., 2012) and across cue-altered environments (Lee et al., 2004), as well as a higher stability of place field dynamics across multiple recording sessions in the same environment (Mizuseki et al., 2012). Consistently, CA3 place representations stabilized more slowly after a change of environment than in CA1 (Leutgeb et al., 2004). The stability, consistency, and slower stabilization of CA3 place fields, in addition to the classical anatomy indicating strong recurrent connectivity (Amaral and Witter, 1989; Ishizuka et al., 1990), lead to a belief that CA3 activity patterns are more reliant on internal network dynamics and less influenced by external sensory inputs. Therefore, we hypothesized that the theta sequence activity in CA3 should be less dependent on the directionality in the behaviors of the animal than CA1.

Our results show that although the extrinsic contribution to theta scale firing is dominant in all subareas, this is indeed least visible in CA3. Moreover, we observe directionality in the phase precession properties so that CA3 displays later spike phases in the running direction opposite to the best firing rate direction.

Materials and Methods

Experimental design and statistical analysis. We reanalyzed a previously published dataset in Mankin et al. (2012, 2015). For a detailed description of the data collection, we refer to the original work. In brief, the dataset involves eight male Long-Evans rats that were trained to forage for randomly scattered cereal crumbs in either a square (80 cm × 80 cm) or a 16-sided polygon (50 cm radius, also referred to as circular) enclosure. The experiment began after animals were trained 9–20 d in the enclosure. Single units were recorded simultaneously from the CA1, CA2, and CA3 subregions for the course of the experiment, which lasted

2 d. On each day the rats completed two blocks of four 10 min sessions, with two sessions in the square enclosure and two sessions in the circular enclosure assigned in random order. The enclosures contain a 20 cm-wide white cue card on an inside wall, and the cue card maintained a constant angle with the cues outside the room.

Data analysis and statistical tests were performed on Python using SciPy (Virtanen et al., 2020), NumPy (Harris et al., 2020) packages, and custom routines based on CircStat toolbox (Philipp, 2009). We used nonparametric Kruskal–Wallis tests with a *post hoc* Dunn's test for statistical comparisons. Normally distributed data were tested using Student's t test. The Watson–Williams test was used for circular data. For categorical data, we used χ^2 and Fisher's exact tests. The p-values were adjusted for multiple comparisons using the Benjamini–Hochberg procedure (Benjamini and Hochberg, 1995). We used two-tailed tests throughout except for binomial tests, and $p = 0.05$ is chosen as the significance level.

Place field detection and delimitation. For each place cell, we computed a spatial map of firing rates from each 10 min session by dividing the spike counts by the occupancy time in each space bin (1 cm × 1 cm). Spikes and occupancy were smoothed by a Gaussian filter with an SD of 3 cm. Place fields were segmented along the closed contour line located at 20% of the maximum rate and accepted if the peak rate exceeds 1 Hz, the field area is larger than 25 cm², and the average firing rate within the field is larger than outside the field. In the analysis, we separated place fields into a border and a nonborder group. The groups are distinguished by the 20% line touching the boundary of the enclosure. Each place cell could have multiple place fields that were analyzed separately.

Two place fields are said to be a pair if both field areas intersect and contain at least 16 spikes of one field that occur next to a spike of the other field within a time window of ±0.08 s (see Fig. 4B). We defined pairs as border pairs if at least one of the place fields touches the border. In nonborder pairs, both place fields do not touch the border.

Directionality of place fields. To obtain the directional tuning curve of place fields, we used a maximum likelihood maximization (MLM) model (Cacucci et al., 2004). In brief, the model assumes an independent relation between positional and directional firing probability distributions, whose product is the firing probability. The product assumption furthermore ensures that directionality tuning is restricted to the place field and that the tuning depends on a weighted sum of position and direction. The solution of the directional term, which is also the estimated directional tuning curve, can be fit by iteratively maximizing firing likelihood to the observation of spikes. This MLM model has an advantage of reducing sampling bias, which usually arises at the enclosure borders where certain heading directions are severely undersampled.

Significance of directionality is determined by comparing the mean resultant vector length (R) of the directional tuning curve to a shuffling distribution, which is obtained by randomly shifting the spike times in a cyclic fashion along a trajectory concatenated from all path segments traversing the place field. The random time shift was repeated 200 times for each place field. A place field is classified as significantly directional if the R value exceeds the 95th percentile of its shuffling distribution. For field pairs, the same method is used to determine the significance of directional selectivity, except that the R is calculated from spike pairs.

Significance of the preferred precession direction is also determined by comparison of R to a distribution obtained from shuffling spike times over all passes through the field. In this case the R value for precession directionality is computed from the directions of field traversals that exhibit phase precession. A pass is labeled as precessing if the phase-position relation of the spikes has a negative slope derived from linear-circular regression (Kempter et al., 2012).

Correlation lags. We produced cross-correlograms for the spike trains of every field pair, with the resolution of 5 ms and a time window between −150 ms and 150 ms. The resultant cross-correlograms were then bandpass filtered (5–12 Hz) to derive the correlation lag as the phase at 0 time lag from the Hilbert transform of the theta filtered correlograms.

Classification of extrinsic and intrinsic pairs. To quantify the dependence of correlation lag on directionality, we devised the measures of

"extrinsicity" and "intrinsicity" for each field pair. The extrinsicity is computed as the Pearson's correlation coefficient between the cross-correlogram for runs from one field to another and the cross-correlogram for runs in the opposite direction but with the sign of time-axis flipped. The Pearson's correlation coefficient (r) is then linearly transformed ($r' = \frac{r+1}{2}$) to be in the range of 0 and 1. The extrinsicity is close to 1 if a field pair was mainly driven by the external sensory input, as the sign of correlation lag would be reversed if the place fields were traversed in a reversed order. Similarly, the intrinsicity is computed as the Pearson's correlation coefficient between the two cross-correlograms without flipping the sign of time-axis. The value of intrinsicity is close to 1 if the correlation lag of a field pair was mainly dependent on its intrinsic dynamics but less on the external sensory-locomotor input, leading to similar correlograms in two running directions. Note that using this definition, extrinsicity and intrinsicity are two independent values that are not necessarily correlated. We classify a field pair as extrinsic (Ex) if its extrinsicity exceeds its intrinsicity and as intrinsic (In) if its intrinsicity exceeds its extrinsicity.

Inclusion criteria for analysis. The animal trajectory is split to passes entering and exiting the place fields or pairs. Intervals in which the speed of the animal is below 5 cm/s were excluded. The passes are then chunked to smaller segments in which the speed was always above 5 cm/s.

The pass segments and their spikes are only included if the pass duration is longer than 0.4 s and satisfies a straightness threshold as in the following:

$$R^2 > \text{mean} + q(\text{std dev}) = \frac{1 + q\sqrt{1 - \frac{1}{n}}}{n},$$

where $q = 5$, R is Rayleigh Vector length of the heading samples of the animal, and n is the number of heading samples. In case the pass is chunked because of low speed, to determine the traveled distance of the animal inside the place field relative to the entry point, only the first pass segment entering the place field is included for analysis. The relative position of the animal can thus be determined by distance traveled divided by the field diameter.

Pair-crossing passes are classified as $A \rightarrow B$ if they start from an area within field A but not field B, and end in an area within field B but not field A. The opposite criteria apply for $B \rightarrow A$ passes. Passes that do not satisfy the above criteria, or cross either one of the field boundaries more than once, are not assigned to any of the directional groups ($A \rightarrow B$ or $B \rightarrow A$). These unassigned passes were also included in computing the firing rate directionality but excluded for cross-correlation analyses. As a result, field pairs that have no spike pairs along the $A \rightarrow B$ or $B \rightarrow A$ passes were further excluded in the cross-correlation analyses.

Model simulation. Romani and Tsodyks (2015) proposed a recurrent network model of the hippocampus, which we adapted and simulated using our trajectory data. Here, we briefly summarize the key equations of the model. The dynamics of firing rate $m_i(t)$ of place cell i at time t is given by the following:

$$\tau \dot{m}_i(t) = -m_i(t) + f\left(I_i^E(t) + I_i^R(t)\right),$$

where $\tau = 10$ ms is the time constant, $f(.)$ is the firing rate function, $I_i^E(t)$ is the sum of external positional and theta oscillatory inputs, and $I_i^R(t)$ is the recurrent input from the other neurons. The latter is computed as follows:

$$I_i^R(t) = \frac{1}{N}\sum_{j=1}^{N} W_{ij} m_j(t) x_j(t),$$

with W_{ij} denoting the synaptic weight from neuron j to i and x_j denoting the depletion state of the synaptic vesicle pool, which is recovering with time constant $\tau_R = 800$ ms as follows:

$$\dot{x}_i(t) = \frac{1 - x_i(t)}{\tau_R} - U x_i(t) m_i(t).$$

The parameter $0 < U \leq 1$ denotes the release probability. The introduction of $x_i(t)$ penalizes the recurrent input from the highly activated place cells with a delay, and therefore it produces asymmetrical weight couplings that are stronger in the forward direction as the animal moves.

We adopted the model parameters from the toroidal environment described in Romani and Tsodyks (2015). The periodicity of the environment was removed by clipping the cosine function $\cos(x)$ at the value of -1 for $|x| > \pi$. Our simulation thus has 32×32 neurons equally spaced across a $2\pi \times 2\pi$ unit squared environment. We randomly chose one recording session in the square arena from the experimental data as the trajectory, and rescaled the trajectory into the range of 0 and 2π and the average speed to be the same as in the original study ($2\pi/5$ unit per second). Simulation was implemented with 1 ms temporal resolution using the Euler method. Spikes from each place cell were then subsampled by a fraction so that the average spike count of all simulated place fields is the same as the experimental data.

Results

Directional tuning of place cells

Directionality of hippocampal place field activity has been reported in a number of previous studies (Leutgeb et al., 2004; Acharya et al., 2016; Mankin et al., 2019), but quantitative comparisons between those studies were hampered because of the use of different methods and behavioral paradigms. Here, we analyze the firing properties of simultaneously recorded CA1, CA2, and CA3 neural networks under identical experimental conditions. We thus first applied one established rate-based directionality analysis on the datasets used in this article (Mankin et al., 2012, 2015) for further comparison. Directional tuning for each place field was quantified using the mean resultant vector length (R) obtained from directionality fields derived by the MLM proposed in Cacucci et al. (2004); Fig. 1A, single examples, 1B populations. Because mean resultant vector lengths are strongly biased by the number of observations (Fig. 1B), we decided to analyze directional tuning as a function of the spike count threshold criterion for including place fields (Fig. 1C) and include only the fields with spike counts higher than 40 in our statistical analysis of place field directionality. We found that all CA regions contain a fraction of directional fields that is above chance level (Binomial test; CA1, 146/800 = 0.1825, $p = 1.8e - 41$; CA2, 111/521 = 0.2131, $p = 2.4e - 38$; CA3, 45/396 = 0.1136, $p = 3.5e - 07$). The amount of directionality in all regions not only depends on the overall spike count threshold of the place field (showing an initial increase that is expected from the gain in statistical power) but also on whether the place field is located at the boundary of the arena (Fig. 1C).

Comparing the place field directionalities between CA regions, CA1 and CA3 have a higher median R than CA2 [Kruskal–Wallis test; CA1 ($n = 800$) vs CA2 ($n = 521$) vs CA3 ($n = 396$), $H_{(2)} = 22.18$, $p = 1.5e - 05$; *post hoc* Dunn's test with Benjamini–Hochberg correction; CA1 vs CA2, $p = 0.0003$, CA2 vs CA3, $p = 3.8e - 05$, CA1 vs CA3, $p = 0.1920$]. The fraction of significantly directional fields in CA3 is lower than in CA1 and CA2 (Fisher's exact test for independence of significant fractions with Benjamini–Hochberg correction; CA1 vs CA2, $p = 0.2656$; CA1 vs CA3, $p = 2.2e - 05$; CA2 vs CA3, $p = 0.0074$). However, as we increase the spike count threshold to admit only fields that are highly sampled, the fraction of significantly directionally tuned fields becomes similar in CA1 and CA3, as far as our data allow such a comparison because of the only very few CA1 and CA3 fields with high spike numbers (Fig. 1D).
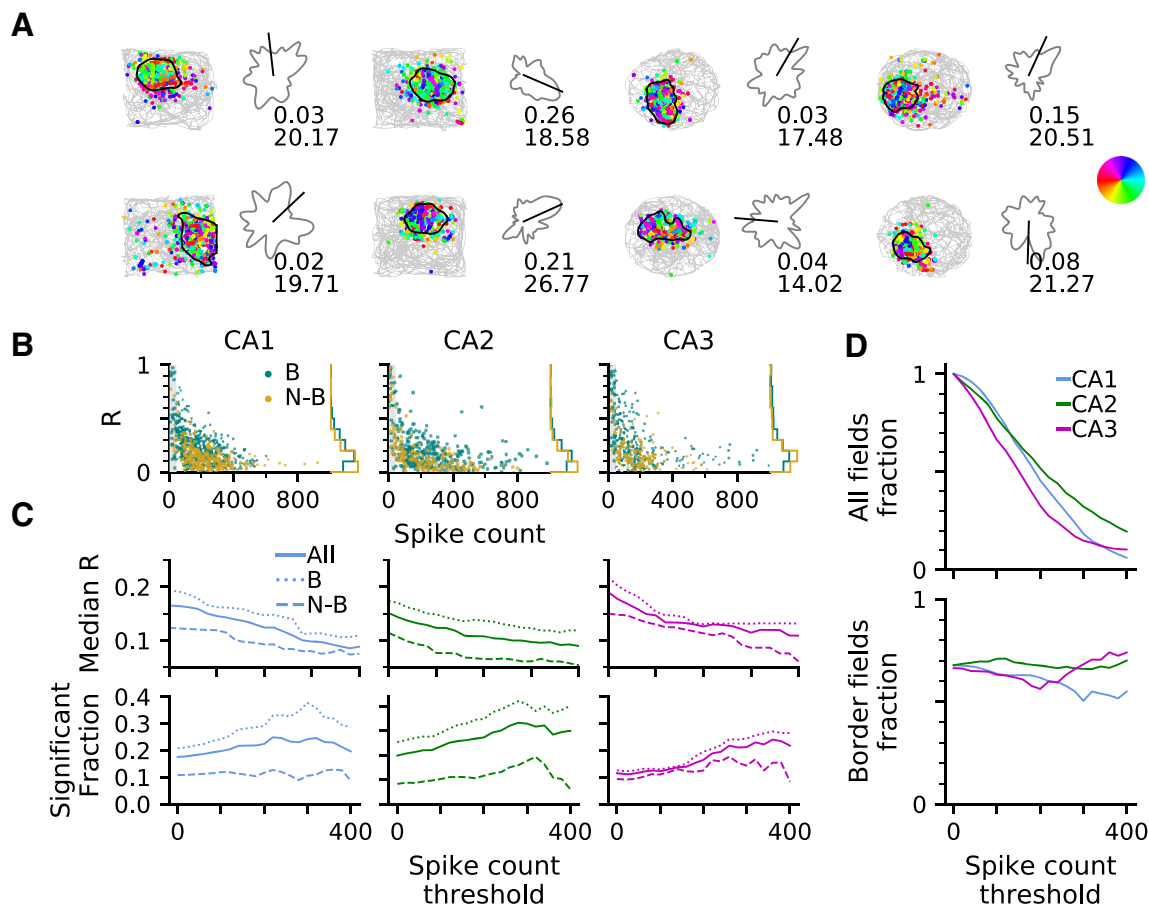
Figure 1. Directionality of place field firing rates. **A**, Examples of place fields in square and circular enclosures of a free-foraging experiment overlaid with the trajectory of the animal in one recording session and spike events color coded by heading direction (color wheel at right). Directional tuning curve is shown to the right of each spike position plot. Mean direction (black bar), mean resultant vector length R (top), peak rate in Hz (bottom). **B**, R and total within-field spike counts of all border (B, teal) and nonborder (N-B, gold) place fields, as well as marginal distribution of R (right). R values are strongly biased by sampling. Therefore, we excluded the fields with spike counts below 40 in our directionality analysis, indicated by the shaded region. **C**, Median R (top row) and fraction of significantly directionally tuned place fields (bottom) by different spike number thresholds for all (solid line), border (dotted line), and nonborder (dashed line) fields in each brain region as indicated. CA1 and CA2 directionality is strongly border driven. **D**, Fraction of all place fields (top) and border fields (bottom) by spike count thresholds.

To accurately interpret the above results, we looked into possible confounds. A major influence on directionality could arise from the presence of arena boundaries, both because they act as salient sensory landmarks and they introduce a behavioral bias. We thus further separated place fields into border and nonborder fields. Including all the place fields regardless of spike counts, we found that border fields in CA1 generally have higher directional selectivity than in the nonborder case [Kruskal–Wallis test; border ($n = 537$) vs nonborder ($n = 263$), $H_{(1)} = 62.33$, $p = 2.9e – 15$; Fisher's exact test; $p = 5.7e – 05$], whereas CA3 exhibits significant border difference in median R [border ($n = 257$) vs nonborder ($n = 139$), $H_{(1)} = 15.31$, $p = 9.1e – 05$] but not in significant fraction (Fisher's exact test; $p = 0.0885$). Similar to CA1, directionality measures in CA2 also exhibit a significant border effect [Kruskal–Wallis test; border ($n = 359$) vs nonborder ($n = 162$), $H_{(1)} = 31.95$, $p = 1.6e – 08$; Fisher's exact test; $p = 3.6e – 07$].

We thus conclude that place field rates in all CA areas encode running direction, and directionality in CA1 and CA2 is more strongly induced by borders, whereas this is not the case for CA3 in which the directionality is more similar between border and nonborder fields. Assuming boundaries to induce a strong sensory-motor constraint, this is already a first hint that CA1 activity is more strongly influenced by extrinsic factors than CA3.

Preferred direction for phase precession in place fields
In addition to the firing rate code, because place field activity is also temporally organized on the theta scale by phase precession (Fig. 2A), we also asked to what extent directionality is also reflected in this temporal code. For each place field, we therefore identified a direction in which phase precession is more likely to occur using single pass phase precession analysis (Schmidt et al., 2009; Kempter et al., 2012; see above, Materials and Methods for inclusion criteria). In brief, we fit a linear-circular regression line for the phase-position relation in every single pass. Passes with negative regression slope between -2π and 0 (per pass length) are classified as phase precessing (Fig. 2B).

First, we computed the density of phase precession occurrences from all passes in all fields as a function of pass direction relative to the preferred firing rate direction of the respective field (Fig. 2C). We find most precessing passes along the best rate direction, reflecting the fact that more spikes should give rise to more detectable phase precession. However, not all spikes may contribute to phase precession to the same degree, either because of different levels of phase noise or because they occur outside theta sequences. If phase precession is directional beyond a simple spike count effect, it needs to show in an analysis per spike. Thus, computing the density of precessing passes per spike (Fig. 2C, right), we found that phase precession is more likely to occur the more the pass direction differs from the preferred rate
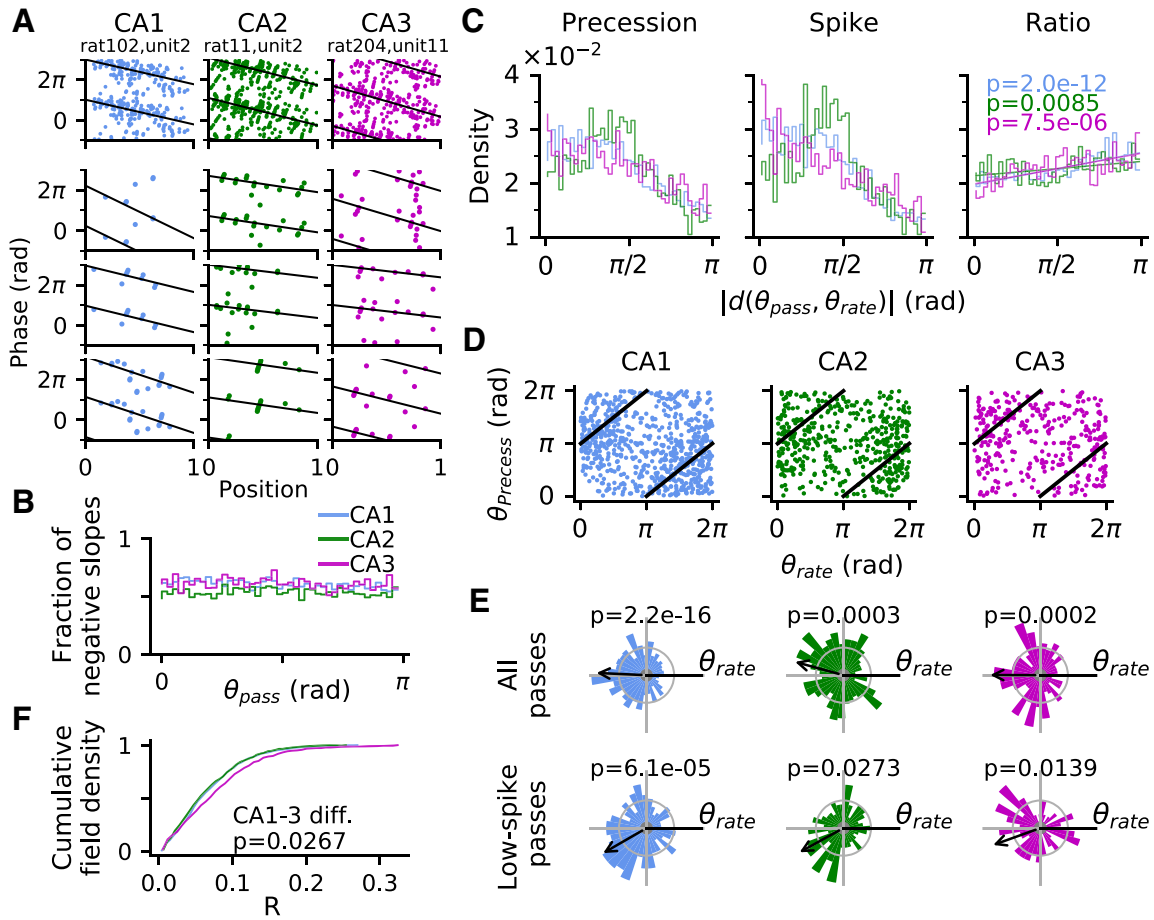
Figure 2. Phase precession per spike is most prevalent opposite to the direction of highest firing rate. ***A***, Top row, Three examples of phase precession pooled over all passes in one recording session. Position is normalized to be between 0 and 1 with respect to the moments of entering and exiting the place field. Linear-circular regression line is indicated in black, characterizing phase precession by its slope and onset phase. Bottom rows, Phase precession in example passes. Passes with slope between -2π and 0 are classified as incidents of phase precession. ***B***, Fraction of fitted negative slopes among all passes as a function of pass direction θ_{pass} for CA1, CA2, and CA3 (color as indicated) indicates a similar amount of precessing passes in all subregions. ***C***, Distribution of phase precessing passes in the whole dataset (left) mirrors the elevated spike count along the preferred rate direction θ_{rate} of the field (middle) pooled over all precessing passes as a function of absolute angular deviation $|d(\theta_{pass}, \theta_{rate})|$ from pass direction θ_{pass}. We therefore normalized the spike distribution by precession occurrences (ratio of left and middle graph) to obtain a distribution of phase precession per spike (right), which increases with angular distance $|d(\theta_{pass}, \theta_{rate})|$ (p-values from Spearman's correlations; CA1, $r_s = 0.83$; CA2, $r_s = 0.39$; CA3, $r_s = 0.62$) indicating an excess of precession at $|d(\theta_{pass}, \theta_{rate})| = \pi$ that cannot just be explained by increased firing. ***D***, The same analysis on a fieldwise level shows preferred precession directions (per spike) $\theta_{precess}$ of single fields and best firing rate direction θ_{rate} to be offset by about π (marked by black line). ***E***, Top, Same as ***D*** shown as normalized polar histograms of $\theta_{precess}$ relative to θ_{rate}. Bottom, Only low-spike passes (25th percentile) are admitted (p-values are derived from V-test vs the null hypothesis of a circular mean at π) to control for high rate bias. Arrow marks direction of the mean resultant vector of the distribution, with the best rate direction pointing to the right. ***F***, Cumulative distribution of R of all place fields in CA1, CA2, and CA3. Kruskal–Wallis test indicates strongest directionality in CA3.

direction of the field (Spearman's correlation; CA1, $r_{s(6719)} = 0.83$, $p = 2.0e - 12$; CA2, $r_{s(4837)} = 0.39$, $p = 0.0085$; CA3, $r_{s(2625)} = 0.62$, $p = 7.5e - 06$), indicating that spike rate and phase precession differentially contribute to rate directionality.

In addition to this population-wide analysis, we also identified the direction in which precession is most probable per spike for each field separately and call it the best precession angle $\theta_{precess}$. Histograms of preferred precession angles from all place fields separately (Fig. 2E, top row) also demonstrate a significant π shift from their preferred firing direction (V-test vs π direction; CA1, $V_{(731)} = 155.54$, $p = 2.2e - 16$; CA2, $V_{(466)} = 51.75$, $p = 0.0003$; CA3, $V_{(341)} = 47.12$, $p = 0.0002$). However, by comparing the R values of precessing passes to a shuffling distribution (see above, Materials and Methods, shuffling procedures), we found that only 24/829 (2.9%), 11/560 (2.0%), and 20/441 (4.5%) of place fields in CA1, CA2, and CA3, respectively, exhibit significant preferred precession direction, which is not significant under binomial tests (CA1, $p = 0.9990$; CA2, $p = 0.9999$; CA3, $p = 0.7034$). We thus conclude that although on the level of the

single field the antiphase relation between spike count and phase precession is weak and does not reach significance (and therefore has likely not been identified previously), there is a strong indication of such a relation on the population level.

To further rule out that the π shift between best rate and best precession direction might arise as an epiphenomenon of different spike counts, with the opposite of the preferred rate direction being overrepresented by the normalization process, we recomputed the histograms of preferred precession angles by limiting the passes to only those with low spike counts ($<25\%$ quantile of all precessing passes in each CA region) so that there is no firing rate directionality left in the used data. Our results show that the place fields in all CA regions still demonstrate a significant π shift from the preferred rate direction (Fig. 2E, bottom row; V-test vs π direction; CA1, $V_{(294)} = 46.58$, $p = 6.1e - 05$; CA2, $V_{(226)} = 20.44$, $p = 0.0273$; CA3, $V_{(120)} = 17.04$, $p = 0.0139$). Thus, on the population level, the direction of best phase precession displays a consistent and significant bias toward the opposite of the direction of best firing rate, corroborating the hypothesis of
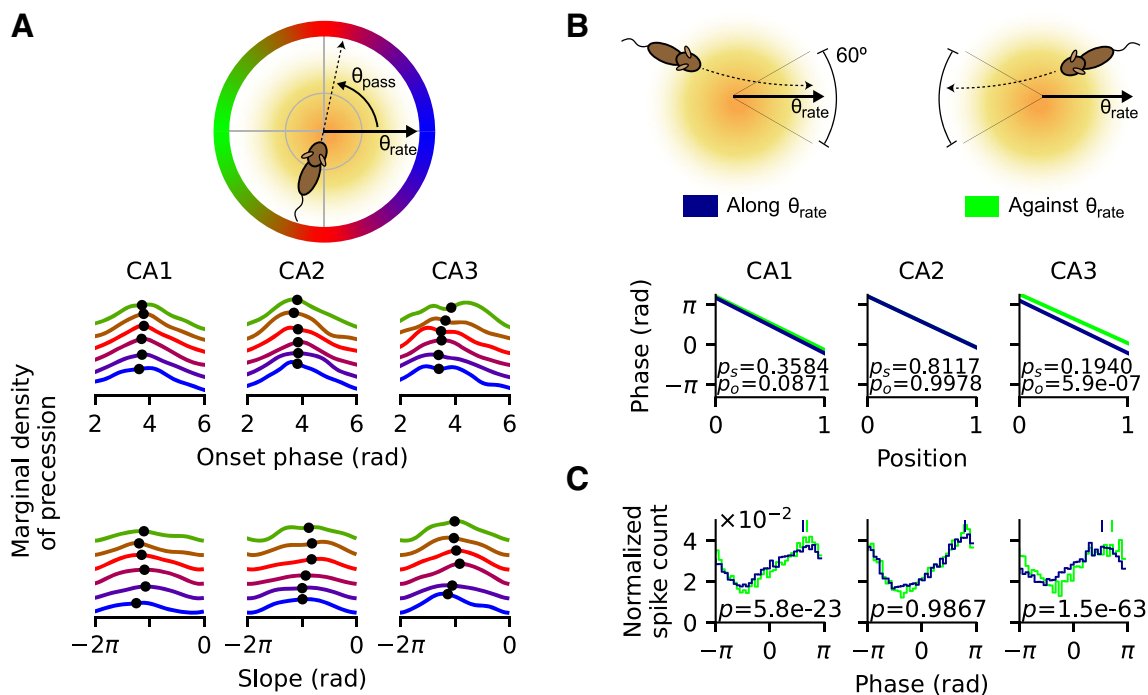
Figure 3. Directional dependence of phase precession properties. **A**, Marginal distributions of precession density as a function of onset phase and slope, color coded by the difference between pass angle θ_{pass} and best rate angle θ_{rate} (top, illustration of the color code). Black dot indicates the circular mean of marginal density. **B**, Average phase-position relations for cases where the animal is running along (blue) and against (green) θ_{rate}. Schematic illustration above. Against-θ_{rate} condition has higher onset than along-θ_{rate} condition; p_o denotes the p-value from Watson–Williams test for onset difference (along-θ_{rate} vs against-θ_{rate}, mean ± SEM in radians; CA1, 3.66 ± 0.04 vs 3.77 ± 0.05, $F_{(1,2073)} = 2.93$, $p = 0.0871$; CA2, 3.78 ± 0.04 vs 3.78 ± 0.05, $F_{(1,1301)} = 0.00$, $p = 0.9978$; CA3, 3.44 ± 0.06 vs 3.94 ± 0.07, $F_{(1,848)} = 25.34$, $p = 5.9e − 07$). There is no difference in slopes between both cases; p_s denotes the p-value from Kruskal–Wallis test for slope difference (mean ± SEM in radians per unit position; CA1, −4.62 ± 0.08 vs −4.54 ± 0.10, $H_{(1)} = 0.84$, $p = 0.3584$; CA2, −4.48 ± 0.10 versus −4.57 ± 0.13, $H_{(1)} = 0.06$, $p = 0.8117$; CA3, −4.44 ± 0.12 vs −4.20 ± 0.14, $H_{(1)} = 1.69$, $p = 0.1940$). **C**, Histograms of spike phases from precession samples show higher spike phase for passes against θ_{rate}; p-values are derived from Watson–Williams test for the difference between the circular means (shown as vertical bars) between the two cases (along-θ_{rate} vs against-θ_{rate}, mean ± SEM in radians; CA1, 3.66 ± 0.04 vs 3.77 ± 0.05, $F_{(1,2073)} = 2.93$, $p = 0.0871$; CA2, 2.50 ± 0.02 vs 2.50 ± 0.02, $F_{(1,19271)} < 0.01$, $p = 0.9867$; CA3, 1.61 ± 0.02 vs 2.22 ± 0.03, $F_{(1,17151)} = 285.63$, $p = 1.5e − 63$).

distinct coding schemes and, hence, input streams, for spike timing and rate (Huxter et al., 2003).

Finally, we also compared distributions of Rayleigh vector lengths R for phase precession tuning and found that although CA1 and CA2 seem to have similar directionality, CA3 exhibits a significantly higher directional selectivity (Fig. 2F; Kruskal–Wallis test; CA1 ($n = 753$) vs CA2 ($n = 485$) vs CA3 ($n = 363$), $H_{(2)} = 9.37$, $p = 0.0092$; post hoc Dunn's test with Benjamini–Hochberg correction; CA1 vs CA2, $p = 0.3351$; CA2 vs CA3, $p = 0.0084$; CA1 vs CA3, $p = 0.0267$), further suggesting that directional information in CA3 place field activity is distinct from CA1 and CA2.

Phase precession properties show dependence on pass direction

To further support the existence of directional effects on phase precession and to elucidate the underlying processes, we searched for directional modulations of phase precession properties by quantifying single pass onset phase and precession slope and plotted their occurrence density (Fig. 3A) for different relative pass directions $|d|$ (defined as the absolute circular difference between pass direction and preferred rate direction of the place field). Although there was no significant correlation between precession slope and $|d|$ in any CA region (CA1, $r_{(5020)} = −0.008$, $p = 0.5768$; CA2, $r_{(3514)} = 0.031$, $p = 0.0564$; CA3, $r_{(2044)} = 0.013$, $p = 0.5558$), we found that phase onsets slightly but significantly increase as the heading deviates more from the preferred rate direction in CA3 ($r_{(2625)} = 0.078$, $p = 5.4e − 05$), also, but barely

significantly, in CA1 ($r_{(6719)} = 0.024$, $p = 0.0459$), but not significantly in CA2 ($r_{(4837)} = −0.023$, $p = 0.0952$). Thus, the opposite directions of best firing rate are signified by later phases, which could reflect more prospective parts of theta sequence activity (Foster and Wilson, 2007).

For illustration, we plotted the typical characteristics of phase precession for cases when the animal runs along ($|d| < 30°$) or against ($|d| > 150°$) the preferred rate direction (θ_{rate}) by separately fitting a regression line for the phase-position relation to passes from all fields in these two cases (Fig. 3B) and found that passes aligned to the opposite of best rate direction indeed have on average a significantly higher onset of precession than those with different directions in CA3 region but not in CA1 and CA2. The average precession slopes do not differ between the two groups of passes.

The difference in onset phases between along-θ_{rate} and against-θ_{rate} passes is also corroborated by the phase histograms (Fig. 3C), where in CA1 and CA3 the against-θ_{rate} group exhibits a significant shift to later phase as compared with along-θ_{rate} group.

Thus, at least in CA3, phase precession tends to start from a higher phase when the running direction of the rat aligns with the opposite of preferred rate direction, corroborating that phase precession exhibits directional modulations.

Directional selectivity in paired place fields

Phase precession is often considered a single-cell reflection of place cell sequences during theta (Dragoi and Buzsáki, 2006;
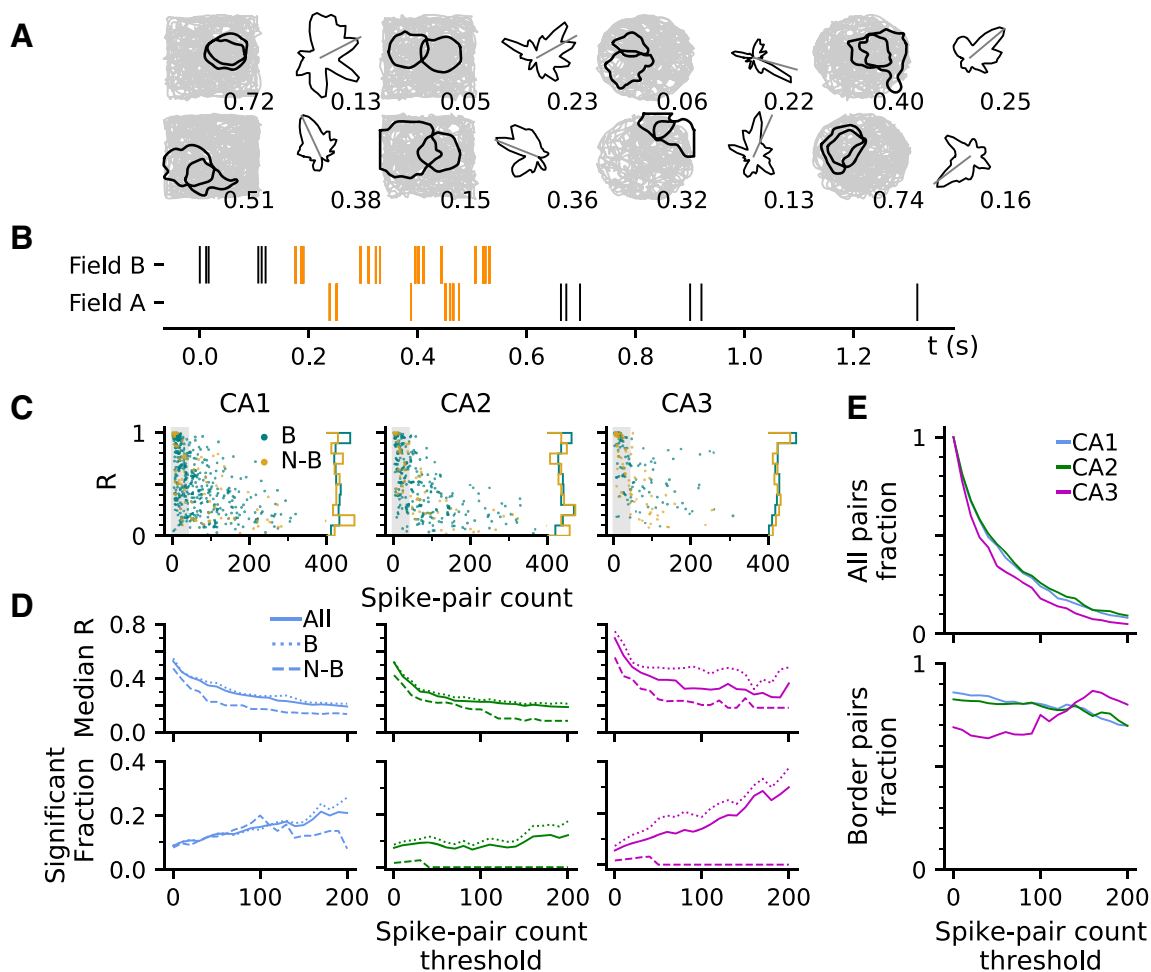
Figure 4. Pair correlations are highly directional in CA3. **A**, Examples of pairs of place fields (black contour lines) and the directional tuning curves of paired spikes. Number below the contour plot indicates the amount of field overlap (calculated as $1 - D_{ks}$, where D_{ks} is 2D Kolmogorov–Smirnov distance between two place fields). Resultant vector length (R) of the directional distribution is printed below the tuning curve. **B**, Raster plots of spike times in a pair of overlapping fields during traversal from field B to A. Admitted paired spikes with time difference <0.08 s between field A and B are in orange. **C**, R and spike-pair count for the whole populations of border and nonborder pairs in CA1, CA2, and CA3. Pairs with spike-pair counts below 40 are excluded in our statistical comparisons, indicated by the shaded region. **D**, Median R (top) and fraction of significantly directional pairs (bottom) by different spike-pair number thresholds. Spike pairs in all CA regions were significantly directional [CA1, 31/258 = 12.02% (Binomial test, $p = 6.9e - 06$); CA2, 17/181 = 9.39% ($p = 0.0097$); CA3, 9/88 = 10.23% ($p = 0.0319$)]. Comparing regions in terms of R, we found that CA3 has higher directional selectivity than CA1 [Kruskal–Wallis test; CA1 ($n = 258$) vs CA2 ($n = 181$) vs CA3 ($n = 88$), $H_{(2)} = 10.82$, $p = 0.0045$; *post hoc* Dunn's test with Benjamini–Hochberg correction; CA1 vs CA2, $p = 0.1413$; CA2 vs CA3, $p = 0.0030$; CA1 vs CA3, $p = 0.0315$]. In CA1, and different from the single spike results in Figure 1, also in CA3 directionality is induced by the proximity to the border in terms of resultant vector lengths [Kruskal–Wallis test; CA1, border ($n = 217$) vs nonborder ($n = 41$), $H_{(1)} = 4.39$, $p = 0.0361$; CA3, border ($n = 56$) versus nonborder ($n = 32$), $H_{(1)} = 9.64$, $p = 0.0019$]. **E**, Fraction of all place fields (top) and border fields (bottom) by spike-pair count thresholds.

Foster and Wilson, 2007; Feng et al., 2015; Leibold, 2020), and as such it should show up in peak lags of pair correlation functions too (Dragoi and Buzsáki, 2006; Huxter et al., 2008; Geisler et al., 2010; Schlesiger et al., 2015). In two-dimensional environments, such correlation lags have been shown to flip signs depending on the order in which a trajectory samples the place fields (Huxter et al., 2008), arguing for strong external (behavioral/sensory) drive of sequence structure. We therefore hypothesized that if phase precession reflects sequence firing, correlation lags should also be tuned to certain directions. To test our assertion, we first identified overlapping pairs of place fields (Fig. 4A) and included only spike pairs that are spaced, at most, 80 ms in time (Fig. 4B). This criterion allowed us to admit only the spike pairs that form part of a putative theta firing sequence.

Overall, directionality results are very comparable between spike pair and single spike analysis from Figure 1. We observe significant directionality in all subregions and a higher median R in CA3 (Fig. 4D; statistics in legend). Most importantly, however, directional tuning of pairs is much higher (in terms of median R) than of single

spikes (Kruskal–Wallis test for median R difference between single spikes and spike pairs at spike count threshold 40; CA1, single ($n = 800$) vs pair ($n = 258$), $H_{(1)} = 153.84$, $p = 2.5e - 35$; CA2, single ($n = 521$) vs pair ($n = 181$), $H_{(1)} = 113.50$, $p = 1.7e - 26$; CA3, single ($n = 396$) vs pair ($n = 88$), $H_{(1)} = 78.70$, $p = 7.2e - 19$), and thus we conclude that spike correlations in theta sequences induce additional directionality in line with our initial hypothesis.

Again, separating field pairs into border and nonborder, we find that pair directionality in CA3 is also border sensitive (Fig. 4, statistics in legend) in contrary to single spike directionality. Particularly, border-sensitive CA3 pairs extend to high R values even for spike-pair counts >100 (Fig. 4C). These findings suggests that border sensitivity in CA3 is specifically tied to the correlation structure, whereas in CA1 it is mostly inherited from the directional firing rates.

Directionality of pair correlation

Because the pair firing rate showed region-dependent differences, we hypothesized that these differences should also transfer
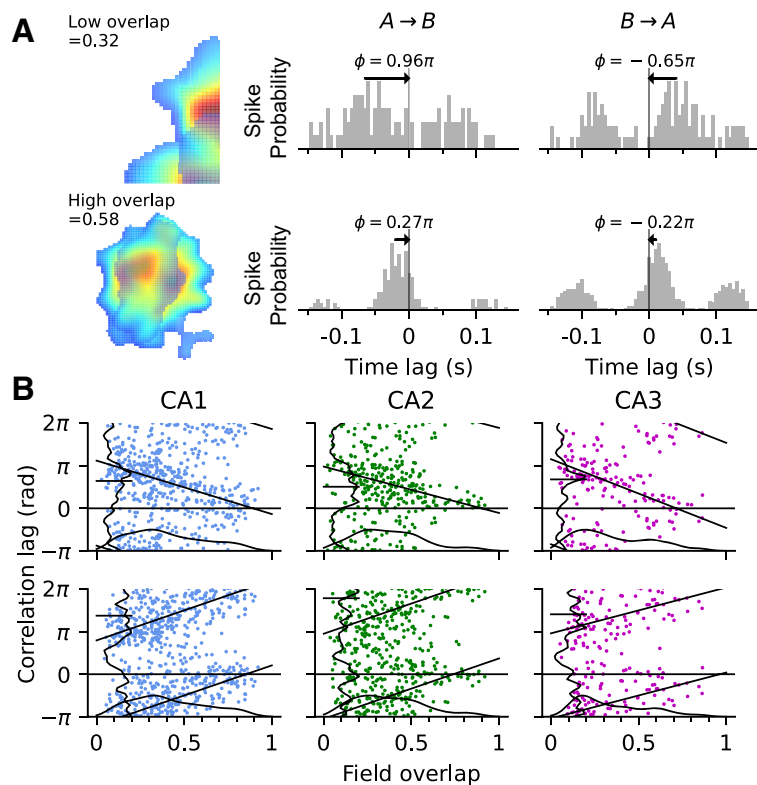
Figure 5. Strong extrinsic effect on correlation lag in all CA regions. **A**, Top row, Examples of a field pair with low overlap (left) and its cross-correlograms when the animal runs from field A to field B (middle) and in the opposite direction from B to A (right). The spike correlation lag ϕ, indicated by the distance of the closest peak to midline, generally flips sign when the direction is reversed. Bottom row, Example of a field pair with high overlap. Note that the magnitude of correlation lag is smaller than the high-overlap example. **B**, The higher the field overlap, the larger the spike correlation lag. Relation between spike correlation lags and the amount of field overlap for all pairs in CA1, CA2, and CA3 when the animal runs from field A to B (top) and from field B to A (bottom). Black straight line shows linear-circular regression line (Direction A to B, CA1, $r_{(412)} = -0.43$, $p < 1.0e - 63$; CA2, $r_{(260)} = -0.39$, $p = 2.9e - 09$; CA3, $r_{(134)} = -0.48$, $p = 6.6e - 08$; Direction B to A, CA1, $r_{(414)} = 0.49$, $p < 1.0e - 63$; CA2, $r_{(280)} = 0.17$, $p = 0.0030$; CA3, $r_{(121)} = 0.39$, $p = 1.3e - 05$). Vertical and horizontal curves are the marginal distribution of spike correlation lags and field overlap, respectively.

to spike timing correlations (Fig. 5A). Huxter et al. (2008) reported that spike correlation lags in CA1 depend on path direction and thus show a strong extrinsic (sensory/behavioral) dependence, and so we followed their approach and confirmed their main results for all three CA regions, that is, correlation lags decrease as the overlaps of the field pairs increase, and the sign of the lags flip if the path direction is reversed (Fig. 5B).

However, a closer inspection of the correlation functions reveals that they often do not have a clear single peak, and thus we devised a new approach, taking into account the symmetries of the full correlation function. Field pairs whose activities rely on intrinsic dynamics and are insensitive to sensory stimulus should show a similar shape of the correlation function regardless of reversing the path direction. In contrast, the correlation lags of extrinsic pairs should flip sign as an effect of direction reversal (Fig. 6A,C, single pass example). Based on this principle, we were able to quantify intrinsicity and extrinsicity of a pair, using the overlap of the correlation functions of both pass directions (original and flipped, extrinsicity; original and original, intrinsicity; Fig. 6B,D; also see above, Materials and Methods). Pairs with higher extrinsicity than intrinsicity are classified as extrinsic and vice versa.

The ratios of extrinsic to intrinsic field pairs in CA1 and CA2 are significantly different from the expected equality, whereas that of CA3 is not (Fig. 6E, top, one-way χ^2 test for

equal proportion of extrinsic and intrinsic pairs: CA1, 184 : 128 = 1.44, $\chi^2_{(1,312)} = 10.05$, $p = 0.0015$; CA2, 113 : 83 = 1.36, $\chi^2_{(1,196)} = 4.59$, $p = 0.0321$; CA3, 37 : 30 = 1.23, $\chi^2_{(1,67)} = 0.73$, $p = 0.3924$). As a further measure for a bias toward extrinsicity or intrinsicity that also takes into account the amount of ex(in)trinsicity, we computed their difference, and found that all regions exhibit a significant bias toward extrinsicity except in CA3 (Fig. 6E, bottom; Student's t test for extrinsicity-intrinsicity with expected value of 0; CA1, mean = 0.0434, $t_{(311)} = 5.56$, $p = 5.8e - 08$; CA2, mean = 0.0453, $t_{(195)} = 3.92$, $p = 0.0001$; CA3, mean = 0.0291, $t_{(66)} = 1.64$, $p = 0.1047$). We therefore conclude that the pair correlations in CA1 and CA2 demonstrate a strong dependence on path directionality but not significantly so in CA3.

The most parsimonious explanation for intrinsic pair correlation structure would be to assume that place cells are bound into rigid sequences that play out independent of running direction. In such a scenario, place field firing should be highly directional, and pairs with similar preferred direction should reveal more of the intrinsic correlation structure than pairs with opposite preferred direction. We thus further separated pairs into those with similar (angle difference $<90°$) and dissimilar ($>90°$) best rate angles (Fig. 6F) and found that pooling over all CA regions, the similar pairs indeed have a lower extrinsic-intrinsic ratio than dissimilar pairs (similar = 203:158 = 1.28; dissimilar = 131:83 = 1.58, Fisher's exact test; $p = 0.0353$). Resolving for the different CA regions, the effect was significant in CA1 (similar = 108:84 = 1.29, dissimilar = 76:44 = 1.73, $p = 0.0441$) and CA3 (similar = 20:23 = 0.87, dissimilar = 17:7 = 2.43, $p = 0.0333$) but not in CA2 (similar = 75:51 = 1.47, dissimilar = 38:32 = 1.19, $p = 0.0930$). Thus place field pairs with similar directional tuning may contribute more to the activation of intrinsic sequence activation at least in CA1 and CA3.

Contrary to the extrinsic pairs, the intrinsic pairs are invariant to sensory inputs and maintain their firing order even when they are reversely sampled (Fig. 6C, single pass example). A possible mechanism could be that intrinsic pairs are asymmetrically connected and bias the generation of theta sequences in one direction. We thus hypothesized that the pair correlation structure reflects two contributions, extrinsic sequences that are produced by sensory inputs and flip order with the running directions and, in addition, intrinsic sequences produced by the internal connections in a fixed order.

To dissociate the intrinsic sequences from the extrinsic ones, we focused on intrinsic pairs, and for those we separated the running trajectories into two groups; either they align with ("Same" group) or are opposite ("Opposite" group) to the intrinsic directional bias that is identified via their cross-correlation signals. A directional bias of $A \rightarrow B$ would mean the correlation signal always has a peak at negative time lag even when the animal
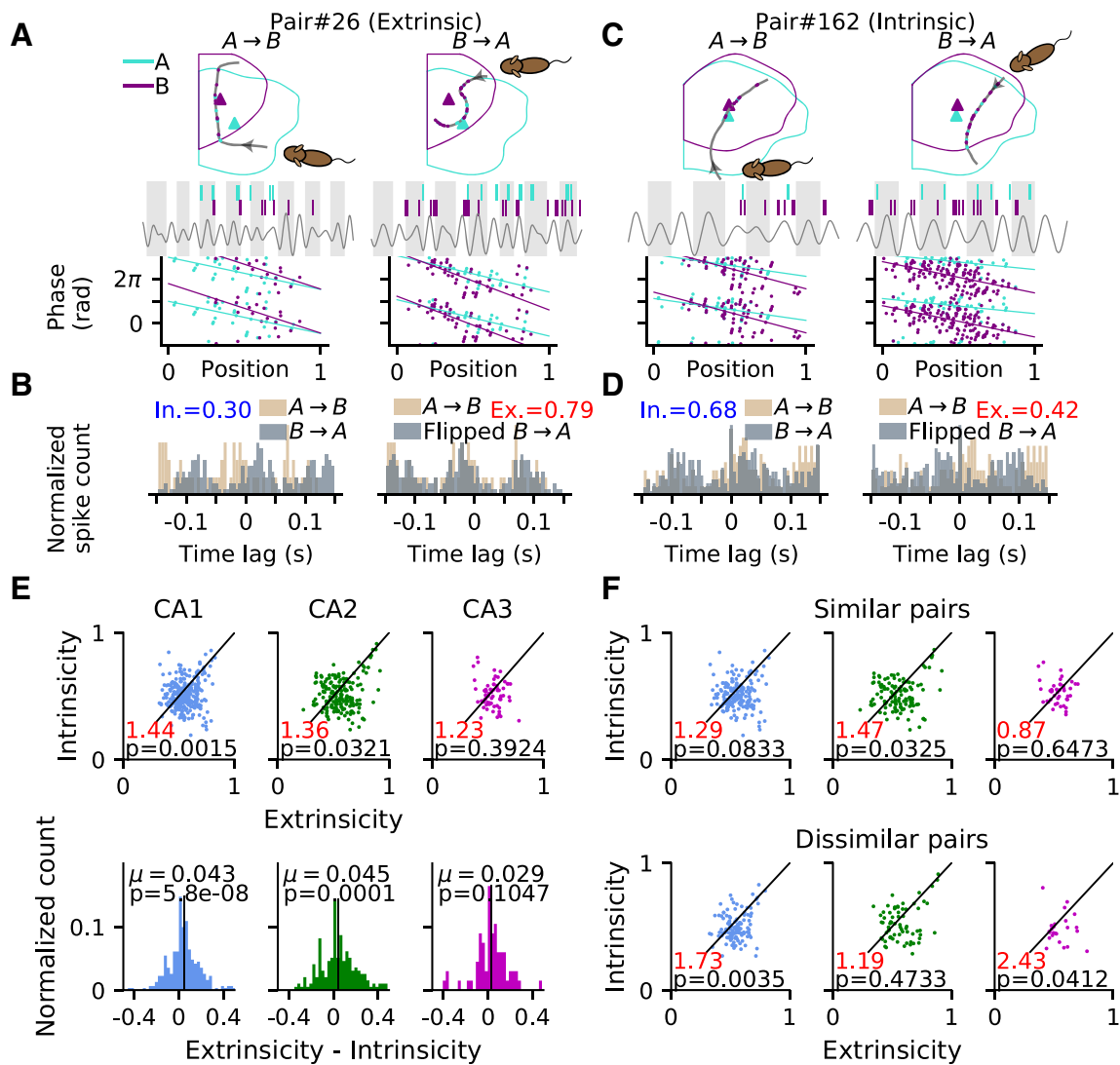
Figure 6. Place field correlations reveal region-specific extrinsic and intrinsic contributions. **A**, Top, Illustration of theta sequence from an example extrinsic pair during a single pass when the rat runs from field A to B ($A \rightarrow B$, left). Place cell A (sky blue) fires ahead of B (purple) in each theta cycle (gray and white shaded intervals). When the trajectory direction is reversed ($B \rightarrow A$, right), place cell B fires ahead of A. Bottom, Phase-position relations of spikes for the example pair in **A**, pooling from all passes in condition $A \rightarrow B$ (left) and $B \rightarrow A$ (right). **B**, Intrinsicity (blue text) is computed by Pearson's correlation (see above, Materials and Methods) between the cross-correlograms of two running directions ($A \rightarrow B$ and $B \rightarrow A$, left), whereas the computation of extrinsicity (red text) takes the cross-correlogram of $A \rightarrow B$ and flipped cross-correlogram of $B \rightarrow A$ (right). **C**, Same as **A**, but an intrinsic pair. Cell B fires ahead of A even in the direction $A \rightarrow B$. **D**, same as **B**, but with higher intrinsicity than extrinsicity. **E**, Top, Scatter plots of intrinsicity versus extrinsicity for all field pairs. The diagonal line represents the decision boundary; pairs above it are classified as intrinsic pairs and pairs below it as extrinsic pairs. Ratio of extrinsic pairs to intrinsic pairs (red number) and p-values (one-way χ^2 test) indicate significant bias toward extrinsicity for CA1. Bottom, Histograms of differences between extrinsicity and intrinsicity. Mean μ (black bar) and p-value of the t test of mean versus zero suggest a bias toward extrinsicity for all brain regions. **F**, Intrinsicity versus extrinsicity for pairs with similar (difference $<90°$, top row) and dissimilar ($>90°$, bottom row) best rate angles. Detailed statistics are reported in the text.

traverses from B to A (Fig. 7A). Similarly, a directional bias of $B \rightarrow A$ is determined by having both correlation peaks at positive time lag (Fig. 7B). In the Same passes, both extrinsic and intrinsic sequences could be present and hardly distinguishable as they have the same firing order. Whereas in the Opposite passes, the occurrence of extrinsic sequences is less, as indicated by the lack of reversal of the cross-correlation signal, and hence the theta sequences would be more representative of the underlying intrinsic firing order. Therefore, a comparison between Same and Opposite passes could reveal the difference between extrinsic and intrinsic sequences. More specifically, we asked whether phase precession, as a potential single-cell reflection of a theta sequence, would differ in onsets, slopes, and phase distributions between Same and Opposite running directions.

In line with our initial hypothesis, we found that precession is more likely to occur when passes align with the directional bias (Fig. 7C). The Same condition has a higher fraction of precession than Opposite condition in all CA regions, but only reaching significance in CA1 and CA2 (Fisher's exact test; CA1, $p = 0.001$; CA2, $p = 0.0284$; CA3, $p = 0.0550$). Considering only the precessing passes, there is no difference in precession slopes between Same and Opposite [Fig. 7E; bottom; Kruskal–Wallis test; CA1, Same ($n = 236$) vs Opposite ($n = 174$), $H_{(1)} = 0.69$, $p = 0.4048$; CA2, Same ($n = 213$) vs Opposite ($n = 164$), $H_{(1)} = 0.15$, $p = 0.7015$; CA3, Same ($n = 61$) vs Opposite ($n = 39$), $H_{(1)} = 2.52$, $p = 0.1126$], but the phase onset of precession exhibits clear regional differences. CA3 has higher phase onset when the passes are opposite to the directional bias (Fig. 7E; top, Watson–Williams test; CA3, $F_{(1,98)} = 5.24$, $p = 0.0243$), whereas such difference is not
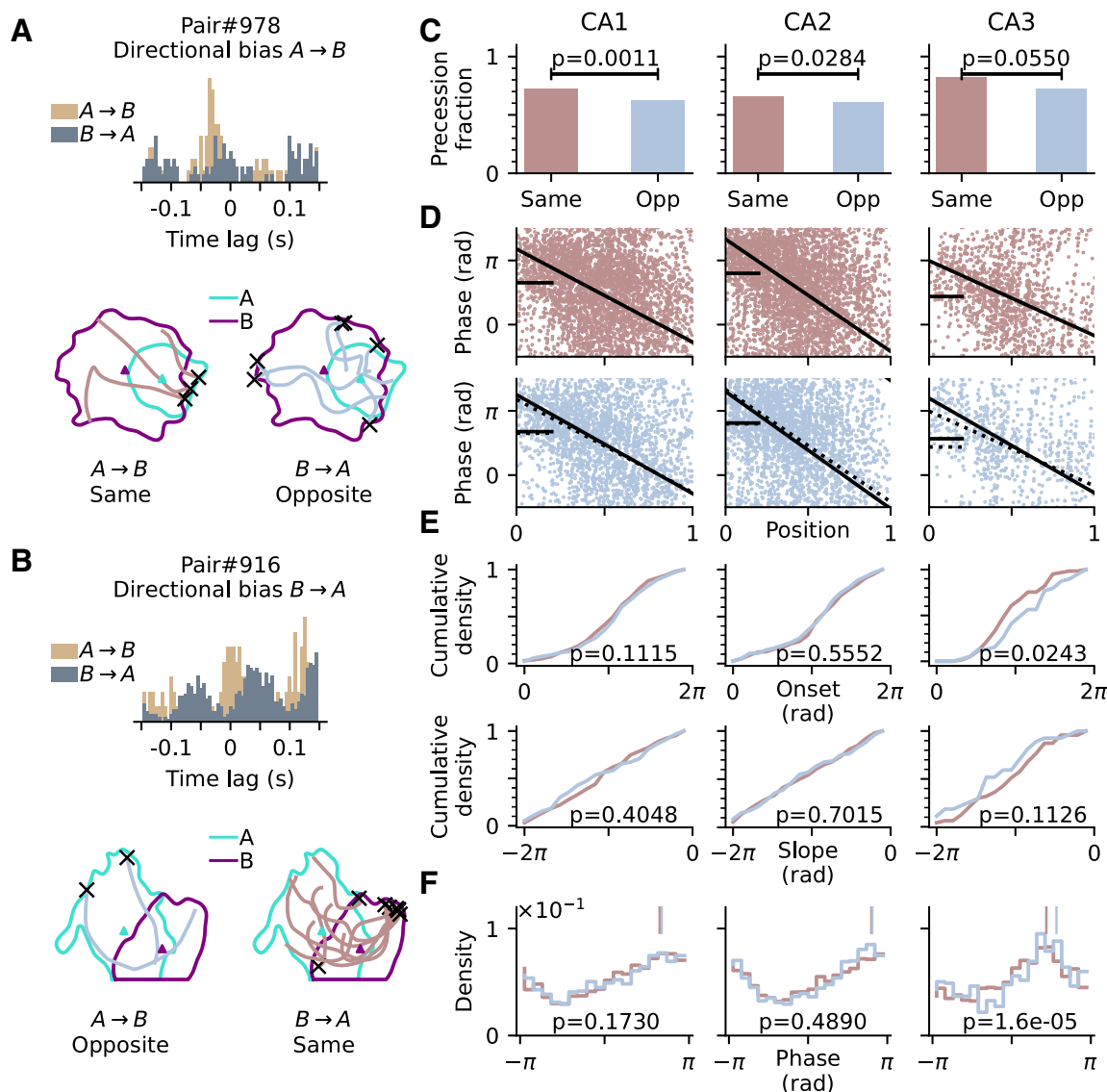
Figure 7. Prospective representation is revealed in CA3 intrinsic pairs. *A*, Top, Correlogram of an example pair with directional bias $A \rightarrow B$ (A always fires before B). Bottom, Passes that align with the directional bias $A \rightarrow B$ (left, brown, denoted as Same), and those are opposite to the directional bias (right, blue, denoted as Opposite). Origins of passes are marked as black crosses. *B*, An example pair with directional bias $B \rightarrow A$. *C*, Fraction of passes that are precessing for Same and Opposite (Opp) conditions; *p*-values are derived from Fisher's exact test. *D*, Top, Phase-position relation for all precessing Same passes. Black solid curve marks the average of all individual linear-circular fits from each precession, and black bar marks the marginal mean phase. Bottom, Same as top but for Opposite condition instead. Linear-circular fit and marginal mean phase for Same passes from the top are also shown in dashed lines here for comparison. *E*, Top, Cumulative density of onsets for all precessing Same and Opposite passes. Colors as in *C*; *p*-values are derived from Watson–Williams test for differences in onset phases. Bottom, Cumulative density of slopes; *p*-values are derived from Kruskal–Wallis test for differences in slopes. *F*, Distribution of spike phases for all precessing Same and Opposite passes; *p*-values are derived from Watson–Williams test for differences in mean phases (vertical bars). See text for detailed statistics.

significant in CA1 ($F_{(1,408)} = 2.54$, $p = 0.1115$) and CA2 ($F_{(1,375)} = 0.35$, $p = 0.5552$). Consistently, pooling the spikes from all precessing passes, the spike phase distribution from Opposite passes shows a significant shift to later phases as compared with Same passes only in CA3 (Fig. 7F; Watson–Williams test; CA3, $F_{(1,2002)} = 18.76$, $p = 1.6e - 05$) but not in CA1 ($F_{(1,6017)} = 1.86$, $p = 0.1730$) and CA2 ($F_{(1,6272)} = 0.48$, $p = 0.4890$).

According to our hypothesis that extrinsic and intrinsic sequences are played out in parallel and that intrinsic pairs result from a suppression of extrinsic sequences in one direction, the association between intrinsic sequences and later spike phases should be more strongly visible in intrinsic pairs than in extrinsic pairs. We thus also inspected the phase distributions in extrinsic pairs. Because by definition, extrinsic pairs do not have a directional bias, we resorted to compare the spike phase distributions from all precessing passes between extrinsic and intrinsic pairs,

regardless of their pass directions. The upward shift of spike phases in intrinsic sequences (if they include more intrinsic pairs), should then show up as a higher marginal spike phase than that of extrinsic pairs. Statistical analysis confirms this prediction and shows that precessing passes from intrinsic pairs indeed exhibit higher spike phases than extrinsic pairs in CA2 and CA3, but not in CA1 (Watson–Williams test, mean ± SEM in radians; CA1, Ex 2.07 ± 0.018 vs In 2.03 ± 0.026, $F_{(1,15816)} = 0.82$, $p = 0.366$; CA2, Ex 2.30 ± 0.020 vs In 2.59 ± 0.032, $F_{(1,9227)} = 45.28$, $p = 1.8e - 11$; CA3, Ex 1.20 ± 0.035 vs In 1.44 ± 0.044, $F_{(1,4232)} = 12.68$, $p = 0.0002$).

Our results support our hypothesis that intrinsic pairs display two types of sequences, extrinsic and intrinsic in the Same direction and predominantly intrinsic sequences in the Opposite direction. Trajectories Opposite to the directional bias of spike pair lags display later spike phases and higher onsets.
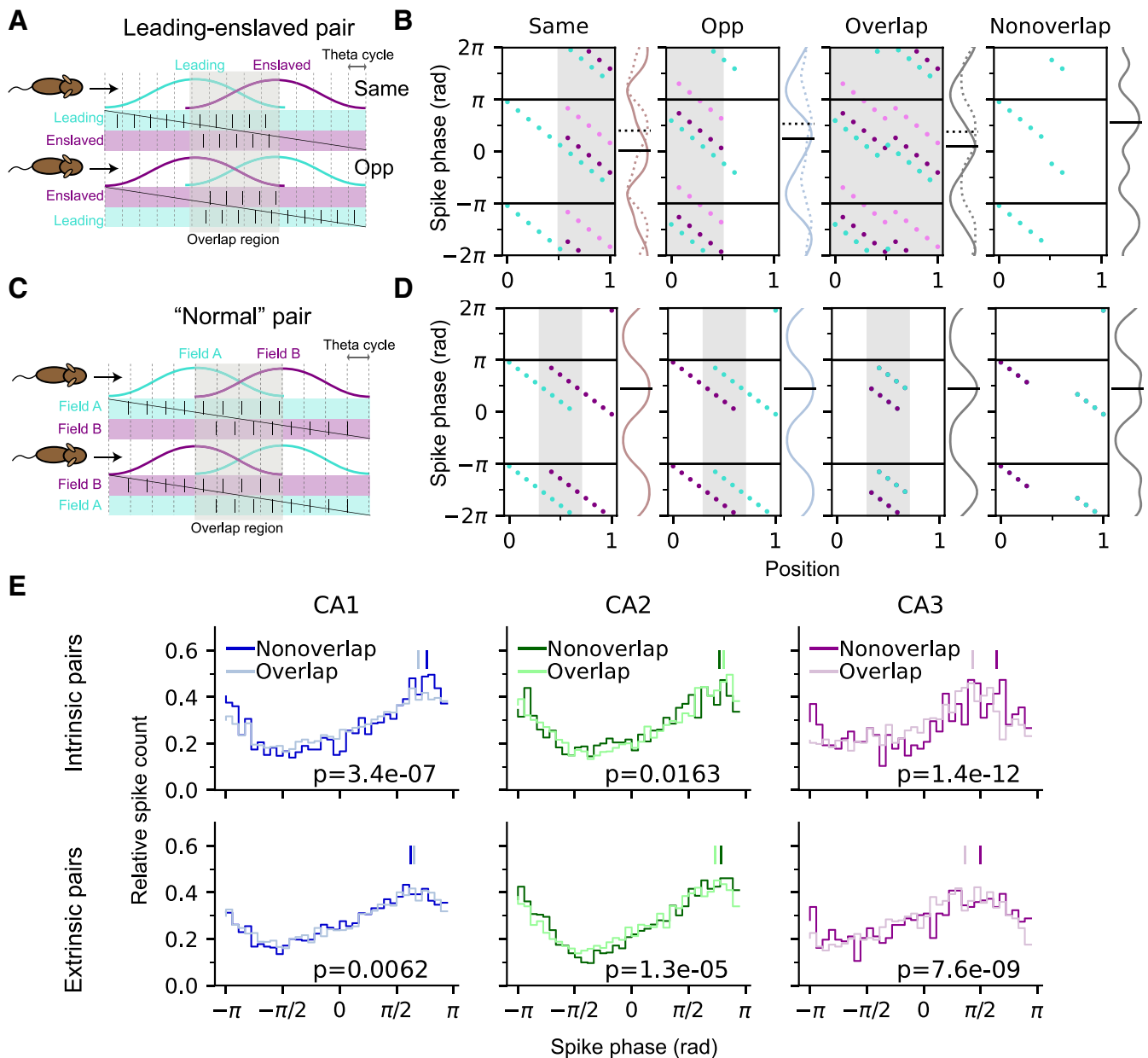
Figure 8. Co-occurrence of phase precession and intrinsic sequences. ***A***, Schematic illustration of how intrinsic sequences arise from enslaved spiking. The enslaved cells only fire at a fixed delay after the leading cell, causing a fixed temporal order even if the animal runs in the opposite (Opp) direction (bottom row). This relation predicts that enslaved cells mostly fire in the overlap region of the two place fields (shaded area). ***B***, Phase precession of leading (cyan dots) and enslaved (dark purple) cells plotted for Same, Opp, within, and outside overlap region, respectively, from left to right. Data were generated artificially for illustration purposes. Marginal distribution of spike phase (solid curve) and its circular mean (solid black bar) are shown on the right of each plot. Light violet dots and dashed lines represent an alternative dataset of enslaved spikes with larger phase shifts from the leading spikes. Note that the phase means of Opp passes and in nonoverlap regions are higher than Same and overlap, respectively. ***C***, Schematics of theta sequences produced by Normal pairs without enslaved spikes. Note that the firing order is reversed when the pair is traversed in the opposite direction and both cells fire symmetrically in the nonoverlap region. ***D***, Phase precession in normal pairs. Note that there is no difference in marginal phase means across all conditions. ***E***, Phase distribution of precession spikes in Overlap and Nonoverlap regions for intrinsic (top) and extrinsic (bottom) pairs in CA1, CA2, and CA3; *p*-values are derived from Watson–Williams test comparing the circular difference of phases between nonoverlapping regions and overlaps. CA3 shows a larger effect in the phase difference as compared with CA1 and CA2. See text for detailed statistics.

It might seem counterintuitive that when the intrinsic pairs are traversed in the opposite direction, sequences play out in a backward order, and yet there is phase precession. We therefore propose a possible explanation for the coexistence of intrinsic sequence and phase precession that is in line with our analysis results by assuming that intrinsic pairs consist of a leading cell and an enslaved cell. The enslaved cell only fires with a delay after the leading cell was active. Consequently, their correlation structure is fixed in both directions. As the leading cell undergoes phase precession, the enslaved cell fires after the precessing

spikes of the leading cell, and, hence, also precesses with a phase shift (Fig. 8A).

The first prediction of the enslavement hypothesis is that the enslaved cell only fires within the overlap region between the two fields. As a result, the Opposite condition would have a higher spike phase than the Same condition because both leading and enslaved spikes are present in the prospective cycles at the beginning of the field (Fig. 8B, left). Whereas in Normal pairs, without enslaved spikes (Fig. 8C), there would be no phase difference between Same and Opposite (Fig. 8D, left). The prediction is
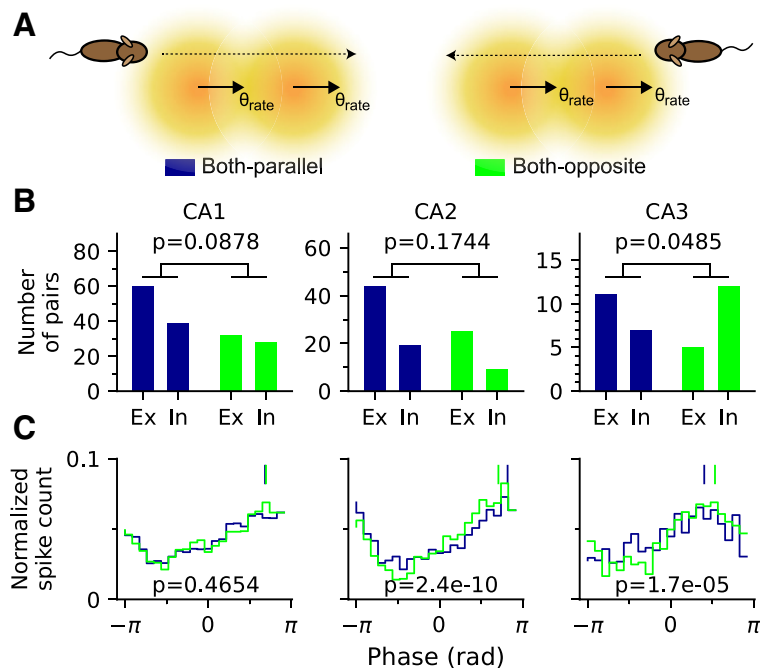
Figure 9. Field pairs in CA3 exhibit higher intrinsicity and fire at later spike phases in the direction opposite to the best rate angles. *A*, Schematic illustration of how trajectories are divided into two groups, Both-parallel (left), if trajectories across a field pair deviate $<90°$ from their best rate angles, and Both-opposite (right), if trajectories deviate $>90°$ from their best rate angles. *B*, Numbers of extrinsic and intrinsic pairs exhibiting phase precession in Both-parallel and Both-opposite cases. In CA3, there is a significantly higher contribution from intrinsic pairs in Both-opposite case than in Both-parallel case; p-values are derived from Fisher's exact test. *C*, Phase distributions of phase precessing passes. The Both-opposite case in CA3 shows a significantly later spike phase than the Both-parallel case. Vertical bars mark the circular means; p-values are derived from Watson–Williams test (Both-parallel vs Both-opposite, mean $\pm$ SEM in radians; CA1, 2.15 $\pm$ 0.0252 vs 2.18 $\pm$ 0.0369, $F_{(1,7917)} = 0.53$, $p = 0.4654$; CA2, 2.57 $\pm$ 0.0321 vs 2.22 $\pm$ 0.0369, $F_{(1,4638)} = 40.31$, $p = 2.4e-10$; CA3, 1.26 $\pm$ 0.0561 vs 1.67 $\pm$ 0.0609, $F_{(1,1841)} = 18.55$, $p = 1.7e-05$).

CA3, the phase difference has decreased as compared with its intrinsic counterpart (CA3 extrinsic, Nonoverlap 1.57 $\pm$ 0.05 vs Overlap 1.14 $\pm$ 0.04, $F_{(1,3813)} = 33.53$, $p = 7.6e-09$), whereas in CA1, there is even a higher mean phase in the Overlap region (CA1 extrinsic, Nonoverlap 1.97 $\pm$ 0.03 vs Overlap 2.06 $\pm$ 0.02, $F_{(1,17\,523)} = 7.48$, $p = 0.0062$), indicating that enslaved spiking is less involved in the extrinsic pairs.

Intrinsic sequences and phase precession are thus not contradicting each other, if we assume that one field exhibits only enslaved spikes. The existence of enslaved spikes can explain both higher spike phase in the opposite traversal direction as well as in the nonoverlap area, which are both in agreement with the data.

Relation between pair correlation and phase precession

Following up the hypothesis from Figure 8 that intrinsic pairs are resulting, at least partly, from enslaved spikes, we suggested that both phase precession and pair correlations contribute different aspects to theta sequences, as proposed previously (Middleton and McHugh, 2016). We thus finally asked whether we can identify a direct relation between the intrinsicity/extrinsicity property and the directionality of phase precession in the data to further corroborate our enslavement hypothesis. To this end, we distinguished trajectories that are either parallel ($<90°$) or opposite ($>90°$) to the best rate angles of the fields of a pair with parallel best rate directions (Fig. 9A) and included only passes with phase precession in both fields. Because the late spike phases appear to be associated with the passes opposite to the best rate angles in single fields (Fig. 2), as well as the intrinsicity in CA3 (Fig. 7), we hypothesized that the association should also transfer to field pairs. Our analyses show that indeed when the trajectories oppose both of the best rate angles, there is a higher proportion of intrinsic pairs contributing to phase precession (Fig. 9B) and a higher marginal spike phase of co-occurring phase precession in CA3 (Fig. 9C) than in the case when the trajectory runs in parallel to both best rate angles. These directional differences are not observed in CA1 pairs. CA2, surprisingly, shows the opposite trend that higher spike phases are more associated with the best rate direction, but there is no difference between the contributions of extrinsic and intrinsic pairs. The findings on CA3 corroborate that both correlation structure and phase precession are direction dependent in CA3, where the intrinsic field pairs seem to lack strong extrinsic drive in one running direction and thus would exhibit enslaved spikes at later spike phases when the running direction opposes their best rate direction. In extrinsic pairs the extrinsic drive seems strong in all running directions to overrule the intrinsic structure and allows cells to fire at earlier phases.

compatible with our experimental findings in Figure 7, where the marginal phase mean and onset in the Opposite condition are higher than in the Same condition, indicating a possible contribution of enslaved spikes to the intrinsic structure of CA3.

Another assumption in the enslavement hypothesis illustrated in Figure 8 is that the precession of leading cells in the Opposite condition would start at a lower onset and last for a shorter number of cycles than in Same because of the diminished forward recurrent connection when the pair is traversed in the opposite order. It would lead to the second prediction that the mean phase in the region where place fields are nonoverlapping should be higher than within the field overlap (Fig. 8B, far right). On the contrary, the "Normal" pairs would show no phase difference between overlap and nonoverlap regions as phase precession is symmetrical in both directions (Fig. 8D, far right).

The prediction of higher overlap phase in nonoverlap regions from the enslavement hypothesis can be tested by comparing the phase distributions between overlap and nonoverlap regions in the experimental data (Fig. 8E, top row). We found that in CA3 intrinsic pairs, nonoverlap spiking indeed has a higher mean phase than in the overlap (mean $\pm$ SEM in radians; Nonoverlap 2.02 $\pm$ 0.07 vs Overlap 1.35 $\pm$ 0.04, Watson–Williams test, $F_{(1,2745)} = 50.69$, $p = 1.4e-12$). A similar trend is also observed in CA1 intrinsic pairs, but the difference is smaller than in CA3 (Nonoverlap 2.41 $\pm$ 0.03 vs Overlap 2.18 $\pm$ 0.02, $F_{(1,9905)} = 26.03$, $p = 3.4e-07$). These results support that in CA1 and CA3, the intrinsic structure is generated by enslaved spikes. As a control, we also inspected the nonoverlap-overlap phase differences in the extrinsic populations (Fig. 8E, bottom row). In

Computational model as control
To further corroborate that the observed directionality effects in place field activity are not just an artifact of running trajectories or data analysis, we applied our analysis to simulations of a

**Figure 10.** Simulation results using the model by Romani and Tsodyks (2015). **A**, Directionality of simulated single fields. Median R (left) and fraction of significantly (Sig. Frac.) directional place fields (middle) by spike count thresholds for all (solid line), border (dotted), and nonborder (dashed) fields. Right, the fraction of all border and nonborder place fields by spike count thresholds. Frac., Fraction. **B**, Distribution of precession incidences (dark blue) and spikes (orange) as a function of $|d(\theta_{pass}, \theta_{rate})|$, the difference between pass direction and best rate direction of the place field. Ratio of blue and orange line in green shows no significant trend (Spearman's correlation, $r_{s(1386)} = -0.27$, $p = 0.0710$). **C**, Scatter plot for the relation between best precession angle $\theta_{precess}$ and rate angle θ_{rate} of all place fields reveals no obvious structures. **D**, Distribution of $\theta_{precess}$ directions of all precessing passes corrected to θ_{rate} shows no significant 180° difference of two best angles. **E**, Distribution of $\theta_{precess}$ directions of low-spike passes. **F**, Average precession slopes (phase-position curves) from precession samples against (green) and along θ_{rate} (blue); p_s and p_o are derived from Kruskal–Wallis test for slope difference and Watson–Williams test for onset difference respectively. **G**, Distribution of spike phases for precession samples against and along θ_{rate}. Vertical bars denote the circular means of the distributions; p-value is derived from Watson–Williams test comparing the difference of two circular means. Detailed statistics are reported in the text.

spiking model that does not include directional information as input (Romani and Tsodyks, 2015) but can be fed with the animal trajectories of our experiments (see above, Materials and Methods for simulation details). In brief, the model neurons integrate place-specific inputs, theta-periodic inputs, and symmetric recurrent connections with short-term synaptic depression. The recurrent connections give rise to omnidirectional phase precession but, because of their symmetry, do not impose preferred intrinsic sequential activity. Also, because the place-specific inputs are not directionally modulated, we reasoned that any directionality and any intrinsicity we find in the model must be artificial. Indeed, as expected, directionality analyses on the single field firing rates showed that the fraction of significantly directional simulated place fields does not exceed chance level of 5% (61/1024 = 5.96%, $p = 0.0936$, Binomial test; Fig. 10A). Similarly, by pooling over all fields again, we did not find a significant correlation of phase precession per spike with the distance to preferred rate direction (Fig. 10B; Spearman's correlation coefficient $r_{s(1386)} = -0.27$, $p = 0.0710$). A further inspection on the distribution of preferred precession angles on a single field basis did not reveal a significant π shift with respect to the preferred rate angles (Fig. 10D; V-test against π; for all passes, $V_{(383)} = -26.21$, $p = 0.9709$; Fig. 10E; for low-spike passes, $V_{(174)} = -30.61$, $p = 0.9995$). After again separating the passes into groups of against-θ_{rate} ($n = 105$) and along-θ_{rate} ($n = 361$), with >150°

and <30° angular difference in radians from the best rate angles, respectively (Fig. 10F), we consistently found no significant difference of their average precession curves (Kruskal–Wallis test for difference in slopes; $H_{(1)} = 0.09$, $p = 0.7591$; Watson–Williams test for difference in onsets; $F_{(1464)} = 0.01$, $p = 0.9415$), and there was also no significant difference in the means of spike phases between groups against-θ_{rate} and along-θ_{rate} (Watson–Williams test; $F_{(1,7639)} = 2.78$, $p = 0.0953$; Fig. 10G). Thus, as expected by model design, properties of phase precession in the model generally do not show a significant dependence on the heading directions of the animal.

A virtue of the investigated Romani and Tsodyks (2015) model is that it contains recurrent synaptic connections, and we asked to what extent they might explain intrinsic correlation structure observed in the data. We thus repeated directionality analysis at the level of field pairs on the simulated data. Similar to the single field results, the fraction of significantly directional pairs never exceed chance level in the model (169/3197 = 5.29%, $p = 0.2394$, Binomial test; Fig. 11A); however, the dependence of correlation lags on place field distance can be well reproduced (Fig. 11B), demonstrating that phase precession induces direction-dependent sequential firing of model place fields.

We next computed extrinsicity and intrinsicity of the model correlations and found a fraction of extrinsic pairs similar to CA1 (Fig. 11C; Ex:In = 1313:851 = 1.54; one-way
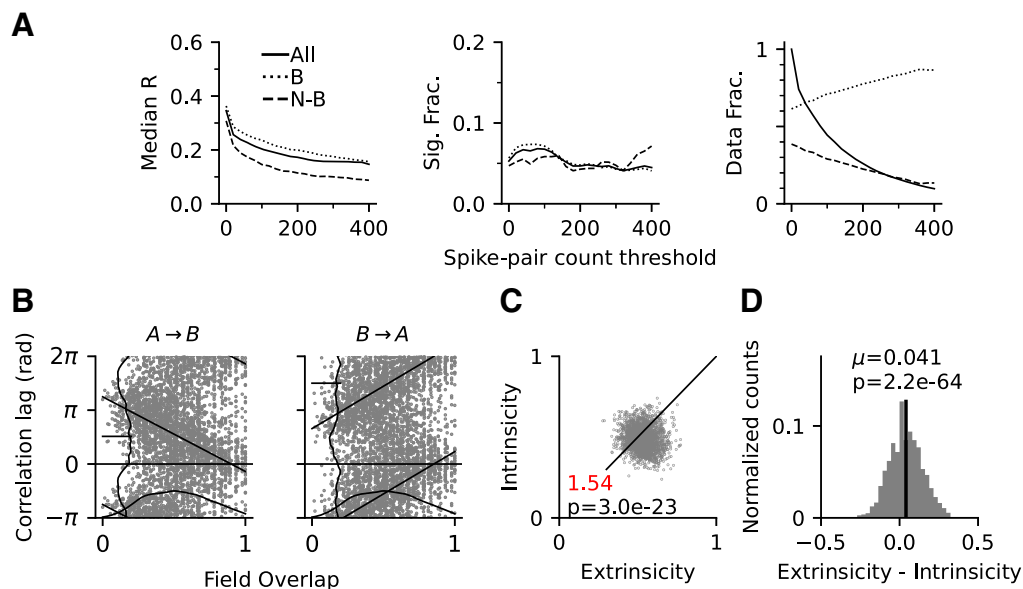
Figure 11. Directionality of pair correlations in model simulations. *A*, Median *R* (left) and fraction of significantly directional pairs (middle) by spike count thresholds for all (solid line), border (dotted), and nonborder (dashed) pairs. Right, Fraction of all, border, and nonborder field pairs. *B*, Relation of spike correlation lags and field overlap of all pairs for direction $A \rightarrow B$ (left) and $B \rightarrow A$ (right). Linear-circular regression line is in black ($A \rightarrow B$, $r_{(2659)} = -0.38$, $p < 1.0e -90$; $B \rightarrow A$, $r_{(2663)} = 0.35$, $p < 1.0e - 90$). Vertical and horizontal curves show the marginal distributions. *C*, Intrinsicity versus extrinsicity for all pairs (one-way χ^2 test of equal extrinsic-intrinsic ratio). *D*, Density of differences between extrinsicity and intrinsicity (mean μ, black bar; *p*-value from Student's *t* test of mean vs 0) show a significant trend toward extrinsicity.

χ^2 test for equal proportion of extrinsic and intrinsic pairs; $\chi^2_{(1,2164)} = 98.63, p = 3.0e - 23$) as well as the bias to extrinsicity (Fig. 11*D*; Student's *t* test for extrinsicity-intrinsicity with expected value of 0; mean = 0.0409, $t_{(2163)} = 17.52$, $p = 2.2e - 64$), suggesting that the balance between spatial inputs and recurrent connections in the Romani and Tsodyks (2015) model has an extrinsic bias most similar to CA1.

To conclude, although a network model with asymmetric weight couplings can reproduce the results of phase precession and correlation lags in a two-dimensional environment including the extrinsic bias prominently observed in CA1 ensembles, further extension is still required to account for directional selectivity in place field networks and their effect on phase precession, specifically on the onset phase, and the less extrinsic dynamics of CA3.

Discussion

We showed that theta-scale timing of place cell activity in all regions of the hippocampus proper exhibits directional modulations. This first applies to phase precession, which is most prominent (per spike) in the direction opposite to the one with the largest firing rate, and this effect is more prevalent and acute in CA3 than in CA1 and CA2. In addition, best precession tuning in CA3 is associated with higher onset phases. Second, by inspecting directionality of spike pairs from two overlapping place fields, we showed that pair correlation exhibits higher directionality than single spikes from individual place fields. Furthermore, using cross-correlation analysis, we demonstrated that CA1 pair correlations are better explained by external sensory inputs induced by overt movement than CA3 pairs. This suggests that CA3 place field correlations are more strongly intrinsically determined. In addition, a closer inspection into the intrinsic pairs revealed that the intrinsic sequences, which are invariant to the sampling order of place fields, are also associated with higher onset and spike phases in CA3 phase precession.

Finally, we used the model by Romani and Tsodyks (2015) and showed that the interaction between directionality and theta activity (described above, Results) cannot be solely explained by an omnidirectional generation mechanism of theta sequences. Nonetheless, the model shares a similar dependence on extrinsic information, thus being more analogous to CA1 rather than CA3.

The directionality of place field firing in 2 d open environments has a long history of debate. Although classical studies on the influence of landmark cues (Kubie and Muller, 1991), as well as early modeling work (Touretzky and Redish, 1996), clearly acknowledge the availability of directional information to the place cell system, there was disagreement about the degree to which this information becomes overt in place field activity (Muller et al., 1994; Anderson et al., 2006; Acharya et al., 2016). In the present study, we have found 10−20% of significantly directional place fields, which is similar to previous reports (Markus et al., 1995; Acharya et al., 2016; Mankin et al., 2019), although directionality seems to strongly depend on the behavioral setting. Markus et al. (1995) found 80% of place cells with significant directionality in eight-arm mazes and 20% in an open circular platform. Acharya et al. (2016) also showed that the significant fraction of heading-direction modulated cells could vary as a function of the width of visual cue on the wall as more place cells were head-direction modulated near the border.

Most interestingly, and consistent with these previous reports, our analysis revealed that directionality of CA1 in familiar environments is heavily induced by proximity to the border, even at a high spike count threshold where the sampling bias is relatively small. However, this border effect is less prominent in simultaneously recorded CA3 place cells. One possible explanation is that there is no border-related directionality in novel environments but develops via learning processes, which is more difficult and, hence, slower in CA3 because of its recurrence. This idea has been suggested in a previous modeling study from Brunel and Trullier (1998), which demonstrated that place cells become less directionally selective through synaptic plasticity when they are

visited in all directions (as in the nonborder case) as compared with the border case when fields are visited only in a subset of directions. Also a second model by Navratilova et al. (2012) suggested that the firing rate of place cells is initially independent of directions but develops to be directionally selective through experience and synaptic plasticity. Assuming that the same learning mechanism further differentiates between border and nonborder directionality, the border difference would thus develop slower in CA3 because of its larger degree of recurrent connectivity. Both models support the idea that the differential directionality between border and nonborder cells in familiar environments could be explained via plasticity induced by early experiences in novel environments. Our finding, however, that borders induce strong directionality of CA3 spike pairs (Fig. 4), questions the assumption of these models that directionality is learned but rather supports the idea that CA3 pair directionality reflects the directional imbalance of extrinsic and intrinsic activity (Fig. 8).

The main conjecture of the present work was that inherent network dynamics could induce directionality of place cell spike timing. Through multiple lines of analysis, we repeatedly found that in our dataset, CA3 exhibits more hints to intrinsic dynamics than CA1. This was, for example, suggested by their theta-scale correlations being more invariant to the trajectory. These findings are very much in accordance with anatomy. Pyramidal cells in CA3 project extensive recurrent collaterals in rodents and primates (Amaral et al., 1984; Anderson et al., 2006), whereas such recurrence is not so much obvious in the CA1 region (but see Deuchars and Thomson, 1996, for rodents). However, a further possibility to explain CA3 bias toward intrinsic dynamics could be its unique position in the mammalian hippocampal-entorhinal circuitry. Sensory information from entorhinal cortex layer II is projected to CA3 not only via the direct perforant pathway but also via mossy fiber pathway of dentate gyrus (DG), contributing to an extra layer of internal processing through the granule and mossy cell loop. Indeed, CA3 activity in rats with DG lesions showed reduced prospective firing in an eight-arm maze (Sasaki et al., 2018), which is strikingly consistent with our observed direction dependence of theta onset phases. The anatomic consistency of the enthorinal-hippocampal formation across mammals, as well as consistent reports on hippocampal phase precession in several mammalian species including *Chiroptera* (Eliav et al., 2018) and primates (Qasim et al., 2021), let us speculate that the bias toward stronger intrinsic sequences in CA3 is a common feature within this animal class as a whole and specifically also expected to be seen for primates and humans despite their less precise spatial firing patterns (Ekstrom et al., 2003).

The directional selectivity of phase precession provides widespread support of our initial hypothesis that directional information should also express itself in hippocampal theta sequences, yet the anatomic foundations of this directional modulation can only be speculated on so far. One possible explanation would be to assume that it is the direct entorhinal inputs to CA3 that induce the directional dependence of firing rate, which would be consistent with directional drive from postsubiculum and entorhinal head direction and conjunctive cells (Sargolini et al., 2006). According to Figures 2D and 7, this input would be reduced in passes opposite to best rate directions. Consequently, intrinsic CA3 activity would then mostly be explained by the indirect DG mossy fiber pathway, which was shown to induce prospective out-of-field spiking (Sasaki et al., 2018), potentially indicating enslaved spikes. In the best rate direction, according to our hypothesis, strong direct entorhinal input should induce

earlier theta spike phases in addition to the DG-induced theta sequences. Conversely, against the best rate direction, DG-induced theta sequences would still play out invariantly despite the weaker entorhinal directional drive. In such a scenario, we would predict that intrinsic pairs would dominate phase precession properties over those extrinsically induced. A direct test of these predictions is provided in Figure 9. Although the outcomes are consistent with our predictions, the conclusiveness is limited because of small sample sizes, particularly in CA3. Yet the above hypotheses could be tested even more directly by acute differential suppression of entorhinal and DG pathways, which we would predict to selectively alter phase precession in the different running directions.

Intrinsic hippocampal correlations are incompatible with the interpretation of the hippocampus as a pure spatial map but rather imply the existence of prestructure (Dragoi and Tonegawa, 2011). The degree to which intrinsic activity is expressed in familiar environments is, however, relatively small and clearly visible only in CA3, thus arguing for a relatively small role of intrinsic structure in supporting spatial navigation in familiar environments. The situation in novel environments, however, might be different with a stronger effect of prestructure on organizing hippocampal representations. This is in line with the finding that theta sequences only develop with time (Feng et al., 2015) as initially some pairs may predominantly fire in the wrong intrinsic order. The idea —contrary to the models of Brunel and Trullier (1998) and Navratilova et al. (2012)—that directional invariance develops in an experience-dependent way on top of prestructured sequences has important implications for theories of spatial memory formation because it would favor the notion of sensory integration into existing temporal structure (cf. Buzsáki and Tingley, 2018; Leibold, 2020).

References

Acharya L, Aghajan ZM, Vuong C, Moore JJ, Mehta MR (2016) Causal influence of visual cues on hippocampal directional selectivity. Cell 164:197–207.

Amaral DG, Insausti R, Cowan WM (1984) The commissural connections of the monkey hippocampal formation. J Comp Neurol 224:307–336.

Amaral DG, Witter MP (1989) The three-dimensional organization of the hippocampal formation: a review of anatomical data. Neuroscience 31:571–591.

Anderson P, Morris R, Amaral D, Bliss T, O'Keefe J (2006) The hippocampus book. New York: Oxford UP.

Benjamini Y, Hochberg Y (1995) Controlling the false discovery rate: a practical and powerful approach to multiple testing. J Roy Stat Soc B Met 57:289–300.

Brunel N, Trullier O (1998) Plasticity of directional place fields in a model of rodent CA3. Hippocampus 8:651–665.

Buzsáki G, Tingley D (2018) Space and time: the hippocampus as a sequence generator. Trends Cogn Sci 22:853–869.

Cacucci F, Lever C, Wills TJ, Burgess N, O'Keefe J (2004) Theta-modulated place-by-direction cells in the hippocampal formation in the rat. J Neurosci 24:8265–8277.

Deuchars J, Thomson AM (1996) CA1 pyramid-pyramid connections in rat hippocampus *in vitro*: dual intracellular recordings with biocytin filling. Neuroscience 74:1009–1018.

Dragoi G, Buzsáki G (2006) Temporal encoding of place sequences by hippocampal cell assemblies. Neuron 50:145–157.

Dragoi G, Tonegawa S (2011) Preplay of future place cell sequences by hippocampal cellular assemblies. Nature 469:397–401.

Ekstrom AD, Kahana MJ, Caplan JB, Fields TA, Isham EA, Newman EL, Fried I (2003) Cellular networks underlying human spatial navigation. Nature 425:184–188.

Eliav T, Geva-Sagiv M, Yartsev MM, Finkelstein A, Rubin A, Las L, Ulanovsky N (2018) Nonoscillatory phase coding and synchronization in the bat hippocampal formation. Cell 175:1119–1130.

Feng T, Silva D, Foster DJ (2015) Dissociation between the experience-dependent development of hippocampal theta sequences and single-trial phase precession. J Neurosci 35:4890–4902.

Foster DJ, Wilson MA (2007) Hippocampal theta sequences. Hippocampus 17:1093–1099.

Geisler C, Diba K, Pastalkova E, Mizuseki K, Royer S, Buzsáki G (2010) Temporal delays among place cells determine the frequency of population theta oscillations in the hippocampus. Proc Natl Acad Sci U S A 107:7957–7962.

Giocomo LM, Stensola T, Bonnevie T, Van Cauter T, Moser MB, Moser EI (2014) Topography of head direction cells in medial entorhinal cortex. Curr Biol 24:252–262.

Harris CR, Millman KJ, van der Walt SJ, Gommers R, Virtanen P, Cournapeau D, Wieser E, Taylor J, Berg S, Smith NJ, Kern R, Picus M, Hoyer S, van Kerkwijk MH, Brett M, Haldane A, del Río JF, Wiebe M, Peterson P, Gérard-Marchant P, et al. (2020) Array programming with NumPy. Nature 585:357–362.

Harris KD, Henze DA, Hirase H, Leinekugel X, Dragoi G, Czurko A, Buzsáki G (2002) Spike train dynamics predicts theta-related phase precession in hippocampal pyramidal cells. Nature 417:738–741.

Huxter J, Burgess N, O'Keefe J (2003) Independent rate and temporal coding in hippocampal pyramidal cells. Nature 425:828–832.

Huxter JR, Senior TJ, Allen K, Csicsvari J (2008) Theta phase-specific codes for two-dimensional position, trajectory and heading in the hippocampus. Nat Neurosci 11:587–594.

Ishizuka N, Weber J, Amaral DG (1990) Organization of intrahippocampal projections originating from CA3 pyramidal cells in the rat. J Comp Neurol 295:580–623.

Jaramillo J, Kempter R (2017) Phase precession: a neural code underlying episodic memory? Curr Opin Neurobiol 43:130–138.

Kempter R, Leibold C, Buzsáki G, Diba K, Schmidt R (2012) Quantifying circular–linear associations: hippocampal phase precession. J Neurosci Methods 207:113–124.

Kubie JL, Muller RU (1991) Multiple representations in the hippocampus. Hippocampus 1:240–242.

Lee I, Yoganarasimha D, Rao G, Knierim JJ (2004) Comparison of population coherence of place cells in hippocampal subfields CA1 and CA3. Nature 430:456–459.

Leibold C (2020) A model for navigation in unknown environments based on a reservoir of hippocampal sequences. Neural Netw 124:328–342.

Leutgeb S, Ragozzino KE, Mizumori SJ (2000) Convergence of head direction and place information in the CA1 region of hippocampus. Neuroscience 100:11–19.

Leutgeb S, Leutgeb JK, Treves A, Moser MB, Moser EI (2004) Distinct ensemble codes in hippocampal areas CA3 and CA1. Science 305:1295–1298.

Mankin EA, Sparks FT, Slayyeh B, Sutherland RJ, Leutgeb S, Leutgeb JK (2012) Neuronal code for extended time in the hippocampus. Proc Natl Acad Sci U S A 109:19462–19467.

Mankin EA, Diehl GW, Sparks FT, Leutgeb S, Leutgeb JK (2015) Hippocampal CA2 activity patterns change over time to a larger extent than between spatial contexts. Neuron 85:190–201.

Mankin EA, Thurley K, Chenani A, Haas OV, Debs L, Henke J, Galinato M, Leutgeb JK, Leutgeb S, Leibold C (2019) The hippocampal code for space in Mongolian gerbils. Hippocampus 29:787–801.

Markus EJ, Qin YL, Leonard B, Skaggs WE, McNaughton BL, Barnes CA (1995) Interactions between location and task affect the spatial and directional firing of hippocampal neurons. J Neurosci 15:7079–7094.

Melamed O, Gerstner W, Maass W, Tsodyks M, Markram H (2004) Coding and learning of behavioral sequences. Trends Neurosci 27:11–14.

Middleton SJ, McHugh TJ (2016) Silencing CA3 disrupts temporal coding in the CA1 ensemble. Nat Neurosci 19:945–951.

Mizuseki K, Royer S, Diba K, Buzsáki G (2012) Activity dynamics and behavioral correlates of CA3 and CA1 hippocampal pyramidal neurons. Hippocampus 22:1659–1680.

Morris RG, Garrud P, Rawlins JN, O'Keefe J (1982) Place navigation impaired in rats with hippocampal lesions. Nature 297:681–683.

Moser E, Moser MB, Andersen P (1993) Spatial learning impairment parallels the magnitude of dorsal hippocampal lesions, but is hardly present following ventral lesions. J Neurosci 13:3916–3925.

Muller RU, Bostock E, Taube JS, Kubie JL (1994) On the directional firing properties of hippocampal place cells. J Neurosci 14:7235–7251.

Nakazawa K, Quirk MC, Chitwood RA, Watanabe M, Yeckel MF, Sun LD, Kato A, Carr CA, Johnston D, Wilson MA, Tonegawa S (2002) Requirement for hippocampal CA3 NMDA receptors in associative memory recall. Science 297:211–218.

Navratilova Z, Hoang LT, Schwindel CD, Tatsuno M, McNaughton BL (2012) Experience-dependent firing rate remapping generates directional selectivity in hippocampal place cells. Front Neural Circuits 6:6.

O'Keefe J, Dostrovsky J (1971) The hippocampus as a spatial map. Preliminary evidence from unit activity in the freely-moving rat. Brain Res 34:171–175.

O'Keefe J, Recce ML (1993) Phase relationship between hippocampal place units and the EEG theta rhythm. Hippocampus 3:317–330.

Philipp B (2009) Circstat: a MATLAB toolbox for circular statistics. J Stat Softw 31: 1–21.

Qasim SE, Fried I, Jacobs J (2021) Phase precession in the human hippocampus and entorhinal cortex. Cell 184:3242–3255.

Romani S, Tsodyks M (2015) Short-term plasticity based network model of place cells dynamics. Hippocampus 25:94–105.

Sargolini F, Fyhn M, Hafting T, McNaughton BL, Witter MP, Moser MB, Moser EI (2006) Conjunctive representation of position, direction, and velocity in entorhinal cortex. Science 312:758–762.

Sasaki T, Piatti VC, Hwaun E, Ahmadi S, Lisman JE, Leutgeb S, Leutgeb JK (2018) Dentate network activity is necessary for spatial working memory by supporting CA3 sharp-wave ripple generation and prospective firing of CA3 neurons. Nat Neurosci 21:258–269.

Schlesiger MI, Cannova CC, Boublil BL, Hales JB, Mankin EA, Brandon MP, Leutgeb JK, Leibold C, Leutgeb S (2015) The medial entorhinal cortex is necessary for temporal organization of hippocampal neuronal activity. Nat Neurosci 18:1123–1132.

Schmidt R, Diba K, Leibold C, Schmitz D, Buzsáki G, Kempter R (2009) Single-trial phase precession in the hippocampus. J Neurosci 29:13232–13241.

Taube JS, Muller RU, Ranck JB Jr. (1990a) Head-direction cells recorded from the postsubiculum in freely moving rats. I. Description and quantitative analysis. J Neurosci 10:420–435.

Taube JS, Muller RU, Ranck JB Jr. (1990b) Head-direction cells recorded from the postsubiculum in freely moving rats. II. Effects of environmental manipulations. J Neurosci 10:436–447.

Touretzky DS, Redish AD (1996) Theory of rodent navigation based on interacting representations of space. Hippocampus 6:247–270.

Virtanen P, Gommers R, Oliphant TE, Haberland M, Reddy T, Cournapeau D, Burovski E, Peterson P, Weckesser W, Bright J, van der Walt SJ, Brett M, Wilson J, Millman KJ, Mayorov N, Nelson ARJ, Jones E, Kern R, Larson E, Carey CJ, et al. (2020) SciPy 1.0: fundamental algorithms for scientific computing in Python. Nat Methods 17:261–272.

2.2 Manuscript II - A Theory of Hippocampal Theta Correlations Accounting for Extrinsic and Intrinsic Sequences

A theory of hippocampal theta correlations accounting for extrinsic and intrinsic sequences

Yuk-Hoi Yiu and Christian Leibold (2023)

Author Contributions

C.L. conceived the project, supervised the simulation and analysis; **Y.-H.Y.** did the modelling, wrote software, implemented the simulation and analysis; C.L. and **Y.-H.Y.** wrote the manuscript.

eLife

A theory of hippocampal theta correlations accounting for extrinsic and intrinsic sequences

Yuk-Hoi Yiu[1,2], Christian Leibold[1,3]*

[1]Fakultät für Biologie & Bernstein Center Freiburg Albert-Ludwigs-Universität Freiburg, Freiburg, Germany; [2]Graduate School of Systemic Neurosciences, Ludwig-Maximilians-Universität München, Munich, Germany; [3]BrainLinks-BrainTools, Albert-Ludwigs-Universität Freiburg, Freiburg, Germany

*For correspondence:
christian.leibold@biologie.uni-freiburg.de

Abstract Hippocampal place cell sequences have been hypothesized to serve as diverse purposes as the induction of synaptic plasticity, formation and consolidation of long-term memories, or navigation and planning. During spatial behaviors of rodents, sequential firing of place cells at the theta timescale (known as theta sequences) encodes running trajectories, which can be considered as one-dimensional behavioral sequences of traversed locations. In a two-dimensional space, however, each single location can be visited along arbitrary one-dimensional running trajectories. Thus, a place cell will generally take part in multiple different theta sequences, raising questions about how this two-dimensional topology can be reconciled with the idea of hippocampal sequences underlying memory of (one-dimensional) episodes. Here, we propose a computational model of cornu ammonis 3 (CA3) and dentate gyrus (DG), where sensorimotor input drives the direction-dependent (extrinsic) theta sequences within CA3 reflecting the two-dimensional spatial topology, whereas the intrahippocampal CA3-DG projections concurrently produce intrinsic sequences that are independent of the specific running trajectory. Consistent with experimental data, intrinsic theta sequences are less prominent, but can nevertheless be detected during theta activity, thereby serving as running-direction independent landmark cues. We hypothesize that the intrinsic sequences largely reflect replay and preplay activity during non-theta states.

eLife assessment

This **important** work presents an interesting perspective for the generation and interpretation of phase precession in the hippocampal formation. Through numerical simulations and comparison to experiments, the study provides a **convincing** theoretical framework explaining the segregation of sequences reflecting navigation and sequences reflecting internal dynamics in the DG-CA3 loop. This study will be of interest for researchers in the spatial navigation and computational neuroscience fields.

Introduction

As a rat navigates in an environment, place cells fire sequentially during one theta cycle (~100 ms) and form time-compressed representations of behavioral experiences (*Skaggs et al., 1996*), called theta sequences. Theta sequences were proposed to be driven by extrinsic (extrahippocampal) sensorimotor input (*Foster and Wilson, 2007*; *Huxter et al., 2008*; *Romani and Tsodyks, 2015*; *Yiu et al., 2022*), since they are played out in the direction of travel during locomotion and, hence, represent current behavioral trajectories. In contrast, various types of hippocampal sequences have also been

proposed to arise from intrinsic hippocampal connectivity. Non-local activation of place sequences during immobile periods was observed in replay of past locations after the space has been explored (*Skaggs and McNaughton, 1996*; *Lee and Wilson, 2002*) as well as in preplay (*Dragoi and Tonegawa, 2011*) of prospective locations before the animal explores a novel environment. In addition, some CA3 place cells exhibit out-of-field firing at reward locations (*Sasaki et al., 2018*). These remote activations of place cells reflect the underlying circuit connectivity rather than the actual location and movement of the animal. Furthermore, a subset of CA3 cell pairs shows rigid theta correlations with peak lags that are independent of the traversal order of their place fields (*Yiu et al., 2022*), suggesting the existence of hard-wired sequences *even* when sensorimotor drive is present. Such intrinsic sequences that are driven by intrahippocampal connectivity (*Tsodyks et al., 1996*), although less predominantly observed during theta (*Yiu et al., 2022*), are generally interpreted as reflecting spatial memories or planning (*Kay et al., 2020*).

Existing models for theta sequences are, however, either fully extrinsic or intrinsic. The former often employ short-term plasticity (*Romani and Tsodyks, 2015*; *Thurley et al., 2008*), which creates synaptic couplings that are temporally stronger along the instantaneous forward direction. In contrast, intrinsic models, such as the *Tsodyks et al., 1996* model, use a fixed asymmetrical weight matrix pre-designed to align with one movement trajectory (for review see *Maurer and McNaughton, 2007*; *Jaramillo and Kempter, 2017*). Neither of these models alone can explain the simultaneous presence of rigid and flexible correlations in theta sequences. Here we present a network model that accounts for both types of correlations by separating their generation into two anatomically distinct layers: CA3 and dentate gyrus (DG). Extrinsic sequences are generated in the CA3 layer by short-term synaptic plasticity mechanisms, while the intrinsic sequences are evoked by the CA3-DG feedback loop with fixed asymmetrical weights, as inspired by the experimental evidence that lesions of DG abolish non-local activation of CA3 place cells (*Sasaki et al., 2018*) and CA3 theta correlations (*Ahmadi et al., 2022*).

In this paper, we present a model for theta correlations that unifies both extrinsic and intrinsic mechanisms. Extrinsic and intrinsic sequences can propagate simultaneously in separate directions, along the movement trajectory and the pre-designed CA3-DG feedback loops, respectively. As a result, spike correlations display directionality as the two sequences cross each other at various angles: The more parallel they are, the stronger the correlation. Our simulations are in quantitative agreement with directionality properties found in experimental data (*Yiu et al., 2022*) and propose that rigid correlation structure can serve as a stable temporal pattern, which is recognizable across multiple movement directions. This temporal 'landmark' pattern allows spatial encoding even if sensory-motor experience is lacking and may reflect the mechanistic basis for replay in non-theta states.

Results

Dependence of theta sequences on heading directions: Extrinsic and intrinsic sequences

Theta-scale correlations of place cells have been explained by previous models using two different types of network mechanisms, intrinsic and extrinsic ones. For *intrinsic* models spike correlations are explained by only the recurrent connectivity of the neuronal network (*Figure 1A*). For *extrinsic* models, the spike correlation is defined by sensory-motor parameters such as movements (*Figure 1B*). We first illustrate how these mechanisms work for two exemplary representatives of these two major model classes.

For intrinsic models, we refer to the *Tsodyks et al., 1996* model where phase precession is generated by the fixed asymmetrical connectivity between place cells. Spike phases of the place cells ahead of the animal decrease as the excitatory drive is gradually increasing, but only along the direction in which the connection strength is asymmetrically stronger (e.g. rightward in *Figure 1A*), called the *asymmetry direction*. Here we simulate a network of CA3 place cells with fixed asymmetrical connectivity (see Methods section: CA3 recurrent connections) as suggested in the *Tsodyks et al., 1996* model and applied our model to behavioral running trajectories in a 2-d open space (*Figure 1C*). Phase precession and spike correlations (*Figure 1D–E*) are compared for opposite running directions. In our simulations, all place cells project excitatory synapses to their counterparts with rightward neighboring place fields. Phase precession therefore is determined by how closely the running direction matches

46
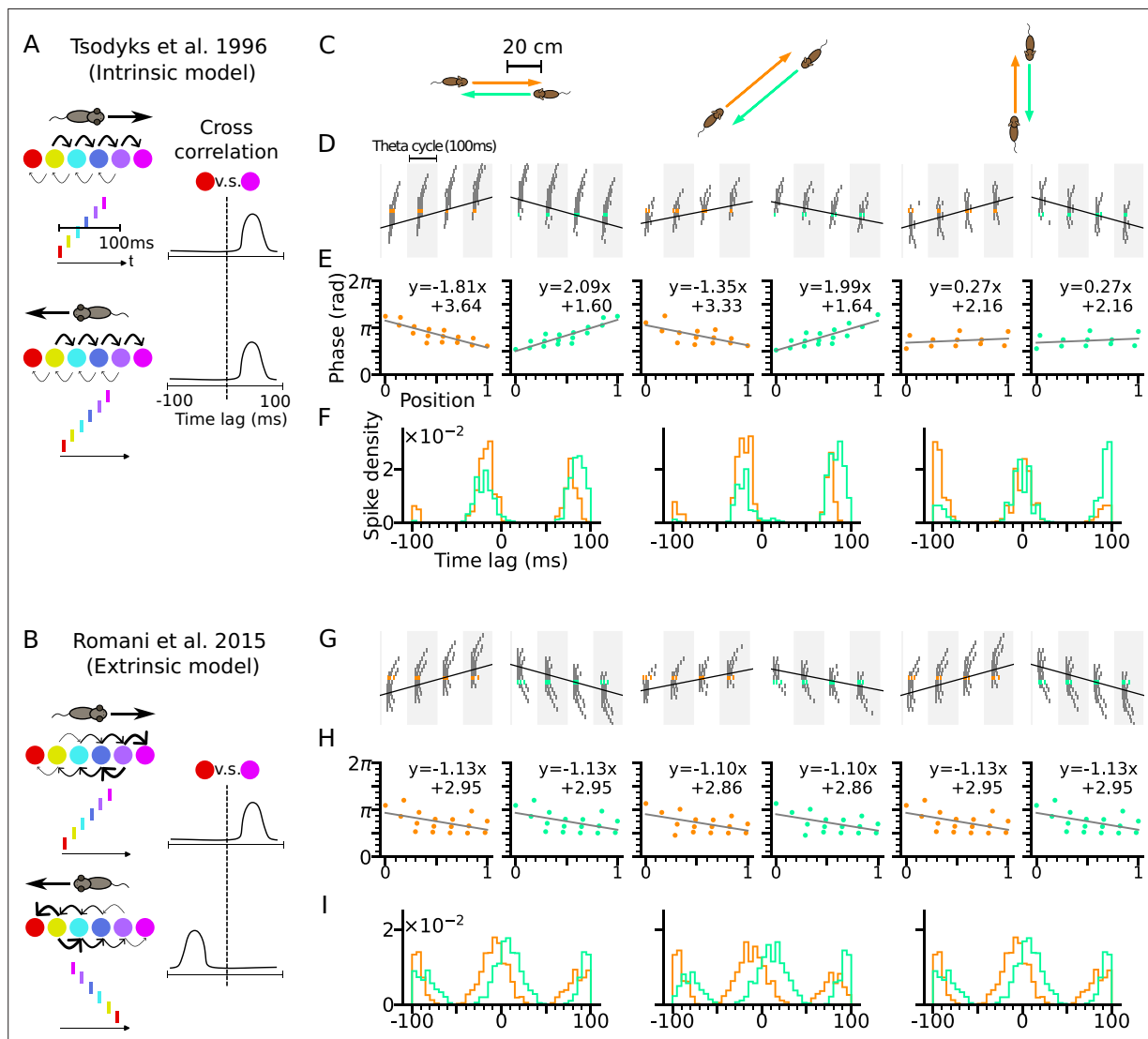
Figure 1. Phase precession depends on running direction in intrinsic models but not extrinsic models. (**A**) Left: Schematic illustration of the intrinsic *Tsodyks et al., 1996* model. When the animal runs through a series of place fields (solid circles) in 1-D, the place cells fire action potentials in sequence at the theta timescale (spike raster with corresponding colors). Recurrent connectivity is pre-configured and asymmetrical (connection strengths indicated by arrow sizes). Right: Cross-correlation function between the red and magenta cell, which remains the same for both running directions. (**B**) Left: Schematic illustration of the extrinsic *Romani and Tsodyks, 2015* model. Recurrent connections behind the animal are temporarily depressed by short-term plasticity, and thereby, become movement-dependent. Right: Cross-correlation flips sign in the opposite running direction. (**C**) Simulated trajectories (duration 2 s) in a 2-d environment (80×80 cm) with speed 20 cm/s in left and right (left column), diagonal (middle), and up and down (right) directions. (**D–F**) Simulation results from the intrinsic model (with fixed asymmetrical connectivity inspired by the *Tsodyks et al., 1996* model). Place cells only project synapses to their right neighbors. (**D**) Spike raster plots of place cells along the orange (left panel) and light green (right panel) trajectories (colors defined in C). Theta sequence order remains the same in the reversed running direction. Black line indicates animal position. (**E**) Phase-position relation for the spikes colored in C. Linear-circular regression (gray line) parameters are indicated on top. Positions of the animal at the first and last spike are normalized to 0 and 1, respectively. (**F**) Averaged cross-correlation of all cell pairs separated by 4 cm along the trajectory. Reversal of running direction does not flip the sign of the peak lags. (**G–I**) Same as D-F, but for the extrinsic model (spike-based variant of *Romani and Tsodyks, 2015* model). Correlation peaks flip after reversal of running direction.

the asymmetry direction imposed by the intrinsic connections. The closer the trajectory angle aligns with this asymmetry direction, the more negative is the slope of phase precession (*Figure 1E*). Since in this case, the theta sequence only propagates rightwards as place cells are sequentially activated from left to right, the signs of spike correlations between cell pairs remain invariant to the movement direction (*Figure 1F*, see Methods section: Cross-correlation analysis). Intrinsic models thus cannot explain

47

experimentally observed directional independence of phase precession and directional dependence of theta spike correlations (*Huxter et al., 2008*).

Our example of an extrinsic model is based on our spiking simulations of the originally rate-based model by *Romani and Tsodyks, 2015*, where phase precession was explained by symmetric recurrent connections that undergo running direction-dependent attenuation by short-term synaptic depression (STD): place fields with centers behind the current animal position on the trajectory thereby received largely reduced recurrent input resulting in recurrently driven theta sequences to play out only in forward direction (see Methods section: CA3 recurrent connections). We simulated our spiking variant of the *Romani and Tsodyks, 2015* model with the same trajectories as the intrinsic model (*Figure 1G–I*), and recovered direction-independent phase precession (*Figure 1H*). Since now, the theta sequences are played out in the same direction as the movement, theta spike correlations are symmetrically reversed (*Figure 1I*) as shown experimentally in CA1 neurons (*Huxter et al., 2008*; *Yiu et al., 2022*).

In area CA3, however, theta spike correlations are neither solely extrinsic (*Yiu et al., 2022*; *Kay et al., 2020*), since phase precession properties change in relation to running directions, nor are they solely intrinsic since reversal of correlation is still observed in most of the sequences (*Huxter et al., 2008*; *Yiu et al., 2022*). We therefore propose a new theory of phase precession for CA3 incorporating both intrinsic and extrinsic factors.
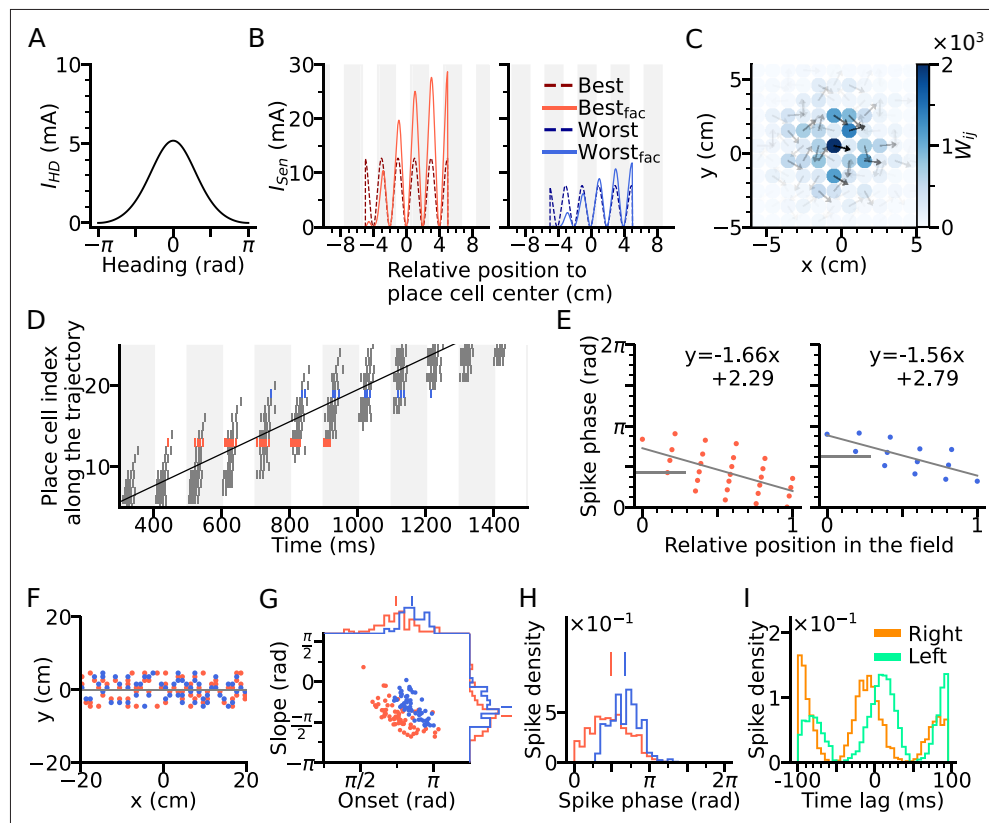
Directional sensory input

To, however, fully explain directional properties of theta phase precession and theta spike correlations by a model, also directional modulations of firing rates (*Yiu et al., 2022*) need to be taken into account.

We therefore included both directional and positional modulation of the sensory input to the model place cells (*Figure 2A–B*) with randomized preferred heading directions (see Methods section: Spatial input). The sensory input is assumed to arise from MEC, and hence, it is also theta-modulated and phase-shifted by 70° with respected to the peak of theta cycle (*Mizuseki et al., 2009*). Furthermore, since the precession slope observed in the *Romani and Tsodyks, 2015* model is limited (-1.13 radians per field size, see *Figure 1H*) as compared to the experimental reports (-4.44 radians (*Yiu et al., 2022*) and about -2.0 radians (*Harris et al., 2002*) per field size), we introduced short-term synaptic facilitation (STF) to the sensory input (*Berretta and Jones, 1996*; *Thurley et al., 2008*) generating temporally asymmetric depolarization as suggested by intracellular recordings in vivo (*Harvey et al., 2009*; *Figure 2B*). STF amplifies the sensory current at the later part of the field, thus creating phase precession with steeper slopes thereby extending the phase range (see Methods section: Spatial input). Finally, we designated the synaptic weights to be stronger between place cells with similar preferred heading directions (*Figure 2C*) as has been proposed (*Brunel and Trullier, 1998*) as a result of Hebbian plasticity applied to directional firing fields.

A simulation of the place cell network was performed for a rightward trajectory through the arena based on our variant of the extrinsic *Romani and Tsodyks, 2015* model (*Figure 2D*). We focus on two sets of place cells, one for which the trajectory aligns with the preferred heading direction of the field (red, denoted as *best* direction) and one for which the trajectory runs opposite the preferred heading direction (denoted as *worst* direction; *Figure 2F*). Phase precession has a lower onset and marginal spike phase along best direction than along the worst (*Figure 2G–H*), which is consistent with experimental data (*Yiu et al., 2022* report mean spike phases ± SEM for best and worst direction of 1.61 ± 0.02 and 2.22 ± 0.03 in radians respectively), reflects that larger depolarizations generally yield shorter latencies. Directionality of the input, although it yields lower spike phases through higher depolarization, does not affect spike pair correlations, which remains solely extrinsic (*Figure 2I*). Thus, even though rate directionality and directional bias in recurrent connectivity can render phase precession directionally dependent, they are not sufficient to account for intrinsic sequences.

Generation of intrinsic sequences by the DG-CA3 recurrent network

To explain the expression of intrinsic sequences in CA3, we propose them to be generated by the interaction of two networks, CA3 and DG (*Figure 3A*). DG is a good candidate region to be involved in phase precession, since lesions of it were shown to reduce prospective spiking (*Sasaki et al., 2018*) and to lower the onset phase of phase precession (*Ahmadi et al., 2022*). In our model, the neurons in

Figure 2. Directional input gives rise to spikes at lower theta phase. (**A**) Directional input component of an example place cell. (**B**) Total sensory input as the sum of directional and positional drive of an example place cell for the animal running along (red dashed line, left) and opposite (blue dashed line, right) the preferred heading direction of the cell, respectively named as *best* and *worst* direction. The sensory input is modelled by oscillatory currents arriving with +70° phase shift relative to theta peaks (gray vertical lines). Place fields are defined by a 5 cm rectangular envelope. Solid lines depict the input current including short-term synaptic facilitation. (**C**) Synaptic weights (W_{ij}, color) from the place cell at the center (the darkest dot) to its neighbors in the 2-d environment. Each dot is a place field center in 2-d space. Arrows depict their preferred heading directions. (**D**) Spike raster plot sorted by visiting order of the place fields along the trajectory. Spikes of the cells with best and worst direction are colored in red and blue, respectively. (**E**) Phase position plots for the cells with best and worst direction from D (labels as in *Figure 1E*). The mean phase is marked as horizontal gray bar. (**F**) Example place cell centers with best (<30° different from the trajectory; red) and worst (>150°; blue) directions relative to the rightward trajectory (gray line). Only centers of cells that fire more than 5 spikes are shown. (**G**) Slopes and onsets of phase precession of the population from (**F**). Marginal slope and onset distributions are plotted on top and right, respectively. Note higher phase onset in the worst-direction case. (**H**) Spike phase distributions. Higher directional inputs generate lower spike phases. (**I**) Average spike correlation between all pairs with 4 cm of horizontal distance difference when the animal runs rightwards and leftwards. Peak lags are flipped as expected from an extrinsic model.

DG receive excitatory synaptic inputs from CA3 place cells (putatively via hilar mossy cells) and project back to the CA3 cells with place field centers at a different location (*Equation 3*) to induce propagation of intrinsic sequences along a specific spatial direction. The CA3 cells at the target location of DG input are then activated and evoke higher depolarization in cells with place fields at the next DG target locations through the feedback. This scheme produces a rigid sequence whose activation order is independent of the movement direction. The connection pattern of DG-CA3 projections (for brevity, we also refer to it as 'DG loop' in the subsequent text) could be determined by pre-existing network structure or past experience through associative learning, or both.

Figure 3, provides schematic illustrations, for a DG layer that either only projects CA3 activity to their rightward neighbours ($\theta_{DG} = 0°$, *Figure 3A*) or only to their leftward neighbors ($\theta_{DG} = 180°$, *Figure 3E*). Simulations for both cases ($\theta_{DG} = 0°$ and $\theta_{DG} = 180°$) assume a rightward trajectory. Apart

49
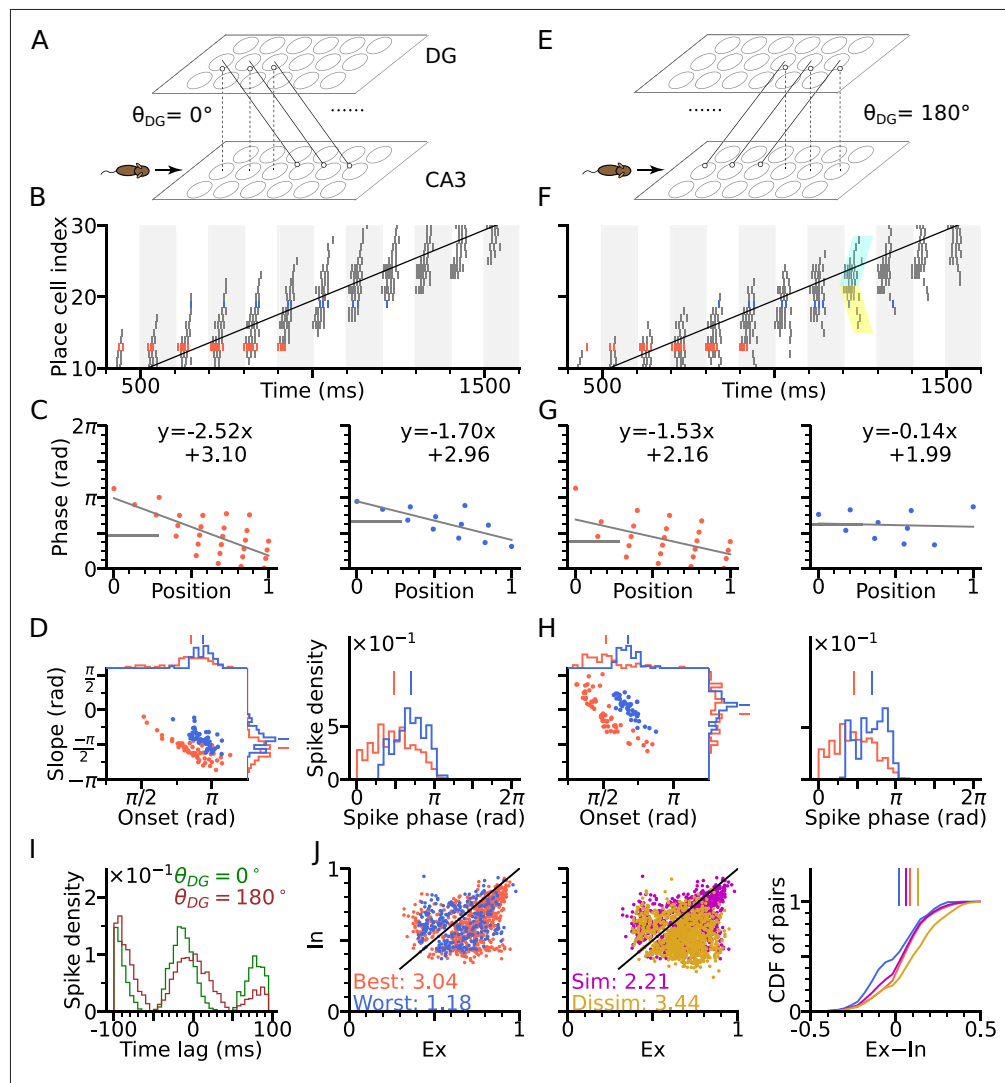
Figure 3. DG-CA3 loop introduces directionality of theta sequences. (**A**) Illustration of synaptic connections from CA3 place cells to DG and vice versa. DG layer mirrors the place cell population in CA3 and redirects the CA3 inputs back to different locations. Here, DG cells project into CA3 place cells with fields 4 cm displaced to the right of the pre-synaptic CA3 cells. θ_{DG} denotes the angular difference between the DG projection direction and the animal's movement direction. (**B**) Spike raster plots sorted by cell indices along the trajectory (2 s duration) from x=-20 cm to x=20 cm. Cells with best and worst angles are marked by red and blue colors, respectively. (**C**) Phase-position plots as is *Figure 2E*. (**D**) Distributions of precession slopes, onsets and spike phases as in *Figure 2G–H*. (**E–H**) Same as A-D, but with DG cells projecting opposite to the animal's movement direction ($\theta_{DG} = 180°$). In F, cyan and yellow shaded regions indicate the examples of forward sequence induced by the movement (extrinsic), and backward sequence induced by the DG recurrence (intrinsic), respectively. (**I**) Average spike correlations for $\theta_{DG} = 0°$ and $\theta_{DG} = 180°$ for pairs separated by 4 cm along the trajectory. Note that for $\theta_{DG} = 180°$, there is a relative excess of spike-pairs with positive lags. (**J**) Left: Intrinsicity and extrinsicity (see Methods) for all pairs from the populations with best (red) and worst (blue) direction. Pair correlations above and below the identity line are classified as intrinsic and extrinsic, respectively. Numbers are the ratios of extrinsically to intrinsically correlated field pairs. Note that the red best direction pairs are more extrinsic than the blue worst direction pairs due to higher sensory input. Middle: Ex/Intrinsicity of pairs with similar (<30°) and dissimilar (>150°) preferred heading angles. Pairs with similar preferred heading angle s are more intrinsic due to stronger DG-CA3 recurrence. Right: Cumulative distribution of the differences between extrinsicity and intrinsicity. Dissimilar and best direction pairs have higher bias to extrinsicity than similar and worst direction pairs, respectively.

The online version of this article includes the following figure supplement(s) for figure 3:

Figure 3 continued on next page

50

from the addition of the DG layer, the model architecture and parameters of CA3 layer are the same as in *Figure 2* (including best and worst direction in place field firing rate), which only generates extrinsic sequences through STD in the CA3 recurrent synaptic connections. DG-loop connectivity is additionally modulated by firing rate directionality of the CA3 place fields. Fields with similar preferred heading directions are more strongly connected via the loop than those with opposite preferred heading directions (see Methods section: DG layer).

We found that, when the simulated animal is running in the same direction as the DG-CA3 projection, phase precession starts from a higher phase (*Figure 3C–D*) due to the forward activation of place cells through DG layer (recovering the effect of asymmetric connectivity in the original *Tsodyks et al., 1996* model), as compared to the model without DG layer (*Figure 2G–H*). Spike phases in best direction remain lower than along the worst direction (*Figure 3D*). When, however, the animal is running against the DG-CA3 projection (*Figure 3E*), extrinsic sequences are still present in forward direction, evoked by the movement of the animal, but the intrinsic sequences are played out backward as determined by the direction of fixed recurrence (see cyan and yellow shaded regions in *Figure 3F*). The latter is reflected by the higher phase at the end of the phase position plots (*Figure 3G*) which leads to flatter precession slopes and decreases the fraction of phase precession (slope <0) of all traversal trials (*Figure 3H*). A closer look into pair correlation reveals that for trajectories opposite to the DG-loop projection ($\theta_{\mathrm{DG}} = 180°$), spike probability is added to positive time lags (*Figure 3I*). Therefore, introducing fixed recurrence through DG loops elicits both extrinsic and intrinsic sequences and qualitatively changes theta sequences.

To quantify the degrees of extrinsic and intrinsic sequence firing in a way allowing comparison to experimental reports, we use the measures *extrinsicity* and *intrinsicity* (*Yiu et al., 2022*) that are based on pairs of place cells with overlapping place fields (see Methods section: Extrinsicity and intrinsicity, and Discussion). In our simulation, extrinsically and intrinsically driven cell pairs are both present in the population (*Figure 3J*), indicating a coexistence of extrinsic and intrinsic sequences. Our model reproduces a greater extrinsicity for cell pair activity when running direction aligns with both best place field directions as compared to when it aligns to both worst field directions, since along the best direction,
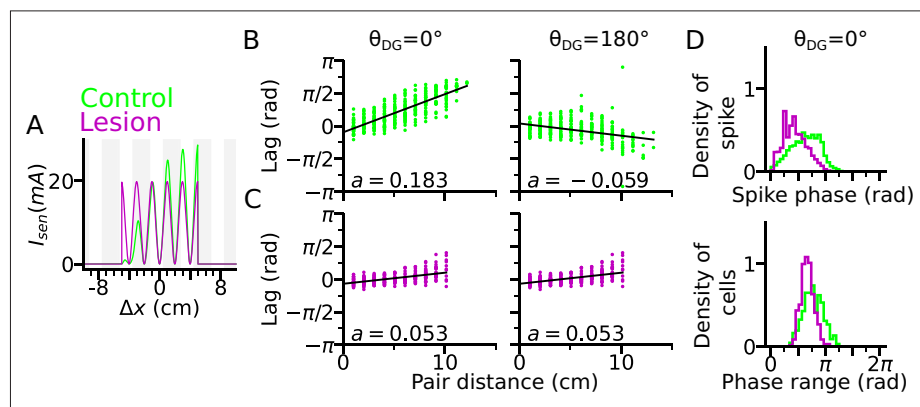
Figure 4. DG lesion reduces theta compression and phase precession range. DG recurrence is turned off to simulate the lesion condition. (**A**) Positional sensory inputs into a place cell in lesion (purple) and control (green) cases. The control case is identical to *Figure 3*. In the lesion case, DG input is compensated by increased sensory input with increased probability of synaptic release, hence reduced short-term synaptic facilitation. (**B**) Theta compression, that is correlation between peak correlation lag and distance of field centers in the control case. Each dot represents a field pair. Linear-circular regression line is indicated in black. Note that the sign of regression slope (a in radians/cm) is determined by the directions of DG loop (negative in $\theta_{\mathrm{DG}} = 180°$). (**C**) same as B, but for the lesion case. Theta compression is reduced as compared to the control condition. (**D**) Top: Distribution of spike phase during phase precession in all active (spike count > 5) cells in control and lesion case. Bottom: Distribution of phase precession range for all active cells.

cells receive more sensory depolarization, and thus, the movement-dependent extrinsic sequences are more activated. The model also explains, why pairs with similar preferred heading directions may be less extrinsic than pairs with approximately opposite preferred heading direction (dissimilar pairs), since the DG loop preferentially connects CA3 place cells with similar preferred heading directions. Both of the results follow the same trend as found in experimental data (*Yiu et al., 2022* report ratios of extrinsically to intrinsically correlated CA3 field pairs of 1.57 for both-best directions, 0.41 for both-worst directions, 0.87 for similar pairs and 2.43 for dissimilar pairs).

Thus, by introducing feedback excitation via the DG layer, intrinsic sequences are able to propagate in fixed directions on top of the movement-dependent extrinsic sequences. Theta sequence directionality is reflected through the change in spike correlation, which varies as a function of the difference between the direction of DG feedback and movement direction. The combination of extrinsic and intrinsic theta sequence activity is robust regarding changes of the parameters of short-term synaptic plasticity (*Figure 3—figure supplement 1*), as well as running speed (*Figure 3—figure supplement 2*), as long as place fields are wide enough to allow spikes in sufficiently many theta cycles.

## Lesion of DG reduces theta compression and phase precession range

One prediction of the DG-loop model, consistent with findings from DG lesion experiments (*Ahmadi et al., 2022*), is that DG would contribute to the temporal organization of spike sequences in CA3. To verify this hypothesis also in the model, we implemented a lesion of DG by disabling activity in the DG layer. To compensate for reduced excitatory drive caused by the lesion, we then increased probability of release of the sensory inputs thereby increasing the initial input amplitudes but removing short-term synaptic facilitation (*Figure 4A*).

We found that a DG lesion would reduce theta compression in sequence activity. Theta compression (*Dragoi and Buzsáki, 2006*) refers to the compression of seconds-long behavioural experience of place-field crossing into a neural representation of spike sequences at a shorter (theta) timescale. To quantify the strength of theta compression, we plotted the pair correlation lags versus the distance between the centers of two fields (abbreviated as 'lags' and 'pair distance' respectively), after simulating a rightward trajectory (*Figure 4B–C*). The magnitude of the linear-circular regression slope a measures how much theta phase encodes a certain interval in space, and therefore, the strength of theta compression. As a result, theta compression is reduced for the DG-lesioned case ($a = 0.053$ radians/cm for both $\theta_{DG} = 0°$ and $\theta_{DG} = 180°$), as compared to the control case ($a = 0.183$ radians/cm for $\theta_{DG} = 0°$ and $a = -0.059$ radians/cm for $\theta_{DG} = 180°$) reproducing the finding (*Ahmadi et al., 2022*) that spatial encoding via theta sequences crucially depends on intact DG and suggesting that the loss of DG inputs could be compensated for by the increase of release probability in the spared afferent synapses from the MEC. The DG lesion also reduces the spike phase and phase range of phase precession (*Figure 4D*), which indicates the participation of DG loops in high-phase spiking. Both weaker phase precession and theta compression stress the important role of DG in temporal organization of CA3 sequences.

Theta sequences in 2-d and out-of-field firing

So far, the model was only evaluated on bidirectional linear tracks, where running directions completely overlapped with the orientation of the DG loop connectivity. Now, we extend our analysis to 2-d space by examining oblique trajectories which cross the orientation of DG-loop projection at certain angles.

We first arrange the DG-loop connections such that the DG-loop orientation crosses a rightward trajectory at 45° and 225° (*Figure 5A–F*). Similar to the cases of $\theta_{DG} = 0°$ and $\theta_{DG} = 180°$ (*Figure 3D and H*), precession slopes are steeper and onsets higher when the trajectory direction aligns more with the orientation of the DG-loop, but with a smaller effect size for oblique crossings (*Figure 5A and C*) since DG-loop connectivity area only overlaps with part of the trajectory near the intersection. We further resolve the precession slope, onset and marginal phase for each place cell into 2-d maps (*Figure 5B and D*). Intrinsic sequences with a higher marginal spike phase can be clearly seen along the belt of DG-loop projections and are even extended to the outside of trajectory predicting 'off-track' spikes at high phases. Depending on the alignment between movement direction and DG-loop orientation, the slope becomes either more negative ($\theta_{DG} = 45°$) or more positive ($\theta_{DG} = 225°$). Analysis of extrinsicity and intrinsicity was conducted for all field pairs and confirmed the same trend as in *Figure 3* that best and dissimilar pairs are more extrinsic than worst and similar pairs, respectively
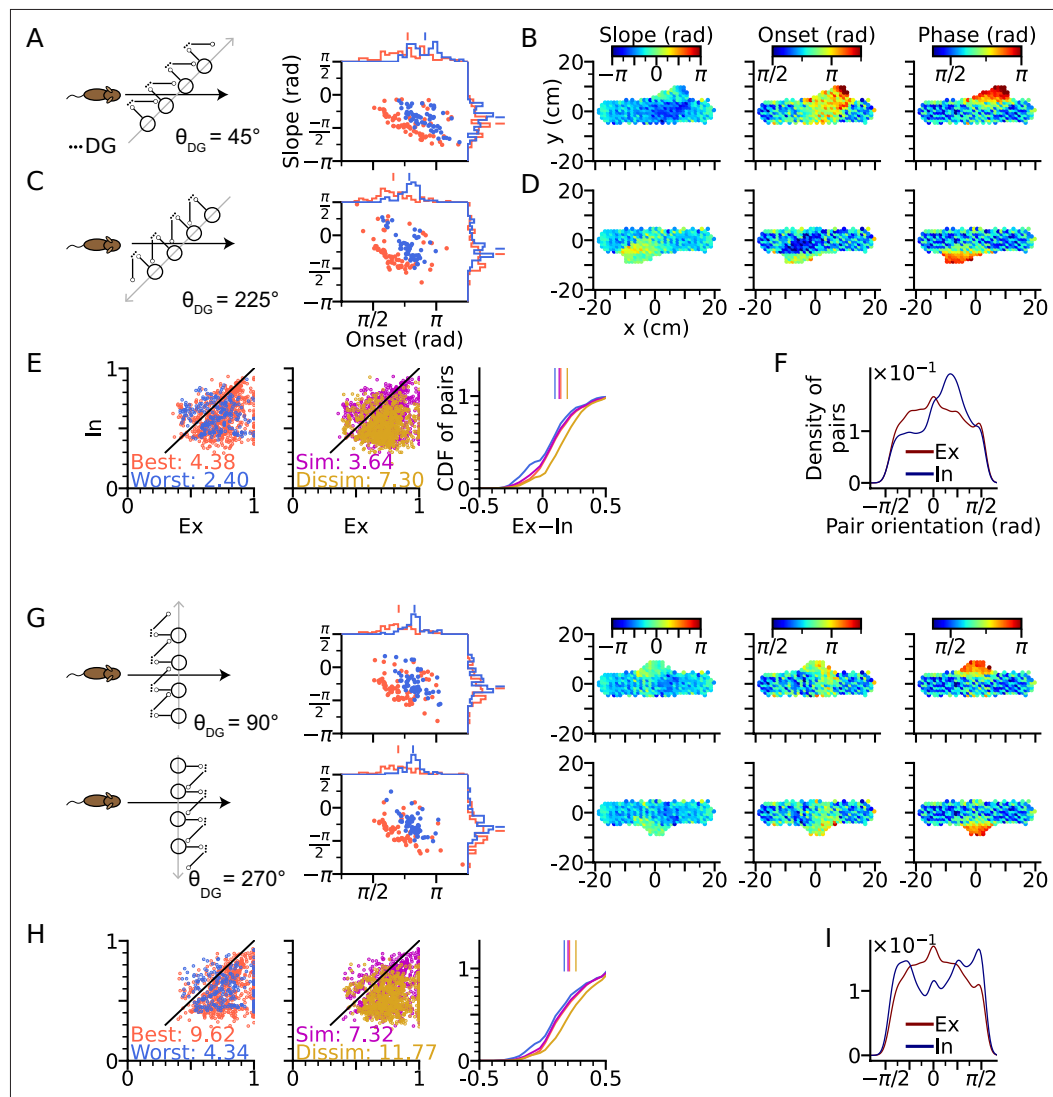
Figure 5. Intrinsic sequences lead to direction dependent 2-d phase precession and out-of-field firing (**A**) Left: Schematic illustration of DG-loop projection being tilted by 45° relative to the trajectory. Right: Distributions of phase precession onsets and slopes from the place cells along the trajectory as in **Figure 2G**. (**B**) Slopes (left), onsets (middle) and mean spike phases (right) of phase precession from the place cells as a function of field center. High spike phases and onsets occur along the DG-loop orientation where intrinsic spiking dominates and yield out-of-field firing (see the extrusions from horizontal dot clouds) with late onsets and phases. (**C–D**) Same as A-B, but DG-loop projection is at 225° relative to trajectory direction. (**D**) For DG loops pointing opposite to the sensorimotor drive, prospective firing along the DG loop yields less steep precession slopes and lower onset. (**E**) Extrinsicity and intrinsicity of all place field pairs along the trajectory as in **Figure 3J**. Some pairs are totally extrinsic (Ex = 1) because DG projection is absent at those parts of the trajectory. (**F**) Density of field pairs with extrinsic/intrinsic correlation as a function of the orientation of field center difference vector relative to the x axis. Intrinsic fields peak at 45°. (**G**) Same as A-D, but DG-loop orientations are perpendicular to the trajectory direction at 90° (top) and 270°. Prospective spikes from intrinsic sequences are initiated in the perpendicular directions. (**H**) Same as E, but with higher Ex-In ratios. (**I**) Field pairs with intrinsic correlations are at ±90°.

(**Figure 5E**). As a quantitative prediction, we computed the angle differences between field centers of cell pairs for the extrinsic and intrinsic populations, and observe that place field center differences in extrinsically correlated field pairs are mostly oriented horizontally (along the running direction) while place field center differences from intrinsically correlated field pairs are oriented along the DG-loop orientation $\theta_{\mathrm{DG}} = 45°$, as by design (**Figure 5F**).

The analysis above is repeated for the geometric configurations that DG-loop connectivity is minimally interacting with the place cell activity induced by movement, that is when DG-loop orientation and the movement direction are perpendicular to each other ($\theta_{\mathrm{DG}} = 90°$ and $\theta_{\mathrm{DG}} = 270°$, **Figure 5G**). Similar effects as in **Figure 5B and D** on precession slope, onset and marginal phases are also observed in the 2-d map, except that the effects are further restricted to the intersection area in the middle. Also, the whole population has become more extrinsic as compared to the 45° and 225° cases (**Figure 5H**, see the numbers for extrinsic-intrinsic ratios) due to the smaller overlapping area between DG-loop projection and the trajectory. Lastly, the pair center difference orientation confirms that field pairs with extrinsic correlations follow the trajectory direction while those with intrinsic correlation are biased towards the DG-loop orientations (90°).

The results demonstrate the distinct roles of extrinsic and intrinsic sequences in 2-d spatial encoding. The former represents trajectory direction while the latter the associative memory towards specific locations. They can be played out at the same time separately in different directions and only interact with each other when they overlap. The interaction is reflected in directional dependence of phase precession properties, most notably the higher spike phases from the DG-CA3 recurrent input, as well as increased intrinsicity of pair correlation and extended firing fields along the orientation of the DG-loop projections. Intrinsic sequences also triggered out-of-field firing (**Figure 5B, D and G**) at late theta phases. In this case, the DG-loop connects to cells with remote place fields. These cells could even display multiple separated place fields, with high spike phases indicating the target location of the intrinsic sequence.

Topology-free mechanisms of extrinsic phase precession

A well-known problem of phase precession models based on recurrent connectivity that applies to both, the original intrinsic **Tsodyks et al., 1996** and **Romani and Tsodyks, 2015** model, is that they do not explain how the topological connectivity matrix (in our case W^{CA3}) is generated (**Lisman and Redish, 2009**; **Jaramillo and Kempter, 2017**). Extrinsic theta sequences in a first exposure to a novel environment should therefore be missing. Although **Feng et al., 2015** find that theta sequences on a first exposure of a novel linear track are indeed much weaker (maybe only reflecting intrinsic sequences), their results nevertheless indicate a very fast learning time scale that is hard to reconcile with recurrent learning of a full spatial topology (particularly the generalization to 2-d). Also their result might be hampered by place field plasticity that biases the decoder towards backward-shifted place maps of later trials (**Parra-Barrero and Cheng, 2023**). We therefore explored, whether extrinsic 2-d sequences could also be generated by a model that is not relying on 2-d topology in the recurrent weights. To this end, we disabled the CA3 recurrence and compensated the missing level of excitation by an increased strength of the spatial input and the DG loops (see Methods section: Parameters of the models). Our simulations show that extrinsic sequences can still be generated by spatial input alone (**Figure 6A**), relying only on the short-term facilitation mechanism. Simulating CA3 activity with lesioned DG similarly abolishes the temporal organization of theta sequence and reduces the phase range (**Figure 6B**). The results demonstrate that the temporal order of extrinsic sequences could be coordinated solely by sensorimotor drive and does not necessarily require CA3 recurrence.

Functional role of intrinsic sequences

While the function of extrinsic theta sequences in encoding the actual trajectory of an animal (connecting the recent past, present and near future locations) is obvious, the potential role of the less readily apparent intrinsic sequences is not straight forward. Simulations of trajectories in 2-d (**Figure 5**) suggest intrinsic activity may serve a role to identify certain location-direction pairs independent of the current trajectory. Here, we follow this idea by evaluating the hypothesis that the intrinsic sequences signal a stable 'landmark' (location/direction pair) cue by a temporal code that is invariant to different directions of approach.

To test our hypothesis, we constructed a downstream readout neuron that would reliably identify the presence of the intrinsic sequence independently of the animal's running direction, whereas it would not be able to do so for only extrinsic sequences. To this end, we trained the synaptic weights using the tempotron learning rule (**Gütig and Sompolinsky, 2006**), which is able to implement binary classification based on temporal relations of input spike patterns (see Methods section: Tempotron). Two tempotrons were trained to recognize the spike patterns from the place cells, one
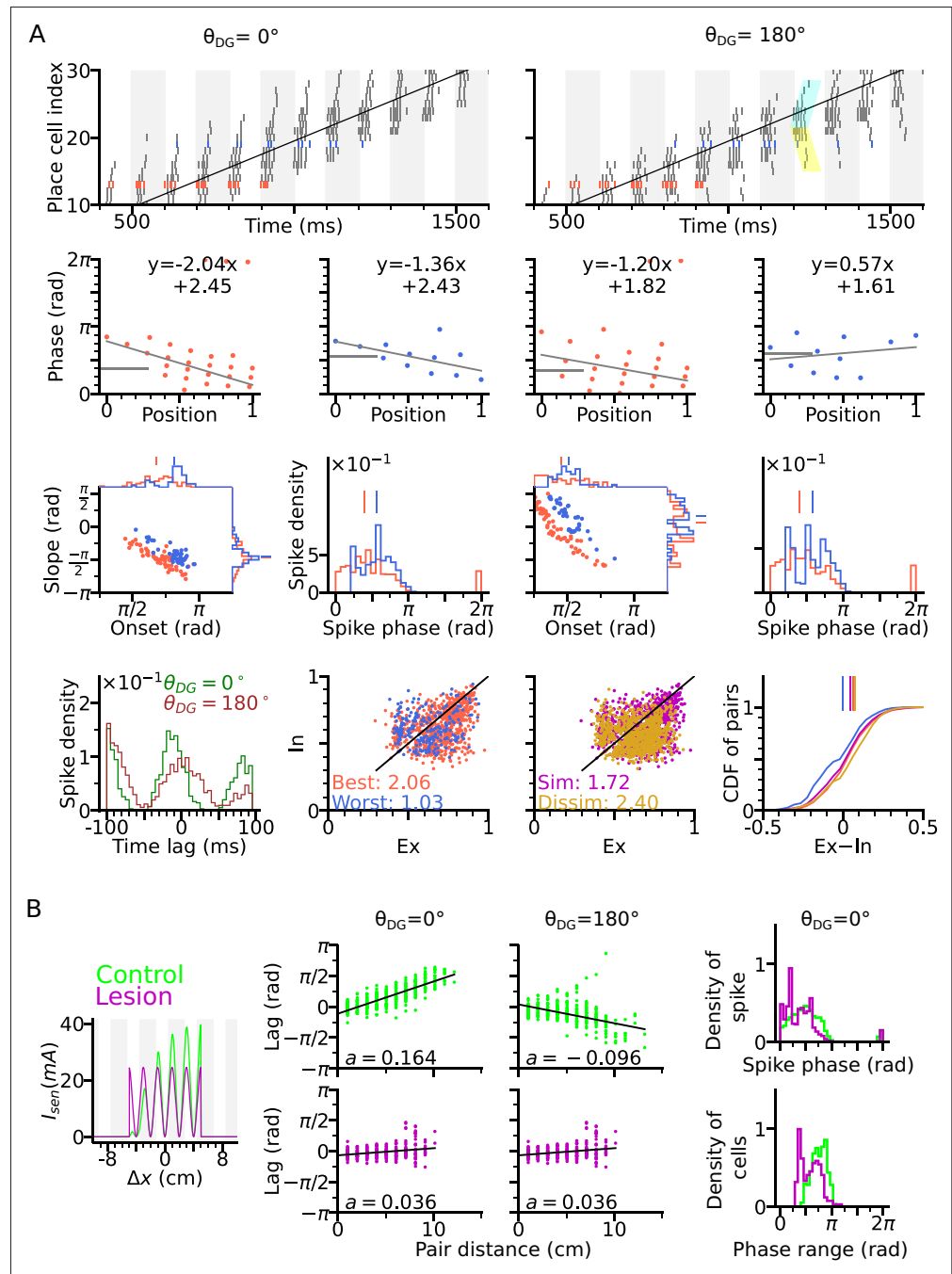
Figure 6. Extrinsically driven theta correlations can be temporally organized by sensorimotor drive alone without CA3-CA3 recurrence. Simulations were performed without CA3-CA3 recurrence but with stronger spatial input. (**A**) Same as *Figure 3*. Extrinsically driven theta correlations and phase precession are still present. (**B**) Same as *Figure 4*. DG is still integral to the theta compression in a network model without CA3-CA3 recurrence.

taking input from a model with DG-loop connectivity at $\theta_{DG} = 0°$, and one without DG-loop connectivity to serve as a control only having access to extrinsic sequences (*Figure 7A*). Non-moving spatial inputs were applied to the CA3 place cells at the centers of with-loop and no-loop populations and their spike patterns in subsequent theta cycle were used as training patterns, mimicking a situation in which network activity is evoked without sensory-motor input as, for example in a offline situation before the animal walks or maybe even has seen the environment. The training patterns have only
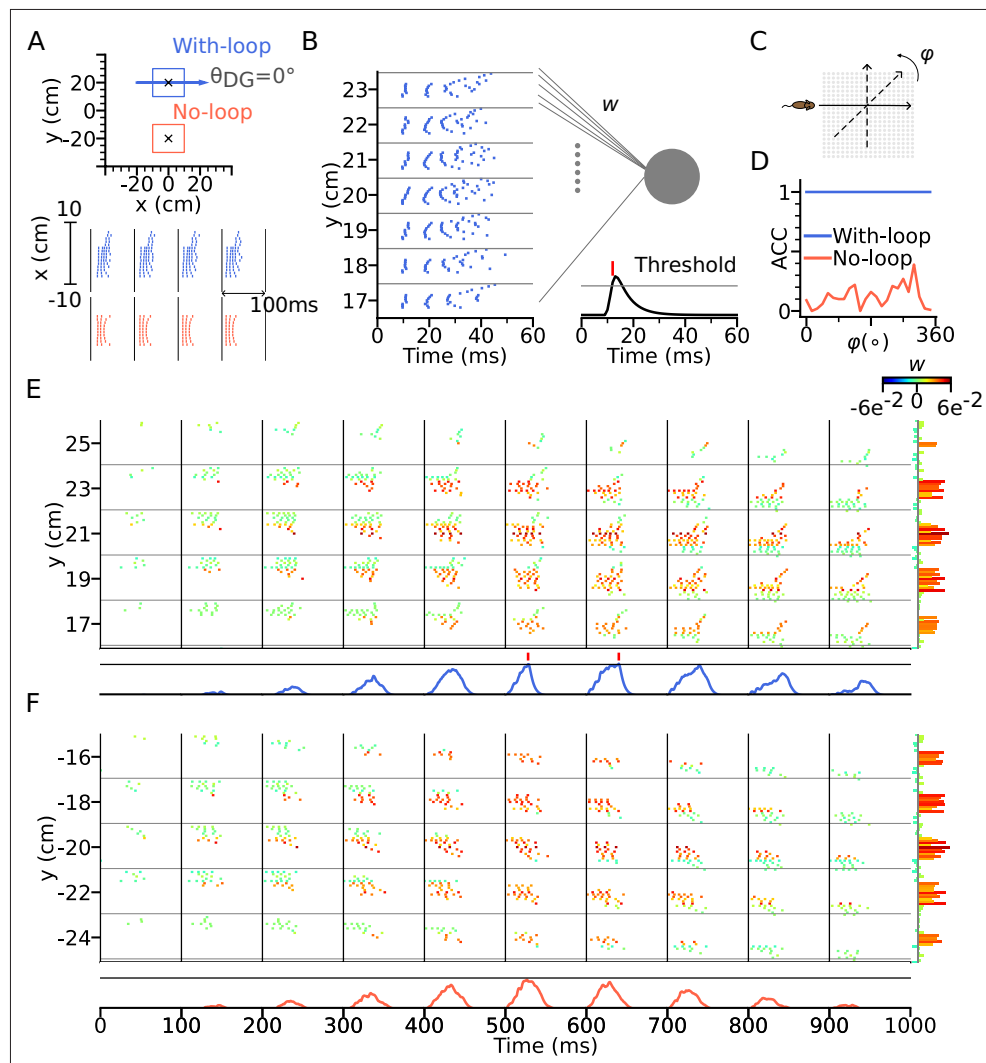
Figure 7. Intrinsic sequences provide a stable landmark for positional decoding using a tempotron. (**A**) Top: Two tempotrons are trained for place cell populations within the top (with DG loop; blue) and bottom (no DG loop; red) squares, to recognize the presence of the corresponding sequence activities. DG-loop rightward projection is indicated by blue arrow and only exists in the blue square. Non-moving spatial inputs are applied to the CA3 network centered at the two locations (marked by black crosses) to evoke spike sequences for training. Bottom: Resulting spikes of the place cell network zoomed in to the subset of field centers from x=-10 to x=10 for y=+20 (with-loop, top raster plot) and y=-20 (no-loop, bottom). Each theta cycle is one (+) training pattern, which the tempotron is trained to detect by eliciting a spike. (**B**) Example training pattern with spikes of place cells from x=-10 to x=10 (in each rectangular row) fixed at different values of y. Only one theta cycle is shown. Each place cell delivers spikes to the dendrite of the tempotron, producing post-synaptic potentials (PSPs) at the soma (line plot at the bottom). Synaptic weights are adapted by the tempotron learning rule such that PSPs can cross the threshold (gray line) and fire for the detection of the sequence. After the tempotron has fired, the PSPs will be shunted. (**C**) Sequence detection is tested while the simulated animal ran on a trajectory with varying direction (φ) from 0° to 360° with a 15° increment to detect the presence of the sequence. (**D**) Detection accuracies (ACC) for with-loop (red line) and no-loop (blue line) input populations. Note that the tempotron cannot detect the no-loop sequences when tested on trajectories at various angles. (**E**) Detection of the intrinsic sequence for a trajectory $\varphi = 180°$ for the DG-loop condition. Spike raster is shown for every two horizontal rows of place cells in the arena and color-coded by the synaptic weights (see color bar on the right). Tempotron soma potential is shown at the bottom for each pattern. (**F**) Same as E, but for no-loop inputs. The tempotron remains silent.

The online version of this article includes the following figure supplement(s) for figure 7:

Figure supplement 1. Decoding of positional landmarks using tempotrons in a network model without CA3-CA3 recurrence.
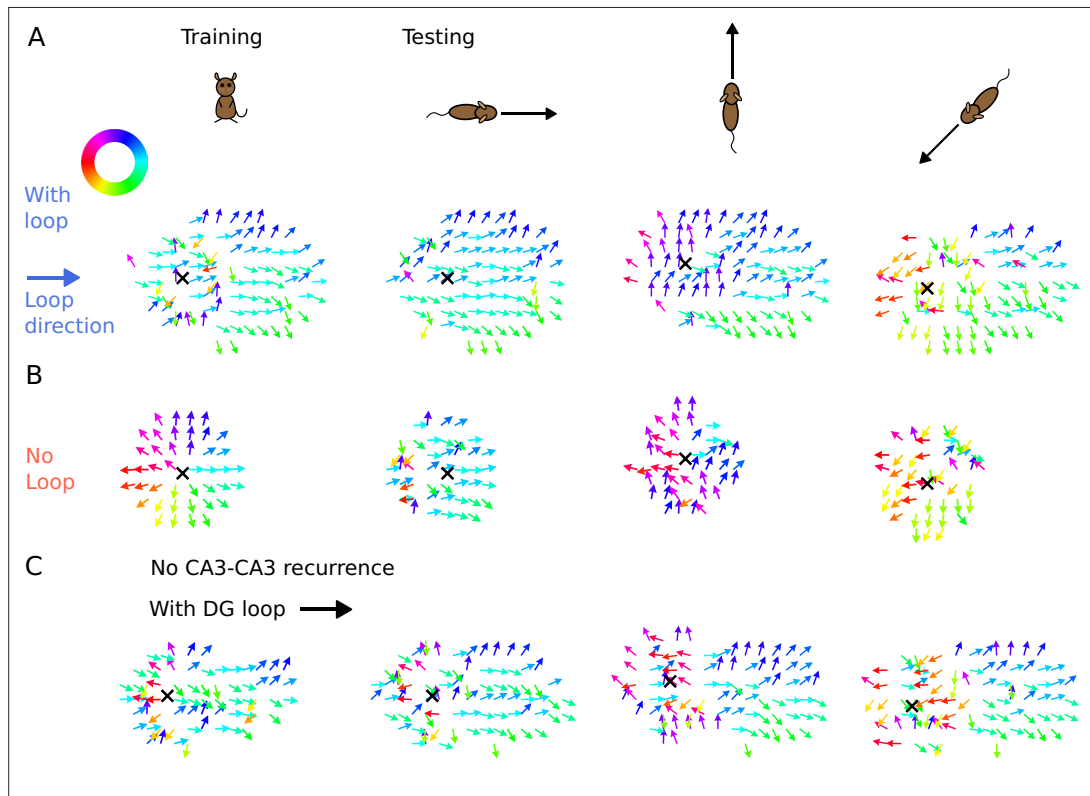
Figure 8. Illustration of spike time gradients in one theta cycle (500–600 ms) with and without DG loop. (**A**) Time gradients with a DG loop projecting to the rightward direction ($\theta_{DG} = 0°$). Each arrow is located at a CA3 place field center. The arrow direction indicates the spike time gradient, equivalently the 'travelling direction' of sequence activity, which is calculated as the sum of the directions to the 8 neighbouring field centers, weighted by the difference between their mean spike times in one theta cycle. Arrow direction is color-coded according to the color wheel. Black cross marks the instantaneous position of the animal. The first column shows the training condition when a non-moving spatial stimulus is applied. The three columns on the right show the testing condition when the rat is running in various directions. The sequence mostly propagates rightwards, following the DG-loop direction even when the animal runs in different directions. (**B**) Same as A without a DG loop. Sequences propagate outward from the animal position as a concentric travelling wave during training. During testing, spike time gradients follow the running direction. (**C**) Same as A, using the network model without CA3 recurrence. As in *Figure 6*, the extrinsic sequence is driven solely by the STF mechanism of the spatial input. Intrinsic sequences in this model still remain invariant to running directions and function as spatial landmarks.

(+) labels, which the tempotrons are trained to recognize by firing a spike (*Figure 7B*). We then test the tempotrons with spike patterns induced by the animal running on different trajectories through the trained location with running directions varying between 0° to 360° (*Figure 7C*). All spikes in each training and testing pattern are individually jittered by adding a noise term $\sigma \sim \mathcal{N}(0, (2\text{ ms})^2)$ for 100 times, producing 100 samples for each pattern. The tempotron is said to successfully recognize the sequence of a trajectory direction if any of the theta cycles throughout the trajectory elicits a spike, that is while running, the readout cell would evaluate the place cell sequence in every theta cycle for information on the trained landmark.

We found that the tempotron trained on the intrinsic sequence from the DG loop is able to recognize the sequence patterns produced for all running directions, while the tempotron trained without a DG-loop fails to identify the extrinsic sequences most of the time (see accuracies in *Figure 7D*). The reason is that the spike patterns induced by intrinsic sequences remain similar to the training pattern despite being approached in other directions (see sequential contributions in *Figure 7E*), while spike patterns for the no-loop condition are different between training and testing (*Figure 7F*). The distinction is further illustrated in *Figure 8*, where 2-d maps of spike time gradients in one theta cycle are plotted with respect to running direction/training condition. Sequences always contain components that propagate along the projection direction of DG loop, while, without such a loop, they only propagate along the running direction. Moreover, during training, the no-loop condition evokes concentric

waves, reflecting the 2-d topology of the recurrent weights. Similar results were also achieved without CA3-CA3 recurrence (*Figure 7—figure supplement 1* and *Figure 8C*).

Our results show that intrinsic sequences can provide a stable correlation signal which allows reliable decoding of locations through temporal correlations. The intrinsic temporal code remains detectable even when mixed with extrinsic sequences.

Discussion

We presented a model of hippocampal theta sequences in 2-d environments, suggesting that both extrinsic and intrinsic mechanisms are required to explain experimental reports that phase precession and spike timing correlations are non-homogeneous across running directions. Although phase precession already becomes directional by including direction-dependent sensory input into a purely extrinsic model, directionality of spike timing correlations cannot be explained by such a model. We, however, demonstrated that the correlation preference could be implemented by fixed recurrent loops via a model DG layer. We further supported the model assumptions by showing that DG lesions plus compensatory sensory drive can abolish the theta compression effect in CA3 spiking activity (*Ahmadi et al., 2022*). By employing a spike-based temporal pattern decoder (tempotron), we showed that the intrinsic sequences could function as stable signatures that act as anchors of the spatial code.

Early intrinsic models (*Tsodyks et al., 1996*) were challenged owing to their inability to generate phase precession in backward travel (*Figure 1E*, also see *Cei et al., 2014*), as well as the predominantly extrinsic correlations observed in CA1 (*Huxter et al., 2008*). In our hybrid model, phase precession still occurs during backward travel ($\theta_{DG} = 180°$) but at a lower probability as indicated by the larger fraction of positive phase-position slopes (*Figure 3H*). Also, extrinsic sequences still dominate over intrinsic sequences as indicated by the majority of field pairs being extrinsic (*Figure 3J*). Both the reduced expression of phase precession in reverse runs and the dominance of extrinsic sequences are in accordance with the experimental data (*Yiu et al., 2022*).

The mixture of extrinsic and intrinsic mechanisms in our theory, naturally gives rise to the directionality of spike correlations and phase distributions. As the trajectory aligns itself with the DG loops, the ratio of intrinsic to extrinsic sequences increases. As a result, spike correlations become more rigid and the phase distribution is shifted upward due to the accumulated synaptic transmission delay from the reverberating activity between CA3 and DG populations. Adding directional sensory input activates extrinsic sequences in the best direction more strongly, and hence, leads to an association between best-angle (worst-angle) pairs and extrinsicity (intrinsicity). These predictions of our model are corroborated by past reports of higher spike phases in the non-preferred arm of a T-maze (*Kay et al., 2020*) as well as the association of rigid correlations with upward shifts in spike phases and an increase in worst-angle pairs (*Yiu et al., 2022*). The experimental distinction between extrinsic and intrinsic components in theta sequences has so far only been achieved in pairs of place cells, owing to the limited number of simultaneously recorded place cells with overlapping fields. Our model predicts that similar distinctions should also be observable in higher-order statistics, obtained from overlapping fields of a larger number of cells. Instead of correlation lags, we suggest to use temporal pattern detection methods (e.g. *Chenani et al., 2019*) to unveil the respective sequence contributions.

Since intrinsic sequences can also propagate outside the trajectory (out-of-field firing in *Figure 5*) and activate place cells non-locally, our model predicts direction-dependent expansion of place fields, or even multiple place fields, with the intrinsic sequence's target location exhibiting late spike phases and higher phase precession onsets. Remote activation during locomotion has already been observed in a previous study (*Sasaki et al., 2018*) where CA3 place cells preferentially firing at one arm of the maze were also activated at reward locations at other arms. In our model, only short-range intrinsic connectivity was considered, thus, place field boundaries expand locally but in a skewed manner matching the sequence direction. Skewness of place fields has been reported by a number of studies (*Mehta et al., 1997*; *Shen et al., 1997*; *Mehta et al., 2000*; *Ekstrom et al., 2001*; *Lee et al., 2004*; *Burke et al., 2008*; *Cei et al., 2014*; *Roth et al., 2012*; *Dong et al., 2021*) showing place fields to be asymmetrically expanded opposite to the direction of travel. This effect was connected to plasticity as it develops after repeated traversal, and due to its dependence on NMDA receptor activation (*Ekstrom et al., 2001*; *Burke et al., 2008*; *Shen et al., 1997*). These plasticity studies show that the hippocampal place code is shaped by intrinsic synaptic computations including temporal activation patterns in theta sequences (*Feng et al., 2015*). Apart from being conducted on linear tracks and not

2-d environments, most of this work focused on CA1 and associated Schaffer collateral plasticity. Yet some prior studies (*Lee et al., 2004*; *Roth et al., 2012*) did show that place fields in CA3 were more skewed than in CA1, which our model would explain by CA3 expressing more intrinsic sequences than CA1 consistent with prior experimental observations (*Yiu et al., 2022* reported ratios of extrinsically to intrinsically driven cell pairs of 1.44 in CA1 and 1.23 in CA3).

A further prediction of hard-wired DG loops is that the resulting activity patterns (intrinsic sequences) should not remap under conditions of global or partial remapping (*Leutgeb et al., 2004*). Instead the same intrinsic sequence components should be observable in multiple environments, however, they might only be seen in a small fraction and thus this prediction is potentially hard to test.

The back-projection from CA3 to DG is a crucial anatomical prerequisite of our model, but was rarely explored compared to the feed-forward inputs via the perforant pathway. The proposed CA3-DG recurrent structure of this model, albeit simplified, is consistent with the anatomical evidence. Pyramidal cells in CA3 innervate the mossy cells at the DG hilus (*Scharfman, 1994*; *Scharfman, 2016*), which then project to granule cells through both excitatory and inhibitory pathways (*Hsu et al., 2016*; *Scharfman, 1995*; *Larimer and Strowbridge, 2008*; *Soriano and Frotscher, 1994*), and subsequently back to CA3 pyramidal cells. An optogenetic study (*Hsu et al., 2016*) showed that the net effect of mossy cells on granule cells was predominantly inhibitory, suggesting that the DG ensembles excited by mossy cell synaptic drive are sparsified by suppressing unwanted out-of-ensemble activity. Indeed, past studies showed that reliable excitatory effect could be observed when granule cells were depolarized (*Scharfman, 1995*) and when they received back-propagation of sharp wave bursts from CA3 population (*Penttonen et al., 1998*). This indicates that the excitatory recurrent pathway from CA3 via DG exists and might allow activity reverberation between two layers. While our model, owing to its simplicity and generality does not require any DG specific pathways and would work equally well with any other anatomical interpretation of the CA3 feedback, we hypothesize the intrinsic feedback connectivity to arise via the DG, particularly because DG lesions were shown to eliminate the coordinated temporal structure of CA3 activity and to be instrumental to sequence organization (*Figure 4* and *Ahmadi et al., 2022*).

Our model assumed a connectivity pattern in the DG loops, in which neurons activate the neighbours along a specific direction, as inspired by Hebb's phase sequences (*Hebb, 1949*) and, hence, replay of the loop would activate a spatially plausible virtual trajectory. The loop connectivity could either arise from previous learning, or might be present already beforehand (*Dragoi and Tonegawa, 2013*), with spatial topology inherited by associating 2-d sensory features to cell ensembles in the loop (*Leibold, 2020*). The resulting topology can exhibit discontinuous long-range jumps to other locations (*Sasaki et al., 2018*) or consist of a discrete set of (behaviorally relevant) locations (*Pfeiffer, 2022*).

Different from other phase precession models, we also included heading direction as part of the sensory input, as inspired by past literature that CA1 (*Markus et al., 1995*; *Acharya et al., 2016*; *Stefanini et al., 2020*), CA3 (*Mankin et al., 2019*), and DG place cells (*Stefanini et al., 2020*) exhibit directional selectivity in firing rates, potentially inherited from the upstream head-direction cells in the medial entorhinal cortex (*Giocomo et al., 2014*) and postsubiculum (*Taube et al., 1990*). As a result, the directional drive immediately translates to phase directionality in theta sequences, partly contributing to the upward shift of the phase distribution in the worst angles. Such phase directionality arises naturally from the intracellular dynamics of a spike-based model, where stronger depolarization causes earlier spiking. This phase-rate dependence has already been used in previous models (*Harris et al., 2002*; *Mehta et al., 2002*; *Thurley et al., 2008*), where the increasing depolarization within place fields directly relates to decreasing spike phases. The causal effect of firing rate on spike phases, however, was disputed by *Huxter et al., 2003* as they showed that precession slopes and spike phases remained the same between high- and low-spiking runs, suggesting that the phase is not single-handedly determined by firing rate. In our model, firing rate is determined by both low-phase spiking from sensory input and high-phase spike arrivals of DG-CA3 loops, both producing opposing effects on the phase distribution. Thus, depending on the strength and geometry of the DG-CA3 connectivity, spike phases are not fully determined by firing rate.

By using a tempotron to decode the spike patterns, we show that the spike patterns of intrinsic sequences can serve as a stable landmark which remains decodable across multiple running directions. The invariant temporal patterns could serve as anchors of spatial memories in a novel environment,

since place fields only stabilize after the animal becomes familiar with the environment (*Wilson and McNaughton, 1993*). The pre-existing sequence motifs, even at times when the spikes of the neurons are not spatially tuned to a location, can still encode the position based on their temporal relations alone. The idea has previously been spelled out (*Cheng, 2013*) and numerically verified (*Leibold, 2020*; *Parra-Barrero and Cheng, 2023*) with multiple fixed sequences that form a decodable spatial representation.

Intrinsic sequences may thus act as a scaffold around which a new spatial code can be built for new but similar behavioral contexts, where similarity could for example be identified by a salient feature. Once the behavioral context of a situation changes, new intrinsic sequences would be observable. These intrinsic landmarks need to be stable across time, as shown for some dentate gyrus representations (*Hainmueller and Bartos, 2018*). We speculate that offline sequences observed during replay and preplay (for review see *Buhry et al., 2011*; *Dragoi and Tonegawa, 2014*), would correspond to the intrinsic activity patterns and indicate the context expectation of an animal (which can be detected by a tempotron). The functional roles of intrinsic sequences may thus not be limited to spatial memories. While, in the spatial domain, intrinsic sequences could be interpreted as spatial trajectories (*Kay et al., 2020*; *Sasaki et al., 2018*), virtual non-spatial trajectories could represent working memories contents (*Jensen et al., 1996*) available for general decision making processes.

Methods

Key resources table

Reagent type (species) or resource	Designation	Source or reference	Identifiers	Additional information
Software, algorithm	Python	Python Software Foundation	https://www.python.org/ RRID:SCR_008394	
Software, algorithm	Linear-circular regression	*Kempter et al., 2012*		The algorithm is customized to our analyses
Software, algorithm	Tempotron	*Gütig and Sompolinsky, 2006*		The algorithm is customized to our analyses

Neuronal model

Generation of neuronal action potentials is modelled according to *Izhikevich, 2003*. The soma potential v and the adaptation variable u of unit i at time t (in ms) follows the equations:

$$\dot{v}_i(t) = 0.04 v_i^2(t) + 5 v_i(t) + 140 - u_i(t) + I_i(t)$$

$$\dot{u}_i(t) = a \left[b\, v_i(t) - u_i(t) \right]$$

$$I_i(t) = I_i^R(t) + I_i^S(t) - I^\theta(t)$$

Any time $v(t)$ crosses the threshold 30 mV from below, we register a spike for the neuron and reset the soma potential by $v(t) \leftarrow c$ and the adaptation variable by $u(t) \leftarrow u(t) + d$. For the excitatory pyramidal place cells, we use parameters $a = 0.035$, $b = 0.2$, $c = -60$ mV, $d = 8$, which provides the neuron with burst firing characteristics. For the inhibitory interneurons, the parameters were $a = 0.02$, $b = 0.25$, $c = -65$ mV, and $d = 2$, which corresponds to fast spiking patterns. $I(t)$ is the total sum of recurrent $I^R(t)$, sensory $I^S(t)$ and oscillatory theta input

$$I^\theta(t) = 7 \left[1 + \cos\left(\frac{2\pi t}{100 \text{ ms}} \right) \right] / 2$$

We chose to use the phenomenological spike generation model of *Izhikevich, 2003*, since it allows to adjust burst firing properties with only few parameters that efficiently emulate the bifurcation structure of spike generation. Synaptic integration below threshold is not affected by the spike generation model and will thus be treated by conventional synaptic models.

Spatial input

The place field centers $\mathbf{p}_i^{CA3} = \left[x_i^{CA3}(t), y_i^{CA3}(t) \right]$ of $80 \times 80 = 6400$ excitatory CA3 cells equally tile the 80 by 80 cm square arena. Place cell firing rates are modelled direction-sensitive, with preferred heading

directions ψ_i^{CA3} semi-randomized among each 2×2 tile of place cells by randomly rotating a set of four equally spaced direction angles by a uniformly distributed angle ξ, that is

$$\left[\psi_i^{CA3}, \psi_{i+1}^{CA3}, \psi_{i+2}^{CA3}, \psi_{i+3}^{CA3}\right] = \left[0°, 90°, 180°, 270°\right] + \xi \mod 360° \, .$$

The sensory input $J_i^S(t)$ into the i-th neuron depends on the instantaneous position, $\mathbf{p}(t) = \left[x(t), y(t)\right]$, and heading direction $\psi(t)$ of the animal as

$$J_i^S(t) \quad = \begin{cases} A_i^S(t)\, I^{MEC}(t) & \text{if } d\big(\mathbf{p}(t), \mathbf{p}_i^{CA3}\big) \leqq 5 \text{ cm} \\ 0 & \text{if } d\big(\mathbf{p}(t), \mathbf{p}_i^{CA3}\big) > 5 \text{ cm} \end{cases}$$

$$A_i^S(t) = A^{pos} + A^{dir} \exp\Big(\cos\big(\psi(t) - \psi_i^{CA3}\big) - 1 \Big)$$

$$I^{MEC}(t) = \frac{1}{2}\left[1 + \cos\left(\frac{2\pi t}{100 \text{ ms}} + 70° \frac{\pi}{180°} \right) \right] \, ,$$

where A^{pos} is the amplitude of positional tuning and $d(\cdot)$ computes the Euclidean distance between two positions. The positional tuning curve is implemented as a rectangular box function, where the place cell only receives sensory input if the animal is within 5 cm from the field center. Directional tuning is implemented as an additional amplitude gain A^{dir} to the positional current depending on the circular difference between the animal's heading and the neuron's preferred heading direction ψ_i^{CA3}. The sensory input is assumed to be modulated by theta oscillations from medial entorhinal cortex (MEC) $I^{MEC}(t)$ with a phase shift of 70° (*Mizuseki et al., 2009*).

The sensory input J^S is subsequently transformed to the input current I^S via short-term facilitation (STF)

$$\dot{s}_i^F(t) = \frac{(S_0^F - s_i^F(t))}{\tau^F} + (S_1^F - s_i^F(t))\Phi^F J_i^S(t)$$

$$I_i^S = J_i^S(t)\left[s_i^F(t)\right]^2 \, ,$$

where the facilitation variable s_i^F decays to S_0^F with a time constant $\tau^F = 500$ ms and increases to S_1^F when the sensory input J_i^S is present. The time constant τ^F of facilitation of neocortical synapses was in the range suggested by *Tsodyks et al., 1998* following previous experimental reports (*Mejías and Torres, 2008*; *Zucker and Regehr, 2002*). Φ^F controls the strength of the STF. The facilitation variable is squared to include non-linear interactions in presynaptic calcium dynamics. As a result, facilitated sensory input I_i^S increases over time and becomes stronger in the later part of the field, thus effectively generating a spatially graded input strength.

Note that only the CA3 place cells receive the sensory input. $I_i^S(t)$ is not applied to the place cells in DG and all of the inhibitory interneurons.

CA3 recurrent connections

Place cells in CA3 connect with each other by excitatory synapses. The excitatory synaptic current $I_i^E(t)$ is conductance-based, and follows the equations:

$$\dot{g}_i^E(t) = \frac{-g_i^E(t)}{\tau^E} + \frac{1}{N_J} \sum_{j,f} W_{ij}\, s_j^D(t)\, \delta(t - t_j^{(f)} - \tau_0) \tag{1}$$

$$I_i^E(t) = \left[V^E - v_i(t)\right] g_i^E(t) \tag{2}$$

The conductance g_i^E of a post-synaptic cell i is increased by the spike arrivals at times $t_j^{(f)}$ from the pre-synaptic cell j, and decay with a time constant $\tau^E = 12$ ms. $N_J = 6,400$ is the number of presynaptic place cells, $V^E = 0$ mV is the reversal potential of the excitatory synapses and $\tau_0 = 2$ ms is the synaptic transmission delay.

The synaptic weights W_{ij} from cell j to cell i depend on the distance between place cell centers and on the similarity of their preferred heading angles, i.e.,

$$W_{ij}^{\text{CA3}} = J_{ij} \left\{ B^{\text{pos}} + B^{\text{dir}} \exp\left[K^{\text{CA3}}\left(\cos(\psi_i^L - \psi_j^L) - 1 \right) \right] \right\} \exp\left(\frac{-d(\mathbf{p}_i^{CA3}, \mathbf{p}_j^{CA3})^2}{2\sigma^2} \right) ,$$

where B^{pos} and $\sigma = 2$ cm correspond to the maximum strength and width of the location-specific interaction, respectively. B^{dir} and K^{CA3} control the maximum strength and the concentration of the directional dependence, respectively. J_{ij} models the rightward asymmetry of the cell connections, which was only turned on when we simulated the 2-d variant of *Tsodyks et al., 1996* model in *Figure 1C–F* and otherwise turned off in the rest of our analysis.

If rightward asymmetry is ON,	$J_{ij} = 1$ if $x_j^{CA3} < x_i^{CA3}$, else 0
If rightward asymmetry is OFF,	$J_{ij} = 1$

Furthermore, the recurrent synaptic conductances underwent short-term synaptic depression (STD), as was proposed in *Romani and Tsodyks, 2015* to serve as sequence generator in 2-d space. The mechanism penalizes the recurrent input into the place cells behind the animal. As a result, the differential recurrence strengths translate to a gradient of spike phases and produces extrinsic sequences in the direction of travel. We model the STD by the variable $s_i^D(t)$ which represents the available synaptic resource and follows the dynamics:

$$\dot{s}_i^D(t) = \frac{1 - s_i^D(t)}{\tau^D} - U^D \delta(t - t_i^{(f)}) ,$$

where s_i^D recovers to 1 with a time constant $\tau^D = 500$ ms and is depleted by a fraction U^D every time a spike occurs. The recovery time constant is comparable to experimentally obtained values of cortical neurons (200–800 ms in *Tsodyks and Markram, 1997*; *Markram et al., 1998*; *Abbott et al., 1997*; *Zucker and Regehr, 2002*) and previous modelling work (450–800 ms in *Romani and Tsodyks, 2015*; *Haga and Fukai, 2018*; *Tsodyks and Markram, 1997*; *Tsodyks et al., 1998*). The STD only applies to synaptic connections when presynaptic cells are CA3 place cells. $s_i^D(t)$ is fixed at 1 when the presynaptic cells are inhibitory interneurons or DG place cells.

DG layer

We simulated $N_{\text{DG}} = 40 \times 40 = 1600$ place cells in the DG layer, with place field centers equally tiling the environment. The DG cells do not receive sensory input. Their positional ($x_i^{\text{DG}}, y_i^{\text{DG}}$) and directional ($\psi_i^{\text{DG}}$) tunings are determining synaptic strengths to and from the CA3 layer. The directional tuning is semi-randomized as described for CA3. The synaptic current dynamics follow *Equations (1) and (2)*. Excitatory synaptic weights from CA3 place cells to DG place cells are defined as

$$W_{ij}^{\text{CA3}-\text{DG}} = C_j^{CA3} B^{\text{DG}} \exp\left[K^{\text{DG}}\left(\cos(\psi_i^{\text{DG}} - \psi_j^{CA3}) - 1 \right) \right] \exp\left(\frac{-d(\mathbf{p}_i^{DG}, \mathbf{p}_j^{CA3})^2}{2\sigma^2} \right) ,$$

which are dependent on the differences in the place field centers and preferred heading angles between the CA3 and DG populations. The variable C_j^{CA3} strengthens outgoing connections from CA3 place cells on the path corresponding to the intrinsic sequence by choosing

$$C_j^{\text{CA3}} = \max_{k \in [-10,10]} \left\{ \exp\left(\frac{-d(\mathbf{p}_k^C, \mathbf{p}_j^{CA3})^2}{2\sigma^2} \right) \right\} ,$$

where $\mathbf{p}_k^C$ varies with the intrinsic path direction θ_{DG} as $\mathbf{p}_k^C = [2k \cos(\theta_{\text{DG}}), 2k \sin(\theta_{\text{DG}})]$.

The excitatory synaptic strengths from DG to CA3 are chosen such that DG cells project back to CA3 cells with place field centers shifted by a vector $\mathbf{r} = [4 \cos(\theta_{\text{DG}}), 4 \sin(\theta_{\text{DG}})]$ of fixed length of 4 cm along the intrinsic path, that is

$$W_{ij}^{\text{DG}-\text{CA3}} = B^{\text{DG}} \exp\left[K^{\text{DG}}\left(\cos(\psi_i^{\text{CA3}} - \psi_j^{\text{DG}}) - 1 \right) \right] \exp\left(\frac{-d(\mathbf{p}_i^{CA3} - \mathbf{r}, \mathbf{p}_j^{DG})^2}{2\sigma^2} \right) . \qquad (3)$$

The model has no synaptic connections between DG excitatory neurons.

Inhibitory synapses

The model additionally contains $N_I = 250$ inhibitory interneurons (denoted as Inh) each for the CA3 and the DG layer. They provide inhibitory feedback separately to the excitatory cells within each layer (CA3-Inh-CA3 and DG-Inh-DG). The dynamics of their synaptic currents mirrors the excitatory synapses, that is

$$\dot{g}_i^I(t) = \frac{-g_i^I(t)}{\tau^I} + \frac{1}{N_I} \sum_j^{N_I} W_{ij}^{X-Y} \delta(t - t_j^{(f)} - \tau_0)$$

$$I_i^I(t) = \left[V^I - v_i(t) \right] g_i^I(t) ,$$

with $\tau^I = 10$ ms, $V^I = -80$ mV. CA3 and DG have all-to-all connections to their inhibitory populations with uniformly randomized strengths, i.e. $W_{ij}^{X-Y} = W_0^{X-Y} \xi$, with $\xi \sim \mathcal{U}(0, 1)$ is the maximum synaptic strength, and the notation X-Y corresponds to Inh-CA3 and Inh-DG connections. There is no synaptic connection between inter-neurons, that is $W^{Inh-Inh} = 0$.

The total recurrent current entering each excitatory neuron is thus the sum of the excitatory and inhibitory current:

$$I_i^R(t) = I_i^I(t) + I_i^E(t)$$

Table 1. Model parameters used in simulations according to Figure panels. In, Ex, C. and L. refer to intrinsic, extrinsic, control and lesion respectively.

Name \ Figure	1 (In)	1 (Ex)	2	3	4 (C.)	4 (L.)	5	6A	6B (C.)	6B (L.)	7
A^{pos}	7.5	9.0	6.5					9.5	7.5		6.5
A^{dir}	0	6						9	8		6
S_0^F	1	0			1.25	0	0.25	0		1.25	0
S_1^F	1	2			1.25	2	1.5	2		1.25	2
Φ^F	0	0.001			0	0.001				0	0.001
B^{pos}	1100	0									
B^{dir}	0	2000	1500				2000	0			1500
K^{CA3}	0	1									
J_{ij}	ON	OFF									
U^D	0	0.9	0.7								
N_{DG}	0			40×40 = 1600							
B^{DG}	0		3000			0	4000		4000	0	4000
K^{DG}	0		1								
N_I	0		250								
$W_0^{CA3-Inh}$	0		50								
$W_0^{Inh-CA3}$	0		5								
W_0^{DG-Inh}	0			350							
W_0^{Inh-DG}	0			35							

Excitatory synapses to interneurons

Interneurons only receive all-to-all excitatory currents from their respective layer. Those currents are modelled according to *Equations 1; 2*. The synaptic weights are constant and denoted by $W_0^{CA3-Inh}$ and W_0^{DG-Inh}.

Parameters of the models

Model parameters that are adjusted in different analyses are listed in *Table 1*. The values of the synaptic weights and spatial input were chosen to allow for a large range of phase precession and stability of the network activity. For the analyses including the DG layer, weights are adjusted to allow coexistence of extrinsic and intrinsic sequences.

Cross-correlation analysis

Cross-correlation represents the probability that a spike of one place cell would occur following a certain time lag from the spike of the another cell. Cross-correlation is always empirically computed as a histogram of time lags between spike pairs with a resolution of 5ms in a window of 200ms. Throughout the present study, the direction of a time lag is designated as the lag of the first encountered cell relative to the next cell along the trajectory, except in *Figure 1*, where the direction of time lag follows the cell order along the 0°, 45°, and 90° trajectory in each comparison group, and in *Figure 2*, where the time lag direction is from left to right cells.

Correlation lag is derived by band-pass (4–12 Hz) filtering the cross-correlation histogram and applying a Hilbert transform on the filtered signal. The phase of the analytic signal at time lag 0 is the correlation lag.

Extrinsicity and intrinsicity

We apply quantitative measures for the extrinsic or intrinsic nature of cross-correlations in a pair of place fields following *Yiu et al., 2022*. We compare the cross-correlation histograms of a field pair for a running direction along the DG loop (θ_{DG}) and opposite to the loop ($\theta_{DG} + 180°$). Extrinsicity (Ex) is computed as the Pearson's correlation (r) between two cross-correlation histograms, and intrinsicity (In) between the histogram of θ_{DG} and the horizontally flipped histogram of $\theta_{DG} + 180°$. The Pearson's correlation is then transformed ($r' = (r + 1)/2$) to be in the range of 0 and 1. An extrinsic correlation would give an extrinsicity near 1, since the effect of DG loop is minimal and correlation histograms are similar in both θ_{DG} and $\theta_{DG} + 180°$ directions. A pair of place fields with intrinsic correlation would see cross-correlation horizontally flipped in the $\theta_{DG} + 180°$ condition due to the large effect of DG loop, and hence, give an intrinsicity near 1. We classify a pair as extrinsic if its extrinsicity exceeds intrinsicity, and vice versa.

Tempotron

A tempotron is a neuronally inspired classifier (readout neuron) whose dendritic synaptic weights can be adapted to recognize temporal patterns of spikes arriving at the afferents (for details, see *Gütig and Sompolinsky, 2006*). Briefly, the soma potential of the tempotron follows the equations

$$V(t) = \sum_i w_i \sum_{i,f} K(t - t_i^{(f)})$$

$$K(t - t_i^{(f)}) = V_0(\exp[-(t - t_i^{(f)})/\tau] - \exp[-(t - t_i^{(f)})/\tau_r]),$$

where w_i is the adaptable weight of the afferent fiber conveying spikes from place cell i to the tempotron. $K(t - t_i^{(f)})$ is a post-synaptic potential (PSP) kernel with decay and rising time constants of $\tau = 5$ ms and $\tau_r = 1.25$ ms respectively. V_0 is a factor which normalizes the PSP kernel to 1. A spike is said to occur if $V(t)$ crosses the firing threshold $V_\Theta = 2$ from below. After threshold crossing, the afferents will be shunted and spike arrivals will not evoke more PSPs for the rest of the pattern. A pattern is defined as the set of spike times of all the pre-synaptic place cells in a theta cycle (100 ms).

The weight w_i follows the update rule

$$\Delta w_i = 0.01 \sum_{t_i^{(f)} < t_{max}} K\left(t_{max} - t_i^{(f)}\right)$$

$$w_i \leftarrow w_i + \Delta w_i \qquad \text{If a } (+) \text{ pattern does not elicit a spike,}$$

$$w_i \leftarrow w_i - \Delta w_i \qquad \text{If a } (-) \text{ pattern does not elicit a spike,}$$

where t_{max} is the time at the peak of the soma potential $V(t)$. The learning rule assigns credit to the afferents based on spike timing. Spike times closer to the peak are considered to have higher contribution to the tempotron firing, hence their afferents are incremented by a larger step. After training, spike times with similar temporal correlations as the (+) patterns would be able to evoke enough PSP in the tempotron's soma and elicit a spike as a positive response of binary classification, while those similar to (-) patterns would not elicit a spike from the tempotron.

We trained the tempotrons to identify the spike patterns of place cells at locations with and without intrinsic connectivity separately. To this end, we modified our network such that DG loops are present at the upper half of the arena, spanning the space from x=-20cm to x=+20 cm at y=+20 cm in direction $\theta_{DG} = 0°$, while the loop is absent in the lower half of the arena.

During training, we applied 'non-moving' spatial inputs to the CA3 place cells at the with-loop (0 cm, 20 cm) and no-loop (0 cm, −20 cm) locations for 1 s, as if the animal were standing still at the locations, evoking the activities representing the two location cues. For computational efficiency, we restricted our analysis to the populations of CA3 place cells within the 20 cm squared boxes centered at the two locations. Each population contains 400 pre-synaptic cells, forming the input space for the tempotron. The spikes from the with-loop population will train the first tempotron and those from the no-loop population will train the second tempotron. Prior to training, the input spikes are sub-divided to 10 patterns based on their theta cycles. Each pattern has a window of 100 ms. We added noise to the patterns by jittering the spikes with Gaussian noise $\mathcal{N} \sim (0, (2\,\text{ms})^2)$ for 100 times. As a result, each tempotron receives 10×100 = 1,000 training patterns from the activity evoked by the location. All training patterns are (+) patterns and there is no (-) pattern.

After training, trajectories (20 cm long, 1 s duration) with running directions from 0° to 360° with 15° increment were simulated to cross each of the locations. The trajectories produce a mix of extrinsic and intrinsic sequences in the with-loop population and only extrinsic sequences in the no-loop population. The patterns evoked by the running trajectories were separately applied to the tempotrons. The input spikes for testing were also subdivided into theta cycles and jittered in the same manner as during training, forming 1000 testing patterns for each running direction. A sequence is said to be correctly identified if the tempotron fires at at least 1 out of 10 theta cycles along the trajectory. The accuracy rate for each running direction of trajectory is computed across the 100 jittered realizations.

Code availability

We used Python 3 for simulations and visualization. The codes are available from a github repository (https://github.com/yyhhoi/directionalnet, copy archived at *Yiu, 2023*).

Additional information

Author contributions

Yuk-Hoi Yiu, Conceptualization, Data curation, Software, Writing - original draft, Writing - review and editing; Christian Leibold, Conceptualization, Supervision, Funding acquisition, Writing - original draft, Writing - review and editing

65

Author ORCIDs
Yuk-Hoi Yiu http://orcid.org/0000-0002-1997-9277
Christian Leibold http://orcid.org/0000-0002-4859-8000

Additional files

Supplementary files
• MDAR checklist

Data availability
The current manuscript is a computational study, so no data have been generated for this manuscript. We used Python 3 for simulations and visualization. The codes are available from https://github.com/yyhhoi/directionalnet (copy archived at *Yiu, 2023*).

References

Abbott LF, Varela JA, Sen K, Nelson SB. 1997. Synaptic depression and cortical gain control. *Science* **275**:220–224. DOI: https://doi.org/10.1126/science.275.5297.221, PMID: 8985017

Acharya L, Aghajan ZM, Vuong C, Moore JJ, Mehta MR. 2016. Causal influence of visual cues on Hippocampal Directional selectivity. *Cell* **164**:197–207. DOI: https://doi.org/10.1016/j.cell.2015.12.015, PMID: 26709045

Ahmadi S, Sasaki T, Sabariego M, Leibold C, Leutgeb S, Leutgeb JK. 2022. Distinct Roles of Dentate Gyrus and Medial Entorhinal Cortex Inputs for Phase Precession and Temporal Correlations in the Hippocampal CA3 Area. *bioRxiv*. DOI: https://doi.org/10.1101/2022.06.07.491859

Berretta N, Jones RS. 1996. Tonic facilitation of glutamate release by presynaptic N-methyl-D-aspartate autoreceptors in the entorhinal cortex. *Neuroscience* **75**:339–344. DOI: https://doi.org/10.1016/0306-4522(96)00301-6, PMID: 8931000

Brunel N, Trullier O. 1998. Plasticity of directional place fields in a model of rodent CA3. *Hippocampus* **8**:651–665. DOI: https://doi.org/10.1002/(SICI)1098-1063(1998)8:6<651::AID-HIPO8>3.0.CO;2-L, PMID: 9882023

Buhry L, Azizi AH, Cheng S. 2011. Reactivation, replay, and preplay: how it might all fit together. *Neural Plasticity* **2011**:203462. DOI: https://doi.org/10.1155/2011/203462, PMID: 21918724

Burke SN, Maurer AP, Yang Z, Navratilova Z, Barnes CA. 2008. Glutamate receptor-mediated restoration of experience-dependent place field expansion plasticity in aged rats. *Behavioral Neuroscience* **122**:535–548. DOI: https://doi.org/10.1037/0735-7044.122.3.535, PMID: 18513124

Cei A, Girardeau G, Drieu C, Kanbi KE, Zugaro M. 2014. Reversed theta sequences of hippocampal cell assemblies during backward travel. *Nature Neuroscience* **17**:719–724. DOI: https://doi.org/10.1038/nn.3698, PMID: 24667574

Chenani A, Sabariego M, Schlesiger MI, Leutgeb JK, Leutgeb S, Leibold C. 2019. Hippocampal CA1 replay becomes less prominent but more rigid without inputs from medial entorhinal cortex. *Nature Communications* **10**:1341. DOI: https://doi.org/10.1038/s41467-019-09280-0, PMID: 30902981

Cheng S. 2013. The CRISP theory of hippocampal function in episodic memory. *Frontiers in Neural Circuits* **7**:88. DOI: https://doi.org/10.3389/fncir.2013.00088, PMID: 23653597

Dong C, Madar AD, Sheffield MEJ. 2021. Distinct place cell dynamics in CA1 and CA3 encode experience in new environments. *Nature Communications* **12**:2977. DOI: https://doi.org/10.1038/s41467-021-23260-3, PMID: 34016996

Dragoi G, Buzsáki G. 2006. Temporal encoding of place sequences by hippocampal cell assemblies. *Neuron* **50**:145–157. DOI: https://doi.org/10.1016/j.neuron.2006.02.023, PMID: 16600862

Dragoi G, Tonegawa S. 2011. Preplay of future place cell sequences by hippocampal cellular assemblies. *Nature* **469**:397–401. DOI: https://doi.org/10.1038/nature09633, PMID: 21179088

Dragoi G, Tonegawa S. 2013. Distinct preplay of multiple novel spatial experiences in the rat. *PNAS* **110**:9100–9105. DOI: https://doi.org/10.1073/pnas.1306031110

Dragoi G, Tonegawa S. 2014. Selection of preconfigured cell assemblies for representation of novel spatial experiences. *Philosophical Transactions of the Royal Society of London. Series B, Biological Sciences* **369**:20120522. DOI: https://doi.org/10.1098/rstb.2012.0522, PMID: 24366134

Ekstrom AD, Meltzer J, McNaughton BL, Barnes CA. 2001. NMDA receptor antagonism blocks experience-dependent expansion of hippocampal "place fields." *Neuron* **31**:631–638. DOI: https://doi.org/10.1016/s0896-6273(01)00401-9, PMID: 11545721

Feng T, Silva D, Foster DJ. 2015. Dissociation between the experience-dependent development of hippocampal theta sequences and single-trial phase precession. *The Journal of Neuroscience* **35**:4890–4902. DOI: https://doi.org/10.1523/JNEUROSCI.2614-14.2015, PMID: 25810520

Foster DJ, Wilson MA. 2007. Hippocampal theta sequences. *Hippocampus* **17**:1093–1099. DOI: https://doi.org/10.1002/hipo.20345, PMID: 17663452

Giocomo LM, Stensola T, Bonnevie T, Van Cauter T, Moser M-B, Moser EI. 2014. Topography of head direction cells in medial entorhinal cortex. *Current Biology* **24**:252–262. DOI: https://doi.org/10.1016/j.cub.2013.12.002, PMID: 24440398

Gütig R, Sompolinsky H. 2006. The tempotron: a neuron that learns spike timing-based decisions. *Nature Neuroscience* **9**:420–428. DOI: https://doi.org/10.1038/nn1643, PMID: 16474393

Haga T, Fukai T. 2018. Recurrent network model for learning goal-directed sequences through reverse replay. *eLife* **7**:e34171. DOI: https://doi.org/10.7554/eLife.34171, PMID: 29969098

Hainmueller T, Bartos M. 2018. Parallel emergence of stable and dynamic memory engrams in the hippocampus. *Nature* **558**:292–296. DOI: https://doi.org/10.1038/s41586-018-0191-2, PMID: 29875406

Harris KD, Henze DA, Hirase H, Leinekugel X, Dragoi G, Czurkó A, Buzsáki G. 2002. Spike train dynamics predicts theta-related phase precession in hippocampal pyramidal cells. *Nature* **417**:738–741. DOI: https://doi.org/10.1038/nature00808, PMID: 12066184

Harvey CD, Collman F, Dombeck DA, Tank DW. 2009. Intracellular dynamics of hippocampal place cells during virtual navigation. *Nature* **461**:941–946. DOI: https://doi.org/10.1038/nature08499, PMID: 19829374

Hebb DO. 1949. *The Organization of Behavior: A Neuropsychological Theory* New York: Wiley.

Hsu TT, Lee CT, Tai MH, Lien CC. 2016. Differential recruitment of dentate Gyrus Interneuron Types by Commissural Versus Perforant Pathways. *Cerebral Cortex* **26**:2715–2727. DOI: https://doi.org/10.1093/cercor/bhv127, PMID: 26045570

Huxter J, Burgess N, O'Keefe J. 2003. Independent rate and temporal coding in hippocampal pyramidal cells. *Nature* **425**:828–832. DOI: https://doi.org/10.1038/nature02058, PMID: 14574410

Huxter JR, Senior TJ, Allen K, Csicsvari J. 2008. Theta phase–specific codes for two-dimensional position, trajectory and heading in the hippocampus. *Nature Neuroscience* **11**:587–594. DOI: https://doi.org/10.1038/nn.2106

Izhikevich EM. 2003. Simple model of spiking neurons. *IEEE Transactions on Neural Networks* **14**:1569–1572. DOI: https://doi.org/10.1109/TNN.2003.820440, PMID: 18244602

Jaramillo J, Kempter R. 2017. Phase precession: a neural code underlying episodic memory? *Current Opinion in Neurobiology* **43**:130–138. DOI: https://doi.org/10.1016/j.conb.2017.02.006, PMID: 28390862

Jensen O, Idiart MA, Lisman JE. 1996. Physiologically realistic formation of autoassociative memory in networks with theta/gamma oscillations: role of fast NMDA channels. *Learning & Memory* **3**:243–256. DOI: https://doi.org/10.1101/lm.3.2-3.243

Kay K, Chung JE, Sosa M, Schor JS, Karlsson MP, Larkin MC, Liu DF, Frank LM. 2020. Constant sub-second cycling between representations of possible futures in the Hippocampus. *Cell* **180**:552–567.. DOI: https://doi.org/10.1016/j.cell.2020.01.014, PMID: 32004462

Kempter R, Leibold C, Buzsáki G, Diba K, Schmidt R. 2012. Quantifying circular-linear associations: hippocampal phase precession. *Journal of Neuroscience Methods* **207**:113–124. DOI: https://doi.org/10.1016/j.jneumeth.2012.03.007, PMID: 22487609

Larimer P, Strowbridge BW. 2008. Nonrandom local circuits in the dentate gyrus. *The Journal of Neuroscience* **28**:12212–12223. DOI: https://doi.org/10.1523/JNEUROSCI.3612-08.2008, PMID: 19020015

Lee AK, Wilson MA. 2002. Memory of sequential experience in the hippocampus during slow wave sleep. *Neuron* **36**:1183–1194. DOI: https://doi.org/10.1016/s0896-6273(02)01096-6, PMID: 12495631

Lee I, Rao G, Knierim JJ. 2004. A double dissociation between hippocampal subfields: differential time course of CA3 and CA1 place cells for processing changed environments. *Neuron* **42**:803–815. DOI: https://doi.org/10.1016/j.neuron.2004.05.010, PMID: 15182719

Leibold C. 2020. A model for navigation in unknown environments based on A reservoir of hippocampal sequences. *Neural Networks* **124**:328–342. DOI: https://doi.org/10.1016/j.neunet.2020.01.014, PMID: 32036230

Leutgeb S, Leutgeb JK, Treves A, Moser MB, Moser EI. 2004. Distinct ensemble codes in hippocampal areas CA3 and CA1. *Science* **305**:1295–1298. DOI: https://doi.org/10.1126/science.1100265, PMID: 15272123

Lisman J, Redish AD. 2009. Prediction, sequences and the hippocampus. *Philosophical Transactions of the Royal Society of London. Series B, Biological Sciences* **364**:1193–1201. DOI: https://doi.org/10.1098/rstb.2008.0316, PMID: 19528000

Mankin EA, Thurley K, Chenani A, Haas OV, Debs L, Henke J, Galinato M, Leutgeb JK, Leutgeb S, Leibold C. 2019. The hippocampal code for space in Mongolian gerbils. *Hippocampus* **29**:787–801. DOI: https://doi.org/10.1002/hipo.23075, PMID: 30746805

Markram H, Wang Y, Tsodyks M. 1998. Differential signaling via the same axon of neocortical pyramidal neurons. *PNAS* **95**:5323–5328. DOI: https://doi.org/10.1073/pnas.95.9.5323

Markus EJ, Qin YL, Leonard B, Skaggs WE, McNaughton BL, Barnes CA. 1995. Interactions between location and task affect the spatial and directional firing of hippocampal neurons. *The Journal of Neuroscience* **15**:7079–7094. DOI: https://doi.org/10.1523/JNEUROSCI.15-11-07079.1995, PMID: 7472463

Maurer AP, Vanrhoads SR, Sutherland GR, Lipa P, McNaughton BL. 2005. Self-motion and the origin of differential spatial scaling along the septo-temporal axis of the hippocampus. *Hippocampus* **15**:841–852. DOI: https://doi.org/10.1002/hipo.20114, PMID: 16145692

Maurer AP, McNaughton BL. 2007. Network and intrinsic cellular mechanisms underlying theta phase precession of hippocampal neurons. *Trends in Neurosciences* **30**:325–333. DOI: https://doi.org/10.1016/j.tins.2007.05.002

67

Mehta MR, Barnes CA, McNaughton BL. 1997. Experience-dependent, asymmetric expansion of hippocampal place fields. *PNAS* **94**:8918–8921. DOI: https://doi.org/10.1073/pnas.94.16.8918

Mehta MR, Quirk MC, Wilson MA. 2000. Experience-dependent asymmetric shape of hippocampal receptive fields. *Neuron* **25**:707–715. DOI: https://doi.org/10.1016/s0896-6273(00)81072-7, PMID: 10774737

Mehta MR, Lee AK, Wilson MA. 2002. Role of experience and oscillations in transforming a rate code into a temporal code. *Nature* **417**:741–746. DOI: https://doi.org/10.1038/nature00807, PMID: 12066185

Mejías JF, Torres JJ. 2008. The role of synaptic facilitation in spike coincidence detection. *Journal of Computational Neuroscience* **24**:222–234. DOI: https://doi.org/10.1007/s10827-007-0052-8, PMID: 17674172

Mizuseki K, Sirota A, Pastalkova E, Buzsáki G. 2009. Theta oscillations provide temporal windows for local circuit computation in the entorhinal-hippocampal loop. *Neuron* **64**:267–280. DOI: https://doi.org/10.1016/j.neuron.2009.08.037, PMID: 19874793

Parra-Barrero E, Cheng S. 2023. Learning to predict future locations with internally generated theta sequences. *PLOS Computational Biology* **19**:e1011101. DOI: https://doi.org/10.1371/journal.pcbi.1011101, PMID: 37172053

Penttonen M, Kamondi A, Sik A, Acsády L, Buzsáki G. 1998. Feed-forward and feed-back activation of the dentate gyrus in vivo during dentate spikes and sharp wave bursts. *Hippocampus* **7**:437–450. DOI: https://doi.org/10.1002/(SICI)1098-1063(1997)7:4<437::AID-HIPO9>3.0.CO;2-F

Pfeiffer BE. 2022. Spatial learning drives Rapid Goal representation in Hippocampal ripples without place field Accumulation or Goal-Oriented Theta Sequences. *The Journal of Neuroscience* **42**:3975–3988. DOI: https://doi.org/10.1523/JNEUROSCI.2479-21.2022, PMID: 35396328

Rivas J, Gaztelu JM, García-Austt E. 1996. Changes in hippocampal cell discharge patterns and theta rhythm spectral properties as a function of walking velocity in the guinea pig. *Experimental Brain Research* **108**:113–118. DOI: https://doi.org/10.1007/BF00242908, PMID: 8721159

Romani S, Tsodyks M. 2015. Short-term plasticity based network model of place cells dynamics. *Hippocampus* **25**:94–105. DOI: https://doi.org/10.1002/hipo.22355, PMID: 25155013

Roth ED, Yu X, Rao G, Knierim JJ. 2012. Functional differences in the backward shifts of CA1 and CA3 place fields in novel and familiar environments. *PLOS ONE* **7**:e36035. DOI: https://doi.org/10.1371/journal.pone.0036035, PMID: 22558316

Sasaki T, Piatti VC, Hwaun E, Ahmadi S, Lisman JE, Leutgeb S, Leutgeb JK. 2018. Dentate network activity is necessary for spatial working memory by supporting CA3 sharp-wave ripple generation and prospective firing of CA3 neurons. *Nature Neuroscience* **21**:258–269. DOI: https://doi.org/10.1038/s41593-017-0061-5, PMID: 29335604

Scharfman HE. 1994. Evidence from simultaneous intracellular recordings in rat hippocampal slices that area CA3 pyramidal cells innervate dentate hilar mossy cells. *Journal of Neurophysiology* **72**:2167–2180. DOI: https://doi.org/10.1152/jn.1994.72.5.2167, PMID: 7884451

Scharfman HE. 1995. Electrophysiological evidence that dentate hilar mossy cells are excitatory and innervate both granule cells and interneurons. *Journal of Neurophysiology* **74**:179–194. DOI: https://doi.org/10.1152/jn.1995.74.1.179, PMID: 7472322

Scharfman HE. 2016. The enigmatic mossy cell of the dentate gyrus. *Nature Reviews. Neuroscience* **17**:562–575. DOI: https://doi.org/10.1038/nrn.2016.87, PMID: 27466143

Shen J, Barnes CA, McNaughton BL, Skaggs WE, Weaver KL. 1997. The effect of aging on experience-dependent plasticity of hippocampal place cells. *The Journal of Neuroscience* **17**:6769–6782. DOI: https://doi.org/10.1523/JNEUROSCI.17-17-06769.1997, PMID: 9254688

Skaggs WE, McNaughton BL. 1996. Replay of neuronal firing sequences in rat hippocampus during sleep following spatial experience. *Science* **271**:1870–1873. DOI: https://doi.org/10.1126/science.271.5257.1870, PMID: 8596957

Skaggs WE, McNaughton BL, Wilson MA, Barnes CA. 1996. Theta phase precession in hippocampal neuronal populations and the compression of temporal sequences. *Hippocampus* **6**:149–172. DOI: https://doi.org/10.1002/(SICI)1098-1063(1996)6:2<149::AID-HIPO6>3.0.CO;2-K, PMID: 8797016

Soriano E, Frotscher M. 1994. Mossy cells of the rat fascia dentata are glutamate-immunoreactive. *Hippocampus* **4**:65–69. DOI: https://doi.org/10.1002/hipo.450040108, PMID: 7914798

Stefanini F, Kushnir L, Jimenez JC, Jennings JH, Woods NI, Stuber GD, Kheirbek MA, Hen R, Fusi S. 2020. A distributed Neural Code in the dentate Gyrus and in CA1. *Neuron* **107**:703–716.. DOI: https://doi.org/10.1016/j.neuron.2020.05.022, PMID: 32521223

Taube JS, Muller RU, Ranck JB. 1990. Head-direction cells recorded from the postsubiculum in freely moving rats. I. Description and quantitative analysis. *The Journal of Neuroscience* **10**:420–435. DOI: https://doi.org/10.1523/JNEUROSCI.10-02-00420.1990, PMID: 2303851

Thurley K, Leibold C, Gundlfinger A, Schmitz D, Kempter R. 2008. Phase precession through synaptic facilitation. *Neural Computation* **20**:1285–1324. DOI: https://doi.org/10.1162/neco.2008.07-06-292, PMID: 18085985

Tsodyks MV, Skaggs WE, Sejnowski TJ, McNaughton BL. 1996. Population dynamics and theta rhythm phase precession of hippocampal place cell firing: A spiking neuron model. *Hippocampus* **6**:271–280. DOI: https://doi.org/10.1002/(SICI)1098-1063(1996)6:3<271::AID-HIPO5>3.0.CO;2-Q, PMID: 8841826

Tsodyks MV, Markram H. 1997. The neural code between neocortical pyramidal neurons depends on neurotransmitter release probability. *PNAS* **94**:719–723. DOI: https://doi.org/10.1073/pnas.94.2.719, PMID: 9012851

Tsodyks M, Pawelzik K, Markram H. 1998. Neural networks with dynamic synapses. *Neural Computation* **10**:821–835. DOI: https://doi.org/10.1162/089976698300017502, PMID: 9573407

Wilson MA, McNaughton BL. 1993. Dynamics of the hippocampal ensemble code for space. *Science* **261**:1055–1058. DOI: https://doi.org/10.1126/science.8351520, PMID: 8351520

Yiu YH, Leutgeb JK, Leibold C. 2022. Directional tuning of phase precession properties in the Hippocampus. *The Journal of Neuroscience* **42**:2282–2297. DOI: https://doi.org/10.1523/JNEUROSCI.1569-21.2021, PMID: 35110389

Yiu YH. 2023. Directionalnet. swh:1:rev:7d87577ddb437b0c5941a29fae1b2f1bed909b33. Software Heritage. https://archive.softwareheritage.org/swh:1:dir:fc7e003de3035b1738384de92550691dc47192b0;origin=https://github.com/yyhhoi/directionalnet;visit=swh:1:snp:e48933641593f2607bf458b9c564be6f773d2abf;anchor=swh:1:rev:7d87577ddb437b0c5941a29fae1b2f1bed909b33

Zucker RS, Regehr WG. 2002. Short-term synaptic plasticity. *Annual Review of Physiology* **64**:355–405. DOI: https://doi.org/10.1146/annurev.physiol.64.092501.114547, PMID: 11826273

69

2.2.1 Supplementary figures
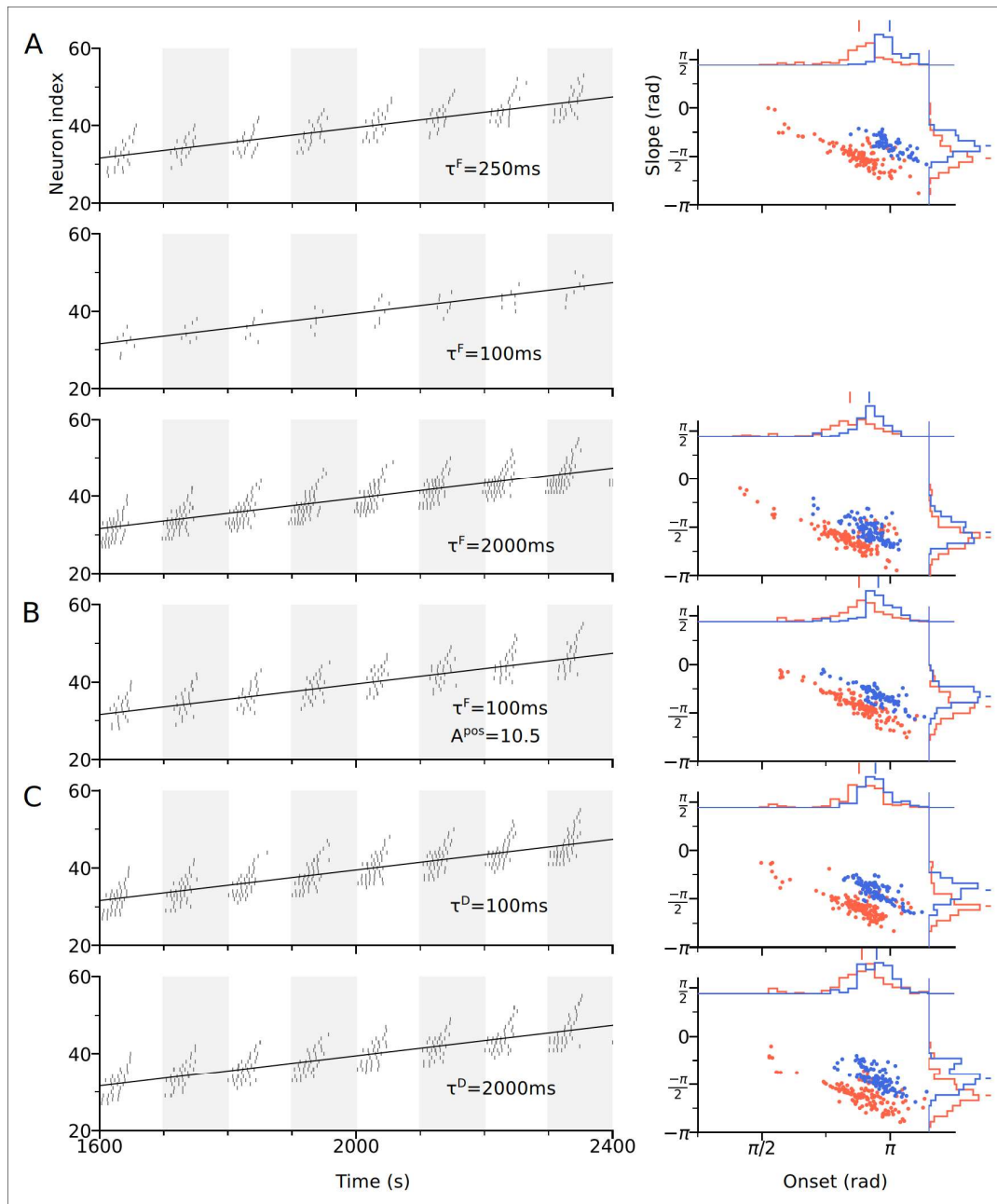
Figure 3—figure supplement 1. Effects of STF and STD time constants on theta sequences. (**A**) Left: Spike raster plot of the CA3 place cells along the trajectory at $= \tau^F$ 250ms (top row), 100ms (middle) and 2000ms (bottom). Conventions follow **Figure 3B**. Decreasing τ^F allows faster recovery time of the sensory input to its resting value, $S_0^F = 0$ thus reducing the amount of depolarization and firing rate, as compared to $= \tau^F$ 500ms used in **Figure 3**. However, the temporal order of theta sequences remains unchanged. Right: Distribution of slopes and onsets of phase precession in the best and worst directions, following the conventions of **Figure 3D**. At $= \tau^F$ 100ms, the place cells do not generate enough spikes (spike count ≤ 5) for the analysis. (**B**) Increasing the amount of sensory input A^{pos} by 60% (from 6.5 in **Figure 3** to 10.5 here) can restore the firing activity and theta sequences at $\tau^F = 100$ms. (**C**) Changing the STD time constant τ^D does not noticeably affect the temporal structure of theta sequences and the distribution of phase precession slopes and onsets.
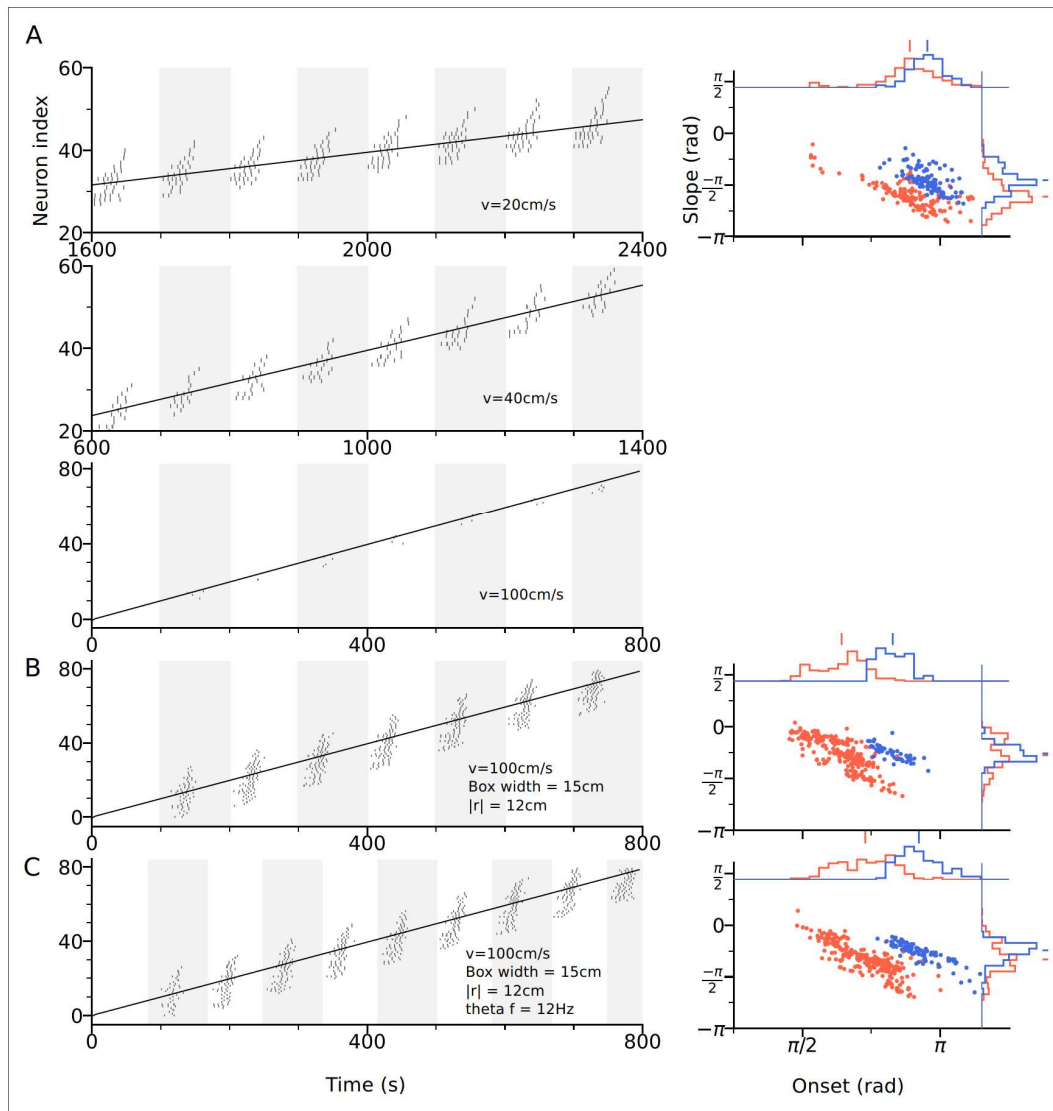
Figure 3—figure supplement 2. Effects of running speed on theta sequences. (**A**) Left: Spike raster plot of the CA3 place cells along the trajectory at running speed v=20 cm/s (top row), 40cm/s (middle) and 100cm/s (bottom). Conventions follow *Figure 3B*. As place cells are traversed at increasing velocities, their firing rate decreases due to insufficient depolarization. Right: Distribution of slopes and onsets of phase precession in the best and worst directions, following the conventions of *Figure 3D*. Only the distribution for running speed at 20 cm/s is shown. At running speed 40 cm/s and 100 cm/s, the place cells do not generate enough spikes (spike count ≤ 5) for the analysis. (**B**) Theta sequences at high running speed (100 cm/s) could be produced by a larger place field size (width of box-shaped input is increased to 15 cm compared to 5 cm in *Figure 3*) and longer DG projection (|**r**|=12 cm compared to 4 cm in *Figure 3*). Phase precession slopes and onsets are lower than in (**A**). (**C**) Increasing theta frequency to 12 Hz can recover the decrease of phase precession slope and onset from the high running speed (*Rivas et al., 1996*; *Maurer et al., 2005*). Model parameters are the same as *Figure 3* in the main text unless specified at the bottom right of the raster plots.
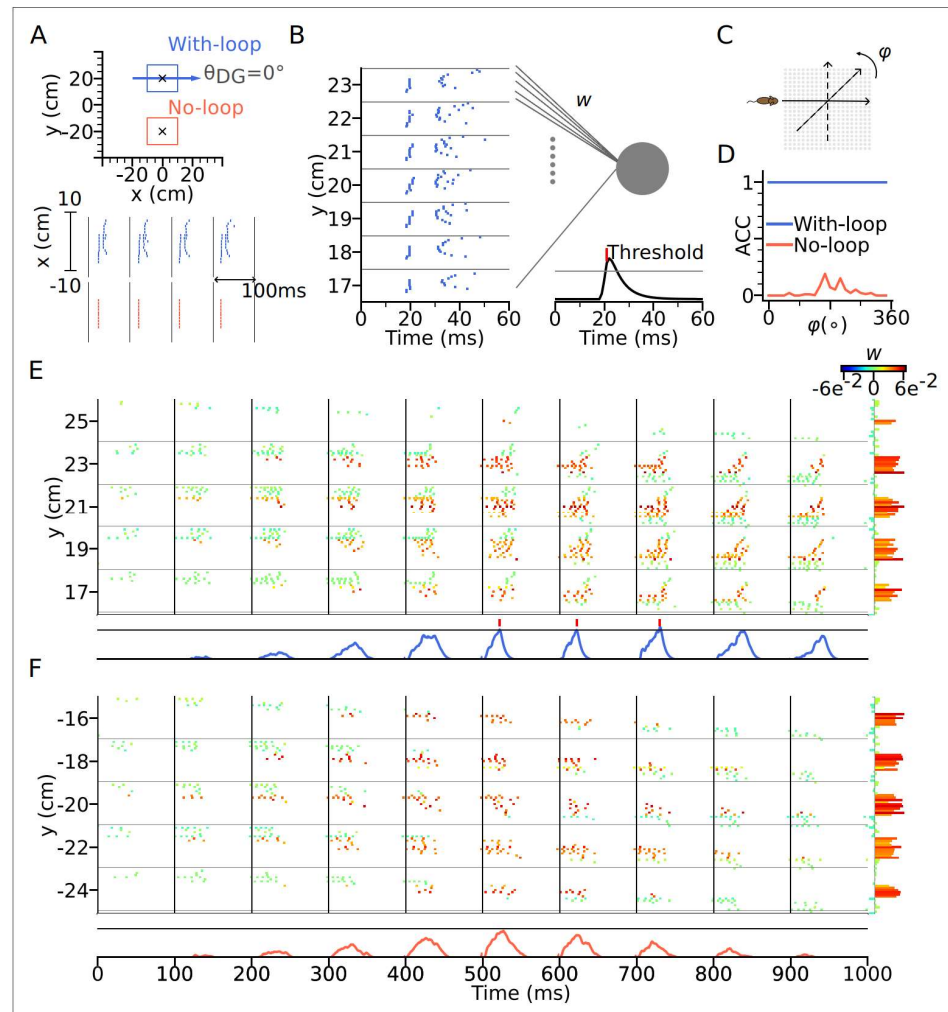
Figure 7—figure supplement 1. Decoding of positional landmarks using tempotrons in a network model without CA3-CA3 recurrence. Figure labels are the same as in *Figure 7*. Compared to the parameters in *Figure 7*, here CA3-CA3 weights were disabled ($B^{\text{dir}} = 0$), but spatial input was increased during testing ($A^{\text{dir}} = 14$, $S_0^F = 0.25$ $S_1^F = 1.5$) and DG-loop strengths were increased ($B^{\text{DG}} = 5500$).

3 Discussion

This thesis explores the spatial representation of temporal sequences in the hippocampus at the theta timescale. Previously, theta sequences were thought to represent the running trajectory, connecting past, present, and future locations. In our first manuscript Yiu et al. (2022), we provided evidence that some place cells exhibit theta correlations that are independent of the running trajectory, reflecting the underlying dynamics of the intra-hippocampal network. The discovery of intrinsic sequences also agrees with the findings of Pastalkova et al. (2008), which showed that the hippocampus could internally generate theta sequences without being dependent on changing external environmental cues or self-motion inputs. In the subsequent manuscript Yiu and Leibold (2023), we proposed that the heterogeneity of theta correlations could be explained by the concurrent propagation of extrinsic and intrinsic sequences, as modeled by a CA3-DG network. Most significantly, our research has elucidated how 1D temporal sequences can represent a 2D spatial environment. Sequences that propagate along 1D manifolds within the 2D topology of place cells—either through the running trajectory (extrinsic) or via pathways determined by the network connectivity (intrinsic)—can support spatial memories through temporal coding.

In this section, we first compare the key findings between the two manuscripts. We then discuss the implications of these key findings, their connections with other aspects of hippocampal temporal coding, and review other theoretical frameworks in light of our results. The thesis concludes with suggestions for future research directions.

3.1 Comparison of key findings between the two manuscripts

3.1.1 Extrinsic and intrinsic sequences

Both manuscripts utilized quantitative measures of extrinsicity and intrinsicity to estimate the trajectory dependency of theta sequences. Our model's prediction of the heterogeneous nature of theta sequences, as presented in the first manuscript, aligns with the trends observed in our experimental findings within the CA3 region, detailed in the second manuscript. Notably, theta sequences exhibit stronger intrinsicity under conditions of minimal sensorimotor inputs (at the non-preferred or worst angle) and when cell pairs are more closely connected and exhibiting similar preferred directions. These results further highlight the dual aspects of temporal codes coordinated separately by external sensorimotor inputs and internal network dynamics.

3.1.2 Directionality of phase precession

Both manuscripts demonstrated that phase precession exhibits directionality, particularly showing higher spike phases when the animal runs in the worst angle. Our model in the second manuscript mechanistically explains the high spike phase as resulting from

both weaker depolarization from spatial inputs and the more pronounced manifestation of intrinsic sequences at the worst angle. This is consistent with the interrelationship between intrinsic sequences, higher spike phases, and worst angles observed in our first manuscript.

3.1.3 Difference between CA1 and CA3

The experimental data in our first manuscript showed that both intrinsically and extrinsically driven theta correlations could be observed across all CA regions. However, compared to CA3, the CA1 region exhibits a stronger bias towards extrinsic sequences, as well as a less significant effect in the directionality of phase precession. While our model in the second manuscript primarily focuses on accounting for the theta sequences observed in CA3, the theoretical framework could also predict consistent observations in the CA1 region. Lacking a recurrent network structure such as back-projections between the CA3 and DG layers, CA1 is likely to produce more extrinsic sequences and thus exhibit less pronounced directionality in phase precession.

Nonetheless, our experimental findings in the first manuscript shows that the intrinsic sequence is still present in the CA1 region despite its primarily feed-forward structure. It can be speculated that the intrinsic sequence in CA1 is derived from upstream CA3 inputs, which are more intrinsically driven and contain higher spike phases. This explanation aligns with the theoretical framework proposed by Chance (2012), which suggested that the high-phase spiking of CA1 place cells during phase precession originated from upstream CA3 inputs.

3.2 Implications of intrinsic sequences

3.2.1 Non-local representations

Both manuscripts point towards the existence of non-local temporal sequences at the theta timescale. "Non-local" refers to temporal sequences that do not represent the immediate nearby locations (as seen in the out-of-field firing in Yiu and Leibold (2023)) or do not follow the actual behavioral order of the animal, as seen in intrinsic theta correlations (Yiu et al., 2022, Yiu and Leibold, 2023).

Historically, non-local hippocampal sequences have been identified primarily at the SWR timescales. A prominent example is hippocampal replay, where sequences may unfold in a forward order from start to goal (Lee and Wilson, 2002, Pfeiffer and Foster, 2013) or in reverse, retracing locations back to the starting point after the animal reaches the goal (Foster and Wilson, 2006, Diba and Buzsáki, 2007). Intriguingly, replay can also activate spatial pathways from previous environments, termed "remote replay," or be initiated by mere visual observation of another rat's task performance (Carr et al., 2011, Mou et al.,

2022).

Theta sequences, despite the forward sweep into prospective locations, have generally been considered as "local", since the prospective representation typically includes only the current position's surroundings and, as a result, is thought to be influenced by sensorimotor input and actual behavioral sequences. However, research has indicated that the non-local representation at the theta timescale, extending beyond the animal's surroundings, is possible. Wikenheiser and Redish (2015) found that the spatial sweep of theta sequences extended farther when the goal was more distant (which cannot be explained by variations in speed and acceleration), indicating a prospective representation that is more dependent on goal-location than the sensorimotor input. Similarly, Kay et al. (2020) demonstrated that, before a rat chose to turn left or right in the middle stem of a T-maze, representations of spatial pathways along both left and right arms were alternating in the theta cycles, showing that theta sequences are able to encode an alternative future that has not been chosen by the animal. These findings further strengthen the notion that spatial representation in theta sequences is not merely coordinated by sensorimotor drive but also potentially by expectation, planning or memory, leading to a non-local representation that extends beyond the immediate surroundings of the animal and encompasses hypothetical pathways.

Our experimental findings demonstrated that non-local representation exists at the theta timescale and could defy the temporal order of sensorimotor drive at its weakest. Our model simulation showed that such non-local theta sequences (intrinsic sequences) can be coordinated by intra-hippocampal connectivity.

In our model, the goal-dependent forward sweep length could be explained by recurrent connections ending at the goal location, leading to a boundary effect that shortens theta sequences near the goal. The representation of possible future pathways, as seen in Kay et al. (2020), may be partially attributed to intrinsic connectivity along previously traversed paths of the left and right arms. However, this explanation may require supplementary mechanisms, such as feedback inhibition via interneurons, to fully account for the observed alternation of different pathways within each theta cycle.

3.2.2 Relation to replay

The intrinsic sequences bear a resemblance to hippocampal replay, as both of their temporal orders are coordinated by intrinsic dynamics and represent non-local spatial sequences. Past studies have posited that theta sequences facilitate replay sequences by associating spatial locations through Hebbian learning during online movements. Given that a SWR event can span 50-200ms, sufficient to cover the duration of a theta sequence, it is conceivable that both replay and intrinsic sequences originate from the same intrinsic circuit generator.

However, evidence for non-local representation in the hippocampus at the theta timescale is limited, this is likely because the presence of sensorimotor drive during locomotion overshadows intrinsic sequences, as evidenced by our experimental results. In contrast, during periods of immobility, the absence of this sensorimotor drive allows the sequential patterns of linked ensembles to become more apparent and emerge as replay or pre-play.

Upcoming experiments could explore the hypothesis of a shared generator between intrinsic sequences and hippocampal replay by analyzing the trajectory dependence of theta correlations between pairs of place cells that have previously participated in replay sequences.

3.2.3 Functional roles

By decoding the temporal patterns via tempotrons, we have demonstrated that intrinsic sequences can serve as a stable "landmark" memory which cannot be degraded by the online sensorimotor input. The finding agrees with Leibold (2020) which showed that spike sequences with temporal order independent of running trajectory can exclusively support spatial memories without explicit rate coding. The "landmark" memory is, therefore, robust to place field remapping in a novel environment since only the spike timing patterns contribute to the neural code but not the location specificity of the firing rate. As a result, the intrinsic sequences might facilitate spatial learning in new environments. In a broader context, our findings highlight a universal mechanism for memory encoding with temporal patterns in parallel with firing rate.

Theta sequences driven by the intrinsic network connectivity have been previously suggested to support the recall of memory sequences Jensen et al. (1996), Lisman et al. (2005). This is because temporal correlation is stored in the connectivity, enabling neural patterns to sequentially activate one another along the causal chain. The intrinsic sequences, given their non-local representation, could facilitate the associative recall of spatial pathways, functioning as working memory for tasks like decision making and planning during movement. Thus, the concurrent propagation of both intrinsic and extrinsic sequences might imply a dual process during spatial navigation: one that represents the memory of the current trajectory (possibly for encoding or planning of immediate chosen movements) and another that retrieves memories of alternative spatial pathways.

3.3 Dual coding in theta oscillations

3.3.1 Differences between phase precession and theta sequence

In the present thesis, we used phase precession as an indicator to gauge the trajectory-dependence of theta sequences based on the notion that the theta sequence is a natural outcome of the phase code across multiple cells. Yet, a growing body of evidence suggests

that phase precession and theta sequences might originate from distinct mechanisms.

This distinction was first highlighted by Foster and Wilson (2007) where they shuffled the spikes while preserving the phase-position relationship within individual cells. The results showed a significant degradation in the temporal order of theta sequences post-shuffling. This implies that the phase precession alone cannot trivially predict the temporal order of theta sequences.

Subsequently, Feng et al. (2015) investigated the evolution of the theta temporal code over time in a novel environment. Their findings revealed that the theta sequences, initially weaker in power, developed to be stronger after the first lap. In contrast, phase precession was evident from the outset. This suggests that while theta sequences are shaped by experience, phase precession is not. Further, Middleton and McHugh (2016) blocked synaptic transmission from CA3 to CA1 neurons. The outcome was a disruption in sequence correlation, but single-cell phase precession in CA1 remained unaffected. This indicates that the CA3 input, predominantly influenced by intrinsic network recurrence, is pivotal for the population temporal code, and EC input, primarily delivering the sensorimotor information and becoming the main input source to CA1 after the blocking, is sufficient to evoke single-cell phase precession in CA1. The finding further supports the notion that the theta sequences and phase precession are not simply the two sides of one coin, and they could arise from distinct processes.

The findings of Feng et al. (2015) and Middleton and McHugh (2016) resonate with the implications of our model. The phase precession and the initially weaker theta sequences in CA1, evident during the first exposure to a new track, might be attributed to extrinsic sequences. The subsequent enhancement in theta sequence power could result from the upstream input from CA3, where intrinsic connectivity has developed over time.

This explanation, however, requires intrinsic sequences to arise from experience-dependent changes. In the present thesis, such learning of intrinsic sequences was not explored, as intrinsic sequences are presumed to arise from pre-existing intra-hippocampal circuitry motivated by the pre-play phenomenon (Dragoi and Tonegawa, 2011). Nevertheless, previous studies on preplay hint at the possibility that the learning of intrinsic theta sequences could be facilitated by the flexible mapping of new memory items onto the pre-existing circuits. Notably, preconfigured sequences in SWRs have been proposed to arise from such mappings, allowing the memory sequence to be rapidly encoded without re-learning a previously known temporal order (Dragoi and Tonegawa, 2011, 2014, Farooq et al., 2019). An alternative explanation, involving the interchange of the roles of intrinsic and extrinsic sequences, can also account for the results presented in Feng et al. (2015). The initially weaker theta sequences could be attributed to pre-existing intrinsic sequences, while extrinsic sequences develop over time, leading to the observed increase

in theta power. Further testing of the exact roles of intrinsic and extrinsic sequences in the experience-dependent modulation of theta power can be achieved by comparing the trajectory-dependent theta correlations over time.

3.3.2 Relation to gamma oscillations

The dual process of theta sequences and phase precession was further elucidated in the context of gamma oscillations (25–100Hz). These faster oscillations co-occur with theta oscillations and can subdivide a single theta cycle into 5–8 shorter gamma cycles, which are thought to encapsulate individual elements within the longer theta sequence (Jensen et al., 1996).

Gamma oscillations are proposed to mediate the dual processes within theta oscillations by differentiating between slow (25–55 Hz) and fast (60–100 Hz, occasionally referred to as "medium" in the literature) gamma frequencies. Prior research (Bieri et al., 2014, Zheng et al., 2016, Guardamagna et al., 2023) have categorized theta cycles based on whether they contain co-occurring slow and fast gamma components. In the CA1 region, slow-gamma theta is found to encode longer and more prospective spatial pathways, exhibiting stronger temporal correlations in spike sequences. These spikes are confined to the late phase of the theta cycle. In contrast, fast-gamma theta primarily encodes the current position within an ongoing trajectory, displaying phase precession with a strong phase-position correlation that spans the full theta range. Notably, slow and fast gamma oscillations in CA1 have distinct origins, arising from CA3 and EC inputs, respectively (Schomburg et al., 2014).

The underlying mechanisms of the dual spatial coding in slow- and fast-gamma theta remain unclear. The most recent explanation was provided by Guardamagna et al. (2023), who suggested that the model by Chance (2012), where EC and CA3 inputs drive the early- and late-phase spiking in CA1 place cells respectively, best aligns with their observations of the dual spatial coding. Our model offers a similar insight, suggesting that intrinsic and extrinsic sequences could give rise to distinctive temporal codes, which might be reflected in the spatial coding of slow- and fast-gamma theta. However, the capacity of our model to predict the mechanisms underlying slow- and fast-gamma spatial coding remains limited, as our theoretical framework does not incorporate gamma oscillations or the CA1 region.

To fully capture the interaction between theta and gamma time codes, our model would need to include fast-spiking inhibitory interneurons. This would allow for the coordination of spike timings within both fast- and slow-gamma ranges. Future research could explore the implications of our model by examining the extrinsic and intrinsic correlations in theta cycles associated with slow and fast gamma oscillations.

3.4 Other theoretical frameworks

3.4.1 Continuous attractor neural network models

In this section, I would like to review how other phase precession models could fit with our findings of extrinsic and intrinsic sequences. One model by Navratilova et al. (2012) is based on continuous attractor neural networks, previously proposed to perform path integration on head-directions and travelled distances (Skaggs et al., 1995, Samsonovich and McNaughton, 1997, Zhang, 1996). In the Navratilova et al. (2012) model, each head-direction cell activates a layer of place-by-direction conjunctive cells, which then project to a layer of place cells with a spatial offset in the preferred direction of the head-direction cell, similar to the projection displacement of CA3-DG recurrence in the present thesis (Yiu and Leibold, 2023). Consequently, movement in a specific direction activates only the associated head-direction cells and propagates the sequential activity through the conjunctive cells with the corresponding projection displacement. The other head-direction cells, except those encode the movement direction, remain inactive; thus, sequence only propagates in the direction of travel. For a linear track, two head-direction cells and their corresponding sets of conjunctive cells would suffice to produce theta sequences in both forward and backward direction. In a 2D open space, multiple sets of head-direction and conjunctive cells would be needed to encode a full angular range of 360 degrees. This model shares similarities with the work of Romani and Tsodyks (2015), although the latter employs the STD mechanism and eliminates the need for multiple layers of conjunctive cells to produce a direction-dependent projection displacement.

The Navratilova et al. (2012) model is primarily extrinsic, as it generates theta sequences that propagate in the direction of forward movement, contingent upon adequate encoding of the angular axis by a sufficient number of head-direction and conjunctive cells. To account for intrinsic sequences, the model would necessitate modifications, such as including a head-direction cell population characterized by broad directional tuning curves. A head-direction cell with a nearly flat tuning curve, while maintaining the same projection offset between the conjunctive and place cells, would replicate the fixed asymmetrical connectivity in the Tsodyks et al. (1996) model. This would enable the place cells to propagate sequences in a predetermined *asymmetry direction*, irrespective of the actual direction of movement. Therefore, the concurrent propagation of both extrinsic and intrinsic sequences could be achieved through a diversified population of head-direction cells with varying degrees of tuning sharpness. This extended model could potentially account for the observed heterogeneity in theta correlations.

3.4.2 Detuned oscillator models

There is also a large family of models based on detuned oscillators (Lengyel et al., 2003). In these models, pyramidal cell receives inhibitory input at a "baseline" theta frequency

(f_b) and excitatory input at an "active" frequency (f_a), according to the equation:

$$f_a(t) = k_v|\mathbf{v}(t)| + f_b(t),$$

where k_v is the modulation strength constant and $|\mathbf{v}(t)|$ is the animal's running speed, which is set to zero when the animal is outside of the place field. As a result, the active frequency remains the same as the baseline frequency when the animal is stationary but increases to be higher than the baseline when the animal moves within the place field. The active frequency is then "detuned" from the baseline frequency when the animal runs across the place field and excites the neuron at progressively earlier theta phase in each theta cycle. The phase advance $\Delta\phi(t) = \phi(t) - \phi(0)$ is dependent on distance traveled $\int_0^t |\mathbf{v}(\tau)|d\tau$ and can be computed by:

$$\Delta\phi = \int_0^t 2\pi[f_a(\tau) - f_b(\tau)]d\tau = 2k_v \int_0^t |\mathbf{v}(\tau)|d\tau$$

The model would be able to explain phase precession in 2-D as the spike phase starts precessing at the time of field entry regardless of the direction of travel (since only the magnitude of the vector $\mathbf{v}(t)$ matters) and thus, belong to the extrinsic family.

A further modification by Burgess (2008) included the directional selectivity:

$$f_a(t) = k_v[\mathbf{v}(t) \cdot \mathbf{d}_L] + f_b(t),$$

which depends on the dot product between the running velocity and the unit vector $\mathbf{d}_L$, denoting the preferred running direction of the neuron. As a result, the slope of phase-position curve is negative when the running direction aligns with the preferred direction, and is positive when the circular difference between the two directions is larger than 90 degrees (because the active frequency is now slower than the baseline frequency). This configuration would produce the same theta correlation in two opposite running directions and aligns with the observation of purely intrinsic sequences (see Figure 1A-F in manuscript II for illustration). However, their study also included the directional tuning of firing rate. In this case, the detuned oscillator only fires and undergoes phase precession in the directions near $\mathbf{d}_L$. The positive phase-position relation in the non-preferred direction is thereby suppressed. Consequently, if a place cell receives upstream inputs from multiple detuned oscillators, with preferred directions covering the full range of running directions, phase precession can then occur in all directions with negative slopes and, in turn, exhibits purely extrinsic theta correlation. Although the study of Burgess (2008) did not discuss the intrinsic and extrinsic correlations, their network could potentially generate both extrinsic and intrinsic sequences using a combination of upstream directionally selective

detuned oscillators.

The major weakness of the detuned oscillator models is that the spike phase is the integration of the phase difference between the active and baseline frequency over time, and thus, depends on the phase history since field entry. Zugaro et al. (2005) has shown that, after resetting the theta phase by silencing the population activity via single-pulse stimulation, single-cell spike phase resumes to phase value just before the interruption and continues precessing. This shows that cells update the phase code in every theta cycle instead of relying on the phase code history of previous cycles, which cannot be reconciled with the prediction of detuned oscillator model where the phase precession is expected to restart from the beginning after phase resetting. In addition, the detuned oscillator models are phenomenological since the neuronal mechanism by which the animal's velocity directly modulates the active frequency was not explained.

3.5   Future directions

The notion of intrinsic sequences in the present thesis is relatively new compared to the traditional view of extrinsic sequences. One aspect of intrinsic sequences that still awaits further experiments is the prediction of non-local sequences by our model simulation. While our first study (Yiu et al., 2022) focused on theta correlations of field pairs along the trajectory, it would be worth investigating the theta correlation of field pairs with one at the current position and another one outside of the trajectory or even outside of its place field. The existence of non-local theta sequences would predict that such out-of-trajectory or out-of-field theta correlation exists, which would further corroborate our theory. However, the search for non-local correlations is limited by recording techniques as it demands recording a large population of place cells that can sufficiently sample the whole spatial environment and overlap with each other's place fields. Recent advances in tetrode arrays such as Guardamagna et al. (2022) which allow for the recording of nearly 100 units per rat, might enable such analysis.

Furthermore, identifying non-local sequences likely require a different data analysis approach. Traditionally hippocampal activity sequences were detected by Bayesian inference of neural activity. However, during mobile periods, the temporal code of non-local sequences might be masked by the firing activity driven by sensorimotor input, particularly in rate-based Bayesian decoders. Our first manuscript Yiu et al. (2022) also suggested that the intrinsic sequences are the most elusive in the best firing direction. This could explain why the non-local sequences were rarely detected during theta states but become more apparent in immobile states such as SWRs. Unsupervised learning techniques for sequential patterns, such as non-negative matrix factorizations (Mackevicius et al., 2019), may offer a more suitable approach for identifying these intrinsic sequences within theta activity.

The present thesis focuses on the theta temporal code; however, the implications extend to the temporal code at other timescales. For instance, spike sequences at both SWR and theta might originate from the same pre-existing intrinsic circuitry and the intrinsic sequences could be coordinated by slow-gamma oscillations. However, the exact interrelationship among theta, gamma and SWR is still unclear. Future research can focus on elucidating the orchestration of temporal sequences across these three frequency bands. Specifically, one could test whether the directionality of phase precession properties and theta correlations differ between slow and fast gamma associated theta cycles, or if the replayed place fields showed stronger intrinsic correlations.

While the present thesis suggests that both extrinsic and intrinsic sequences are required to explain the heterogeneity of theta correlations, the short-term plasticity and asymmetric recurrence may not be the exclusive generation mechanisms. As discussed before, further extensions of the continuous attractor neural networks by Navratilova et al. (2012) could potentially explain the extrinsic and intrinsic correlations, by using head-direction signals to limit in which direction the sequence activity should propagate within a 2-D topology of place cells. The head-direction signal in the present thesis has so far been interpreted and implemented as a variation in the amount of sensorimotor drive without directly modulating phase precession properties or the propagation directions of theta sequences. Further work could investigate the more active role of head-direction signals in coordinating the theta temporal code.

3.6 Conclusion

I want to conclude the thesis with a quote from Aristotle "The whole is greater than the sum of its parts." The hippocampal sequence is a very representative example of this saying. Spike sequences formed by multiple place cells do not merely represent multiple places but deliver greater functions, such as representations of local and non-local spatial pathways, and memories stored as temporal correlations alternative to firing rate. Spikes when put in the right timings could in concert support various functions, including stable landmark memories, memory encoding and retrieval. To unravel the spatial representation of the hippocampus, one must understand the interplay between individual neurons and the complex network dynamics they form. The same can also be said for any other neural structures. The journey through this thesis has reminded us that in the complex world of neuroscience, the mystery often lies in the connections, the patterns, and the holistic view of the system.

References

Acharya, L., Aghajan, Z., Vuong, C., Moore, J., and Mehta, M. (2016). Causal Influence of Visual Cues on Hippocampal Directional Selectivity. *Cell*, 164(1-2):197–207.

Addis, D. R., Moscovitch, M., Crawley, A. P., and McAndrews, M. P. (2004). Recollective qualities modulate hippocampal activation during autobiographical memory retrieval. *Hippocampus*, 14(6):752–762.

Aksoy-Aksel, A. and Manahan-Vaughan, D. (2013). The temporoammonic input to the hippocampal CA1 region displays distinctly different synaptic plasticity compared to the Schaffer collateral input in vivo: significance for synaptic information processing. *Frontiers in Synaptic Neuroscience*, 5.

Alger, B. and Teyler, T. (1976). Long-term and short-term plasticity in the CA1, CA3, and dentate regions of the rat hippocampal slice. *Brain Research*, 110(3):463–480.

Allen, T. A., Salz, D. M., McKenzie, S., and Fortin, N. J. (2016). Nonspatial Sequence Coding in CA1 Neurons. *The Journal of Neuroscience*, 36(5):1547–1563.

Amaral, D. and Witter, M. (1989). The three-dimensional organization of the hippocampal formation: A review of anatomical data. *Neuroscience*, 31(3):571–591.

Amilhon, B., Huh, C., Manseau, F., Ducharme, G., Nichol, H., Adamantidis, A., and Williams, S. (2015). Parvalbumin Interneurons of Hippocampus Tune Population Activity at Theta Frequency. *Neuron*, 86(5):1277–1289.

Anagnostaras, S. G., Maren, S., and Fanselow, M. S. (1999). Temporally Graded Retrograde Amnesia of Contextual Fear after Hippocampal Damage in Rats: Within-Subjects Examination. *The Journal of Neuroscience*, 19(3):1106–1114.

Andersen, P., Morris, R., Amaral, D., Bliss, T., and O'Keefe, J., editors (2006). *The Hippocampus Book*. Oxford University Press.

Aronov, D., Nevers, R., and Tank, D. W. (2017). Mapping of a non-spatial dimension by the hippocampal–entorhinal circuit. *Nature*, 543(7647):719–722.

Benarroch, E. E. (2013). HCN channels: Function and clinical implications. *Neurology*, 80(3):304–310.

Bennett, M. R., Gibson, W. G., and Robinson, J. (1994). Dynamics of the CA3 pyramidial neuron autoassociative memory network in the hippocampus. *Philosophical Transactions of the Royal Society of London. Series B: Biological Sciences*, 343(1304):167–187.

Bett, D., Stevenson, C. H., Shires, K. L., Smith, M. T., Martin, S. J., Dudchenko, P. A., and Wood, E. R. (2013). The Postsubiculum and Spatial Learning: The Role of Postsubicular Synaptic Activity and Synaptic Plasticity in Hippocampal Place Cell, Object, and Object-Location Memory. *The Journal of Neuroscience*, 33(16):6928–6943.

Bezaire, M. J., Raikov, I., Burk, K., Vyas, D., and Soltesz, I. (2016). Interneuronal mechanisms of hippocampal theta oscillations in a full-scale model of the rodent CA1 circuit. *eLife*, 5:e18566.

Bi, G.-q. and Poo, M.-m. (1998). Synaptic Modifications in Cultured Hippocampal Neurons: Dependence on Spike Timing, Synaptic Strength, and Postsynaptic Cell Type. *The Journal of Neuroscience*, 18(24):10464–10472.

Bieri, K., Bobbitt, K., and Colgin, L. (2014). Slow and Fast Gamma Rhythms Coordinate Different Spatial Coding Modes in Hippocampal Place Cells. *Neuron*, 82(3):670–681.

Bittner, K. C., Milstein, A. D., Grienberger, C., Romani, S., and Magee, J. C. (2017). Behavioral time scale synaptic plasticity underlies CA1 place fields. *Science*, 357(6355):1033–1036.

Bland, B. H., Colom, L. V., Konopacki, J., and Roth, S. H. (1988). Intracellular records of carbachol-induced theta rhythm in hippocampal slices. *Brain Research*, 447(2):364–368.

Bland, B. H., Oddie, S. D., and Colom, L. V. (1999). Mechanisms of Neural Synchrony in the Septohippocampal Pathways Underlying Hippocampal Theta Generation. *The Journal of Neuroscience*, 19(8):3223–3237.

Bliss, T. V. P. and Lømo, T. (1973). Long-lasting potentiation of synaptic transmission in the dentate area of the anaesthetized rabbit following stimulation of the perforant path. *The Journal of Physiology*, 232(2):331–356.

Bolding, K. A., Ferbinteanu, J., Fox, S. E., and Muller, R. U. (2020). Place cell firing cannot support navigation without intact septal circuits. *Hippocampus*, 30(3):175–191.

Burgess, N. (2008). Grid cells and theta as oscillatory interference: Theory and predictions. *Hippocampus*, 18(12):1157–1174.

Buzsáki, G. (2002). Theta Oscillations in the Hippocampus. *Neuron*, 33(3):325–340.

Buzsáki, G. and Moser, E. I. (2013). Memory, navigation and theta rhythm in the hippocampal-entorhinal system. *Nature Neuroscience*, 16(2):130–138.

Cacucci, F. (2004). Theta-Modulated Place-by-Direction Cells in the Hippocampal Formation in the Rat. *Journal of Neuroscience*, 24(38):8265–8277.

Carr, M. F., Jadhav, S. P., and Frank, L. M. (2011). Hippocampal replay in the awake state: a potential substrate for memory consolidation and retrieval. *Nature Neuroscience*, 14(2):147–153.

Cei, A., Girardeau, G., Drieu, C., Kanbi, K. E., and Zugaro, M. (2014). Reversed theta sequences of hippocampal cell assemblies during backward travel. *Nature Neuroscience*, 17(5):719–724.

Chance, F. S. (2012). Hippocampal Phase Precession from Dual Input Components. *The Journal of Neuroscience*, 32(47):16693–16703.

Clark, R. E., Broadbent, N. J., Zola, S. M., and Squire, L. R. (2002). Anterograde Amnesia and Temporally Graded Retrograde Amnesia for a Nonspatial Memory Task after Lesions of Hippocampus and Subiculum. *The Journal of Neuroscience*, 22(11):4663–4669.

Colgin, L. L. (2013). Mechanisms and Functions of Theta Rhythms. *Annual Review of Neuroscience*, 36(1):295–312.

Crutcher, K., Madison, R., and Davis, J. (1981). A study of the rat septohippocampal pathway using anterograde transport of horseradish peroxidase. *Neuroscience*, 6(10):1961–1973.

Deshmukh, S. S. and Knierim, J. J. (2013). Influence of local objects on hippocampal representations: Landmark vectors and memory. *Hippocampus*, 23(4):253–267.

Diba, K. and Buzsáki, G. (2007). Forward and reverse hippocampal place-cell sequences during ripples. *Nature Neuroscience*, 10(10):1241–1242.

Dong, C., Madar, A. D., and Sheffield, M. E. J. (2021). Distinct place cell dynamics in CA1 and CA3 encode experience in new environments. *Nature Communications*, 12(1):2977.

Dragoi, G. and Buzsáki, G. (2006). Temporal Encoding of Place Sequences by Hippocampal Cell Assemblies. *Neuron*, 50(1):145–157.

Dragoi, G. and Tonegawa, S. (2011). Preplay of future place cell sequences by hippocampal cellular assemblies. *Nature*, 469(7330):397–401.

Dragoi, G. and Tonegawa, S. (2013). Distinct preplay of multiple novel spatial experiences in the rat. *Proceedings of the National Academy of Sciences*, 110(22):9100–9105.

Dragoi, G. and Tonegawa, S. (2014). Selection of preconfigured cell assemblies for representation of novel spatial experiences. *Philosophical Transactions of the Royal Society B: Biological Sciences*, 369(1635):20120522.

Dvorak-Carbone, H. and Schuman, E. M. (1999). Long-Term Depression of Temporoammonic-CA1 Hippocampal Synaptic Transmission. *Journal of Neurophysiology*, 81(3):1036–1044.

Ego-Stengel, V. and Wilson, M. A. (2009). Disruption of ripple-associated hippocampal activity during rest impairs spatial learning in the rat. *Hippocampus*, 20(1):1–10.

Eichenbaum, H. (2014). Time cells in the hippocampus: a new dimension for mapping memories. *Nature Reviews Neuroscience*, 15(11):732–744.

Farooq, U., Sibille, J., Liu, K., and Dragoi, G. (2019). Strengthened Temporal Coordination within Pre-existing Sequential Cell Assemblies Supports Trajectory Replay. *Neuron*, 103(4):719–733.e7.

Feng, T., Silva, D., and Foster, D. J. (2015). Dissociation between the Experience-Dependent Development of Hippocampal Theta Sequences and Single-Trial Phase Precession. *Journal of Neuroscience*, 35(12):4890–4902.

Foster, D. J. and Wilson, M. A. (2006). Reverse replay of behavioural sequences in hippocampal place cells during the awake state. *Nature*, 440(7084):680–683.

Foster, D. J. and Wilson, M. A. (2007). Hippocampal theta sequences. *Hippocampus*, 17(11):1093–1099.

Fox, S. E., Wolfson, S., and Ranck, J. B. (1986). Hippocampal theta rhythm and the firing of neurons in walking and urethane anesthetized rats. *Experimental Brain Research*, 62(3):495–508.

Frank, L. M., Stanley, G. B., and Brown, E. N. (2004). Hippocampal Plasticity across Multiple Days of Exposure to Novel Environments. *The Journal of Neuroscience*, 24(35):7681–7689.

Fried, I., MacDonald, K. A., and Wilson, C. L. (1997). Single Neuron Activity in Human Hippocampus and Amygdala during Recognition of Faces and Objects. *Neuron*, 18(5):753–765.

George, T. M., De Cothi, W., Stachenfeld, K. L., and Barry, C. (2023). Rapid learning of predictive maps with STDP and theta phase precession. *eLife*, 12:e80663.

Giocomo, L., Stensola, T., Bonnevie, T., Van Cauter, T., Moser, M.-B., and Moser, E. (2014). Topography of Head Direction Cells in Medial Entorhinal Cortex. *Current Biology*, 24(3):252–262.

Girardeau, G., Benchenane, K., Wiener, S. I., Buzsáki, G., and Zugaro, M. B. (2009). Selective suppression of hippocampal ripples impairs spatial memory. *Nature Neuroscience*, 12(10):1222–1223.

Goodridge, J. P., Dudchenko, P. A., Worboys, K. A., Golob, E. J., and Taube, J. S. (1998). Cue Control and Head Direction Cells. *Behavioral Neuroscience*, 112(4):749–761.

Goutagny, R., Jackson, J., and Williams, S. (2009). Self-generated theta oscillations in the hippocampus. *Nature Neuroscience*, 12(12):1491–1493.

Greicius, M. D., Krasnow, B., Boyett-Anderson, J. M., Eliez, S., Schatzberg, A. F., Reiss, A. L., and Menon, V. (2003). Regional analysis of hippocampal activation during memory encoding and retrieval: fMRI study. *Hippocampus*, 13(1):164–174.

Grosmark, A., Long, J., and Buzsáki, G. (2016). Recordings from hippocampal area CA1, PRE, during and POST novel spatial learning. Artwork Size: 143 GB Pages: 143 GB.

Grosmark, A. D. and Buzsáki, G. (2016). Diversity in neural firing dynamics supports both rigid and learned hippocampal sequences. *Science*, 351(6280):1440–1443.

Gu, Z. and Yakel, J. L. (2017). Inducing theta oscillations in the entorhinal hippocampal network in vitro. *Brain Structure and Function*, 222(2):943–955.

Guardamagna, M., Eichler, R., Pedrosa, R., Aarts, A., Meyer, A. F., and Battaglia, F. P. (2022). The Hybrid Drive: a chronic implant device combining tetrode arrays with silicon probes for layer-resolved ensemble electrophysiology in freely moving mice. *Journal of Neural Engineering*, 19(3):036030.

Guardamagna, M., Stella, F., and Battaglia, F. P. (2023). Heterogeneity of network and coding states in mouse CA1 place cells. *Cell Reports*, 42(2):112022.

Guzman, S. J., Schlögl, A., Espinoza, C., Zhang, X., Suter, B. A., and Jonas, P. (2021). How connectivity rules and synaptic properties shape the efficacy of pattern separation in the entorhinal cortex–dentate gyrus–CA3 network. *Nature Computational Science*, 1(12):830–842.

Hangya, B., Borhegyi, Z., Szilagyi, N., Freund, T. F., and Varga, V. (2009). GABAergic Neurons of the Medial Septum Lead the Hippocampal Network during Theta Activity. *Journal of Neuroscience*, 29(25):8094–8102.

Harris, K. D., Henze, D. A., Hirase, H., Leinekugel, X., Dragoi, G., Czurkó, A., and Buzsáki, G. (2002). Spike train dynamics predicts theta-related phase precession in hippocampal pyramidal cells. *Nature*, 417(6890):738–741.

Heusser, A. C., Poeppel, D., Ezzyat, Y., and Davachi, L. (2016). Episodic sequence memory is supported by a theta–gamma phase code. *Nature Neuroscience*, 19(10):1374–1380.

Hollup, S. A., Molden, S., Donnett, J. G., Moser, M.-B., and Moser, E. I. (2001). Accumulation of Hippocampal Place Fields at the Goal Location in an Annular Watermaze Task. *The Journal of Neuroscience*, 21(5):1635–1644.

Huxter, J. R., Senior, T. J., Allen, K., and Csicsvari, J. (2008). Theta phase–specific codes for two-dimensional position, trajectory and heading in the hippocampus. *Nature Neuroscience*, 11(5):587–594.

Hüfner, K., Strupp, M., Smith, P., Brandt, T., and Jahn, K. (2011). Spatial separation of visual and vestibular processing in the human hippocampal formation: Hüfner et al. *Annals of the New York Academy of Sciences*, 1233(1):177–186.

Ishizuka, N., Weber, J., and Amaral, D. G. (1990). Organization of intrahippocampal projections originating from CA3 pyramidal cells in the rat. *The Journal of Comparative Neurology*, 295(4):580–623.

Jensen, O., Idiart, M. A., and Lisman, J. E. (1996). Physiologically realistic formation of autoassociative memory in networks with theta/gamma oscillations: role of fast NMDA channels. *Learning & Memory*, 3(2-3):243–256.

Karlsson, M. P. and Frank, L. M. (2009). Awake replay of remote experiences in the hippocampus. *Nature Neuroscience*, 12(7):913–918.

Kay, K., Chung, J. E., Sosa, M., Schor, J. S., Karlsson, M. P., Larkin, M. C., Liu, D. F., and Frank, L. M. (2020). Constant Sub-second Cycling between Representations of Possible Futures in the Hippocampus. *Cell*, 180(3):552–567.e25.

Kim, J. J. and Fanselow, M. S. (1992). Modality-Specific Retrograde Amnesia of Fear. *Science*, 256(5057):675–677.

Knierim, J., Kudrimoti, H., and McNaughton, B. (1995). Place cells, head direction cells, and the learning of landmark stability. *The Journal of Neuroscience*, 15(3):1648–1659.

Knudsen, E. B. and Wallis, J. D. (2021). Hippocampal neurons construct a map of an abstract value space. *Cell*, 184(18):4640–4650.e10.

Konopacki, J., Maciver, M., Bland, B. H., and Roth, S. H. (1987). Theta in hippocampal slices: Relation to synaptic responses of dentate neurons. *Brain Research Bulletin*, 18(1):25–27.

Le Duigou, C., Simonnet, J., Teleñczuk, M. T., Fricker, D., and Miles, R. (2014). Recurrent synapses and circuits in the CA3 region of the hippocampus: an associative network. *Frontiers in Cellular Neuroscience*, 7.

Lee, A. K. and Wilson, M. A. (2002). Memory of Sequential Experience in the Hippocampus during Slow Wave Sleep. *Neuron*, 36(6):1183–1194.

Leibold, C. (2020). A model for navigation in unknown environments based on a reservoir of hippocampal sequences. *Neural Networks*, 124:328–342.

Lengyel, M., Szatmáry, Z., and Érdi, P. (2003). Dynamically detuned oscillations account for the coupled rate and temporal code of place cell firing: Modeling the Rate and Temporal Code of Place Cells. *Hippocampus*, 13(6):700–714.

Leutgeb, J. K., Leutgeb, S., Moser, M.-B., and Moser, E. I. (2007). Pattern Separation in the Dentate Gyrus and CA3 of the Hippocampus. *Science*, 315(5814):961–966.

Li, X.-G., Somogyi, P., Ylinen, A., and Buzsáki, G. (1994). The hippocampal ca3 network: An in vivo intracellular labeling study. *Journal of Comparative Neurology*, 339(2):181–208.

Lisman, J. E., Talamini, L. M., and Raffone, A. (2005). Recall of memory sequences by interaction of the dentate and CA3: A revised model of the phase precession. *Neural Networks*, 18(9):1191–1201.

Lubenov, E. V. and Siapas, A. G. (2009). Hippocampal theta oscillations are travelling waves. *Nature*, 459(7246):534–539.

Lømo, T. (2003). The discovery of long-term potentiation. *Philosophical Transactions of the Royal Society of London. Series B: Biological Sciences*, 358(1432):617–620.

Mackevicius, E. L., Bahle, A. H., Williams, A. H., Gu, S., Denisenko, N. I., Goldman, M. S., and Fee, M. S. (2019). Unsupervised discovery of temporal sequences in high-dimensional datasets, with applications to neuroscience. *eLife*, 8:e38471.

Mankin, E. A., Thurley, K., Chenani, A., Haas, O. V., Debs, L., Henke, J., Galinato, M., Leutgeb, J. K., Leutgeb, S., and Leibold, C. (2019). The hippocampal code for space in Mongolian gerbils. *Hippocampus*, 29(9):787–801.

Markus, E., Qin, Y., Leonard, B., Skaggs, W., McNaughton, B., and Barnes, C. (1995). Interactions between location and task affect the spatial and directional firing of hippocampal neurons. *The Journal of Neuroscience*, 15(11):7079–7094.

McNaughton, B. L., Barnes, C. A., and O'Keefe, J. (1983). The contributions of position, direction, and velocity to single unit activity in the hippocampus of freely-moving rats. *Experimental Brain Research*, 52:41–49.

Mehta, M. R., Lee, A. K., and Wilson, M. A. (2002). Role of experience and oscillations in transforming a rate code into a temporal code. *Nature*, 417(6890):741–746.

Middleton, S. J. and McHugh, T. J. (2016). Silencing CA3 disrupts temporal coding in the CA1 ensemble. *Nature Neuroscience*, 19(7):945–951.

Mitchell, S., Rawlins, J., Steward, O., and Olton, D. (1982). Medial septal area lesions disrupt theta rhythm and cholinergic staining in medial entorhinal cortex and produce impaired radial arm maze behavior in rats. *The Journal of Neuroscience*, 2(3):292–302.

Montoya, C. and Sainsbury, R. (1985). The effects of entorhinal cortex lesions on type 1 and type 2 theta. *Physiology & Behavior*, 35(1):121–126.

Morris, N. P., Fyffe, R. E., and Robertson, B. (2004). Characterisation of hyperpolarization-activated currents (Ih) in the medial septum/diagonal band complex in the mouse. *Brain Research*, 1006(1):74–86.

Morris, R. G. M., Garrud, P., Rawlins, J. N. P., and O'Keefe, J. (1982). Place navigation impaired in rats with hippocampal lesions. *Nature*, 297(5868):681–683.

Moser, M.-B. and Moser, E. I. (1998). Functional differentiation in the hippocampus. *Hippocampus*, 8(6):608–619.

Mou, X., Pokhrel, A., Suresh, P., and Ji, D. (2022). Observational learning promotes hippocampal remote awake replay toward future reward locations. *Neuron*, 110(5):891–902.e7.

Muller, R., Bostock, E., Taube, J., and Kubie, J. (1994). On the directional firing properties of hippocampal place cells. *The Journal of Neuroscience*, 14(12):7235–7251.

Muller, R. and Kubie, J. (1987). The effects of changes in the environment on the spatial firing of hippocampal complex-spike cells. *The Journal of Neuroscience*, 7(7):1951–1968.

Munn, R. G. and Giocomo, L. M. (2020). Multiple head direction signals within entorhinal cortex: origin and function. *Current Opinion in Neurobiology*, 64:32–40.

Myers, C. E. and Scharfman, H. E. (2009a). A role for hilar cells in pattern separation in the dentate gyrus: A computational approach. *Hippocampus*, 19(4):321–337.

Myers, C. E. and Scharfman, H. E. (2009b). A role for hilar cells in pattern separation in the dentate gyrus: A computational approach. *Hippocampus*, 19(4):321–337.

Myers, C. E. and Scharfman, H. E. (2011). Pattern separation in the dentate gyrus: A role for the CA3 backprojection. *Hippocampus*, 21(11):1190–1215.

Navratilova, Z., Giocomo, L. M., Fellous, J.-M., Hasselmo, M. E., and McNaughton, B. L. (2012). Phase precession and variable spatial scaling in a periodic attractor map model of medial entorhinal grid cells with realistic after-spike dynamics. *Hippocampus*, 22(4):772–789.

O'Keefe, J. (1976). Place units in the hippocampus of the freely moving rat. *Experimental Neurology*, 51(1):78–109.

O'Keefe, J. and Dostrovsky, J. (1971). The hippocampus as a spatial map. Preliminary evidence from unit activity in the freely-moving rat. *Brain Research*, 34(1):171–175.

O'Keefe, J. and Recce, M. L. (1993). Phase relationship between hippocampal place units and the EEG theta rhythm. *Hippocampus*, 3(3):317–330.

O'Neill, J., Senior, T. J., Allen, K., Huxter, J. R., and Csicsvari, J. (2008). Reactivation of experience-dependent cell assembly patterns in the hippocampus. *Nature Neuroscience*, 11(2):209–215.

Pastalkova, E., Itskov, V., Amarasingham, A., and Buzsáki, G. (2008). Internally Generated Cell Assembly Sequences in the Rat Hippocampus. *Science*, 321(5894):1322–1327.

Patel, J., Fujisawa, S., Berényi, A., Royer, S., and Buzsáki, G. (2012). Traveling Theta Waves along the Entire Septotemporal Axis of the Hippocampus. *Neuron*, 75(3):410–417.

Penttonen, M., Kamondi, A., Sik, A., Acsády, L., and Buzsáki, G. (1998). Feed-forward and feed-back activation of the dentate gyrus in vivo during dentate spikes and sharp wave bursts. *Hippocampus*, 7(4):437–450.

Petersen, P. C. and Buzsáki, G. (2020). Cooling of Medial Septum Reveals Theta Phase Lag Coordination of Hippocampal Cell Assemblies. *Neuron*, 107(4):731–744.e3.

Pfeiffer, B. E. (2022). Spatial learning drives rapid goal representation in hippocampal ripples without place field accumulation or goal-oriented theta sequences. *The Journal of Neuroscience*, 42(19):3975–3988.

Pfeiffer, B. E. and Foster, D. J. (2013). Hippocampal place-cell sequences depict future paths to remembered goals. *Nature*, 497(7447):74–79.

Quian Quiroga, R., Kraskov, A., Koch, C., and Fried, I. (2009). Explicit Encoding of Multimodal Percepts by Single Neurons in the Human Brain. *Current Biology*, 19(15):1308–1313.

Quiroga, R. Q., Reddy, L., Kreiman, G., Koch, C., and Fried, I. (2005). Invariant visual representation by single neurons in the human brain. *Nature*, 435(7045):1102–1107.

Remondes, M. and Schuman, E. M. (2003). Molecular Mechanisms Contributing to Long-Lasting Synaptic Plasticity at the Temporoammonic–CA1 Synapse. *Learning & Memory*, 10(4):247–252.

Robinson, N. T., Descamps, L. A., Russell, L. E., Buchholz, M. O., Bicknell, B. A., Antonov, G. K., Lau, J. Y., Nutbrown, R., Schmidt-Hieber, C., and Häusser, M. (2020). Targeted Activation of Hippocampal Place Cells Drives Memory-Guided Spatial Behavior. *Cell*, 183(6):1586–1599.e10.

Romani, S. and Tsodyks, M. (2015). Short-term plasticity based network model of place cells dynamics. *Hippocampus*, 25(1):94–105.

Roux, C. M., Leger, M., and Freret, T. (2021). Memory Disorders Related to Hippocampal Function: The Interest of 5-HT4Rs Targeting. *International Journal of Molecular Sciences*, 22(21):12082.

Samsonovich, A. and McNaughton, B. L. (1997). Path Integration and Cognitive Mapping in a Continuous Attractor Neural Network Model. *The Journal of Neuroscience*, 17(15):5900–5920.

Santos, B. A., Gomes, R. M., and Husbands, P. (2021). The role of rebound spikes in the maintenance of self-sustained neural spiking activity. *Nonlinear Dynamics*, 105(1):767–784.

Sasaki, T., Piatti, V. C., Hwaun, E., Ahmadi, S., Lisman, J. E., Leutgeb, S., and Leutgeb, J. K. (2018). Dentate network activity is necessary for spatial working memory by supporting CA3 sharp-wave ripple generation and prospective firing of CA3 neurons. *Nature Neuroscience*, 21(2):258–269.

Sato, N. and Yamaguchi, Y. (2009). Relationship between an Input Sequence and Asymmetric Connections Formed by Theta Phase Precession and STDP. In Köppen, M., Kasabov, N., and Coghill, G., editors, *Advances in Neuro-Information Processing*, volume 5506, pages 186–193. Springer Berlin Heidelberg, Berlin, Heidelberg. Series Title: Lecture Notes in Computer Science.

Scarpetta, S. and Marinaro, M. (2005). A learning rule for place fields in a cortical model: Theta phase precession as a network effect. *Hippocampus*, 15(7):979–989.

Scharfman, H. E. (1994). Evidence from simultaneous intracellular recordings in rat hippocampal slices that area CA3 pyramidal cells innervate dentate hilar mossy cells. *Journal of Neurophysiology*, 72(5):2167–2180.

Scharfman, H. E. (1995). Electrophysiological evidence that dentate hilar mossy cells are excitatory and innervate both granule cells and interneurons. *Journal of Neurophysiology*, 74(1):179–194.

Scharfman, H. E. (2007). The CA3 "backprojection" to the dentate gyrus. In *Progress in Brain Research*, volume 163, pages 627–637. Elsevier.

Scharfman, H. E. (2016). The enigmatic mossy cell of the dentate gyrus. *Nature Reviews Neuroscience*, 17(9):562–575.

Schomburg, E., Fernández-Ruiz, A., Mizuseki, K., Berényi, A., Anastassiou, C., Koch, C., and Buzsáki, G. (2014). Theta Phase Segregation of Input-Specific Gamma Patterns in Entorhinal-Hippocampal Networks. *Neuron*, 84(2):470–485.

Schwartzkroin, P. A. and Wester, K. (1975). Long-lasting facilitation of a synaptic potential following tetanization in thein vitro hippocampal slice. *Brain Research*, 89(1):107–119.

Scoville, W. B. and Milner, B. (1957). Loss of recent memory after bilateral hippocampal lesions. *Journal of Neurology, Neurosurgery & Psychiatry*, 20(1):11–21.

Shahbaba, B., Li, L., Agostinelli, F., Saraf, M., Cooper, K. W., Haghverdian, D., Elias, G. A., Baldi, P., and Fortin, N. J. (2022a). Hippocampal ensembles represent sequential relationships among an extended sequence of nonspatial events. *Nature Communications*, 13(1):787.

Shahbaba, B., Li, L., Agostinelli, F., Saraf, M., Cooper, K. W., Haghverdian, D., Elias, G. A., Baldi, P., and Fortin, N. J. (2022b). Hippocampal ensembles represent sequential relationships among an extended sequence of nonspatial events. *Nature Communications*, 13(1):787.

Shen, E., Wang, R., and Zhang, Z. (2008). Theta Phase Precession Enhance Single Trial Learning in an STDP Network. In Wang, R., Shen, E., and Gu, F., editors, *Advances in Cognitive Neurodynamics ICCN 2007*, pages 109–114. Springer Netherlands, Dordrecht.

Silva, D., Feng, T., and Foster, D. J. (2015). Trajectory events across hippocampal place cells require previous experience. *Nature Neuroscience*, 18(12):1772–1779.

Skaggs, W. E., Knierim, J. J., Kudrimoti, H. S., and McNaughton, B. L. (1995). A model of the neural basis of the rat's sense of direction. *Advances in Neural Information Processing Systems*, 7:173–180.

Skaggs, W. E. and McNaughton, B. L. (1996). Replay of Neuronal Firing Sequences in Rat Hippocampus During Sleep Following Spatial Experience. *Science*, 271(5257):1870–1873.

Skaggs, W. E., McNaughton, B. L., Wilson, M. A., and Barnes, C. A. (1996). Theta phase precession in hippocampal neuronal populations and the compression of temporal sequences. *Hippocampus*, 6(2):149–172.

Sliwa, J., Planté, A., Duhamel, J.-R., and Wirth, S. (2016). Independent Neuronal Representation of Facial and Vocal Identity in the Monkey Hippocampus and Inferotemporal Cortex. *Cerebral Cortex*, 26(3):950–966.

Sotty, F., Danik, M., Manseau, F., Laplante, F., Quirion, R., and Williams, S. (2003). Distinct electrophysiological properties of glutamatergic, cholinergic and GABAergic rat septohippocampal neurons: novel implications for hippocampal rhythmicity. *The Journal of Physiology*, 551(3):927–943.

Squire, L. R. and Alvarez, P. (1995). Retrograde amnesia and memory consolidation: a neurobiological perspective. *Current Opinion in Neurobiology*, 5(2):169–177.

Squire, L. R., Genzel, L., Wixted, J. T., and Morris, R. G. (2015). Memory Consolidation. *Cold Spring Harbor Perspectives in Biology*, 7(8):a021766.

Stackman, R. W. and Herbert, A. M. (2002). Rats with lesions of the vestibular system require a visual landmark for spatial navigation. *Behavioural Brain Research*, 128(1):27–40.

Stefanini, F., Kushnir, L., Jimenez, J. C., Jennings, J. H., Woods, N. I., Stuber, G. D., Kheirbek, M. A., Hen, R., and Fusi, S. (2020). A Distributed Neural Code in the Dentate Gyrus and in CA1. *Neuron*, 107(4):703–716.e4.

Steward, O. (1976). Topographic organization of the projections from the entorhinal area to the hippocampal formation of the rat. *The Journal of Comparative Neurology*, 167(3):285–314.

Taube, J., Muller, R., and Ranck, J. (1990a). Head-direction cells recorded from the postsubiculum in freely moving rats. I. Description and quantitative analysis. *The Journal of Neuroscience*, 10(2):420–435.

Taube, J., Muller, R., and Ranck, J. (1990b). Head-direction cells recorded from the postsubiculum in freely moving rats. II. Effects of environmental manipulations. *The Journal of Neuroscience*, 10(2):436–447.

Thurley, K., Leibold, C., Gundlfinger, A., Schmitz, D., and Kempter, R. (2008). Phase Precession Through Synaptic Facilitation. *Neural Computation*, 20(5):1285–1324.

Toth, K., Borhegyi, Z., and Freund, T. (1993). Postsynaptic targets of GABAergic hippocampal neurons in the medial septum-diagonal band of broca complex. *The Journal of Neuroscience*, 13(9):3712–3724.

Tsodyks, M. V. and Markram, H. (1997). The Neural Code between Neocortical Pyramidal Neurons Depends on Neurotransmitter Release Probability. *Proceedings of the National Academy of Sciences of the United States of America*, 94(2):719–723.

Tsodyks, M. V., Skaggs, W. E., Sejnowski, T. J., and McNaughton, B. L. (1996). Population dynamics and theta rhythm phase precession of hippocampal place cell firing: A spiking neuron model. *Hippocampus*, 6(3):271–280.

Tóth, K., Freund, T. F., and Miles, R. (1997). Disinhibition of rat hippocampal pyramidal cells by GABAergic afferents from the septum. *The Journal of Physiology*, 500(2):463–474.

Varga, V., Hangya, B., Kránitz, K., Ludányi, A., Zemankovics, R., Katona, I., Shigemoto, R., Freund, T. F., and Borhegyi, Z. (2008). The presence of pacemaker HCN channels identifies theta rhythmic GABAergic neurons in the medial septum: Characterization of medial septal HCN neurons. *The Journal of Physiology*, 586(16):3893–3915.

Vertes, R. P., Hoover, W. B., and Di Prisco, G. V. (2004). Theta Rhythm of the Hippocampus: Subcortical Control and Functional Significance. *Behavioral and Cognitive Neuroscience Reviews*, 3(3):173–200.

Wallace, D. G., Hines, D. J., Pellis, S. M., and Whishaw, I. Q. (2002). Vestibular Information Is Required for Dead Reckoning in the Rat. *The Journal of Neuroscience*, 22(22):10009–10017.

Wallenstein, G. V. and Hasselmo, M. E. (1997). GABAergic Modulation of Hippocampal Population Activity: Sequence Learning, Place Field Development, and the Phase Precession Effect. *Journal of Neurophysiology*, 78(1):393–408.

Weisskopf, M. G., Zalutsky, R. A., and Nicoll, R. A. (1993). The opioid peptide dynorphin mediates heterosynaptic depression of hippocampal mossy fibre synapses and modulates long-term potentiation. *Nature*, 362(6419):423–427.

Wikenheiser, A. M. and Redish, A. D. (2015). Hippocampal theta sequences reflect current goals. *Nature Neuroscience*, 18(2):289–294.

Wilson, M. A. and McNaughton, B. L. (1994). Reactivation of Hippocampal Ensemble Memories During Sleep. *Science*, 265(5172):676–679.

Winocur, G. (1990). Anterograde and retrograde amnesia in rats with dorsal hippocampal or dorsomedial thalamic lesions. *Behavioural Brain Research*, 38(2):145–154.

Witter, M. P., Griffioen, A. W., Jorritsma-Byham, B., and Krijnen, J. L. (1988). Entorhinal projections to the hippocampal CA1 region in the rat: An underestimated pathway. *Neuroscience Letters*, 85(2):193–198.

Witter, M. P., Naber, P. A., Van Haeften, T., Machielsen, W. C., Rombouts, S. A., Barkhof, F., Scheltens, P., and Lopes Da Silva, F. H. (2000). Cortico-hippocampal communication by way of parallel parahippocampal-subicular pathways. *Hippocampus*, 10(4):398–410.

Xu, C., Datta, S., Wu, M., and Alreja, M. (2004). Hippocampal theta rhythm is reduced by suppression of the H-current in septohippocampal GABAergic neurons. *European Journal of Neuroscience*, 19(8):2299–2309.

Yiu, Y.-H. and Leibold, C. (2023). A theory of hippocampal theta correlations accounting for extrinsic and intrinsic sequences. *eLife*, 12:RP86837.

Yiu, Y.-H., Leutgeb, J. K., and Leibold, C. (2022). Directional Tuning of Phase Precession Properties in the Hippocampus. *The Journal of Neuroscience*, 42(11):2282–2297.

Yoder, R. M. and Pang, K. C. (2005). Involvement of GABAergic and cholinergic medial septal neurons in hippocampal theta rhythm. *Hippocampus*, 15(3):381–392.

Yoder, R. M. and Taube, J. S. (2014). The vestibular contribution to the head direction signal and navigation. *Frontiers in Integrative Neuroscience*, 8.

Zalutsky, R. A. and Nicoll, R. A. (1990). Comparison of Two Forms of Long-Term Potentiation in Single Hippocampal Neurons. *Science*, 248(4963):1619–1624.

Zhang, K. (1996). Representation of spatial orientation by the intrinsic dynamics of the head-direction cell ensemble: a theory. *The Journal of Neuroscience*, 16(6):2112–2126.

Zheng, C., Bieri, K., Hsiao, Y.-T., and Colgin, L. L. (2016). Spatial Sequence Coding Differs during Slow and Fast Gamma Rhythms in the Hippocampus. *Neuron*, 89(2):398–408.

Zola-Morgan, S. M. and Squire, L. R. (1990). The Primate Hippocampal Formation: Evidence for a Time-Limited Role in Memory Storage. *Science*, 250(4978):288–290.

Zugaro, M. B., Monconduit, L., and Buzsáki, G. (2005). Spike phase precession persists after transient intrahippocampal perturbation. *Nature Neuroscience*, 8(1):67–71.

Appendices

Appendix A: Permission for reuse of figure in Figure 2B

License Number	5592980990224
License date	Jul 20, 2023
Licensed Content Publisher	Elsevier
Licensed Content Publication	Cell
Licensed Content Title	Causal Influence of Visual Cues on Hippocampal Directional Selectivity
Licensed Content Author	Lavanya Acharya,Zahra M. Aghajan,Cliff Vuong,Jason J. Moore,Mayank R. Mehta
Licensed Content Date	Jan 14, 2016
Licensed Content Volume	164
Licensed Content Issue	1-2
Licensed Content Pages	11
Start Page	197
End Page	207
Type of Use	reuse in a thesis/dissertation
Portion	figures/tables/illustrations
Number of figures/tables/illustrations	1
Format	both print and electronic
Are you the author of this Elsevier article?	No
Will you be translating?	No
Title	Linking hippocampal sequences and spatial representations
Institution name	Ludwig Maximilian University of Munich
Expected presentation date	Aug 2023
Order reference number	2
Portions	Figure 1D
Requestor Location	Mr. Yuk Hoi Yiu
	Freiburg im Breisgau, 79108 Germany Attn: Yuk Hoi Yiu
Publisher Tax ID	GB 494 6272 12
Total	**0.00 EUR**
Terms and Conditions	

Appendix B: Permission for reuse of figure in Figure 3A and 3B

License Number	5593551377543
License date	Jul 21, 2023
Licensed Content Publisher	John Wiley and Sons
Licensed Content Publication	Hippocampus
Licensed Content Title	Phase relationship between hippocampal place units and the EEG theta rhythm
Licensed Content Author	Michael L. Recce, John O'Keefe
Licensed Content Date	Oct 13, 2004
Licensed Content Volume	3
Licensed Content Issue	3
Licensed Content Pages	14
Type of Use	Dissertation/Thesis
Requestor type	University/Academic
Format	Print and electronic
Portion	Figure/table
Number of figures/tables	2
Will you be translating?	No
Title	Linking hippocampal sequences and spatial representations
Institution name	Ludwig Maximilian University of Munich
Expected presentation date	Aug 2023
Order reference number	3
Portions	Figure 2 and 3
Requestor Location	Mr. Yuk Hoi Yiu
	Freiburg im Breisgau, 79108 Germany Attn: Yuk Hoi Yiu
Publisher Tax ID	EU826007151
Total	**0.00 EUR**

Appendix C: Permission for reuse of figure in Figure 5 and 6

Appendix D: Permission for reuse of figure in Figure 8

<div align="center">

SPRINGER NATURE LICENSE
TERMS AND CONDITIONS

</div>

Oct 12, 2023

This Agreement between Mr. Yuk Hoi Yiu ("You") and Springer Nature ("Springer Nature") consists of your license details and the terms and conditions provided by Springer Nature and Copyright Clearance Center.

License Number	5604810578218
License date	Aug 09, 2023
Licensed Content Publisher	Springer Nature
Licensed Content Publication	Nature Neuroscience
Licensed Content Title	Hippocampal replay in the awake state: a potential substrate for memory consolidation and retrieval
Licensed Content Author	Margaret F Carr et al
Licensed Content Date	Jan 26, 2011
Type of Use	Thesis/Dissertation
Requestor type	academic/university or research institute
Format	print and electronic
Portion	figures/tables/illustrations
Number of figures/tables/illustrations	1
Would you like a high resolution image with your order?	no
Will you be translating?	no
Circulation/distribution	30 - 99
Author of this Springer Nature content	no
Title	Linking hippocampal sequences and spatial representations
Institution name	Ludwig Maximilian University of Munich
Expected presentation date	Aug 2023
Order reference number	6
Portions	Figure 1
Requestor Location	Mr. Yuk Hoi Yiu ██████████████ Freiburg im Breisgau, 79108 Germany Attn: Yuk Hoi Yiu
Total	**0.00 EUR**

Terms and Conditions

Springer Nature Customer Service Centre GmbH Terms and Conditions

Appendix E: Permission for reuse of figure in Figure 8

License Number	5604820832876
License date	Aug 09, 2023
Licensed Content Publisher	Springer Nature
Licensed Content Publication	Nature Neuroscience
Licensed Content Title	Forward and reverse hippocampal place-cell sequences during ripples
Licensed Content Author	Kamran Diba et al
Licensed Content Date	Sep 2, 2007
Type of Use	Thesis/Dissertation
Requestor type	academic/university or research institute
Format	print and electronic
Portion	figures/tables/illustrations
Number of figures/tables/illustrations	1
Would you like a high resolution image with your order?	no
Will you be translating?	no
Circulation/distribution	30 - 99
Author of this Springer Nature content	no
Title	Linking hippocampal sequences and spatial representations
Institution name	Ludwig Maximilian University of Munich
Expected presentation date	Aug 2023
Order reference number	7
Portions	Figure 1a
Requestor Location	Mr. Yuk Hoi Yiu Freiburg im Breisgau, 79108 Germany Attn: Yuk Hoi Yiu
Total	**0.00 EUR**
Terms and Conditions	

Springer Nature Customer Service Centre GmbH Terms and Conditions

Curriculum vitae

Personal Information

First name, last name	Yuk Hoi, Yiu
Position	PhD candidate, Theoretical Systems Neuroscience
Work address	Room 00.042, Bernstein Center Freiburg
	Hansastr. 9a, 79104 Freiburg, Germany

Education

11.2019 – Present	PhD in Systemic Neurosciences
	Graduate School of Systemic Neurosciences
	Ludwig Maximilian University of Munich, Germany
10.2017 – 10.2019	Master of Science in Neuro-Cognitive Psychology
	Ludwig Maximilian University of Munich, Germany
08.2013 – 07.2017	Bachelor of Engineering in Biomedical Engineering
	The Chinese University of Hong Kong, Hong Kong

Working Experience

11.2021 – Present	Full-time PhD candidate
	Prof. Dr. Christian Leibold's lab, Theoretical Systems Neuroscience
	Albert Ludwigs Universität Freiburg, Germany
10.2019 – 10.2021	Full-time PhD candidate
	Prof. Dr. Christian Leibold's lab, Computational Neuroscience
	Ludwig Maximilian University of Munich, Germany
11.2018 – 02.2019	Part-time Research Assistant
	Dr. rer. nat. Seyed-Ahmad Ahmadi's lab, German Center for Vertigo and Balance Disorders
	Ludwig Maximilian University of Munich, Germany

Publications

Yiu, Y.-H., Aboulatta, M., Raiser, T., Ophey, L., Flanagin, V. L., zu Eulenburg, P., & Ahmadi, S.-A. (2019). DeepVOG: Open-source pupil segmentation and gaze estimation in neuroscience using deep learning. *Journal of Neuroscience Methods*, *324*, 108307. https://doi.org/10.1016/j.jneumeth.2019.05.016

Yiu, Y.-H., & Leibold, C. (2023). A theory of hippocampal theta correlations accounting for extrinsic and intrinsic sequences. *eLife*, *12*, RP86837. https://doi.org/10.7554/eLife.86837.4

Yiu, Y.-H., Leutgeb, J. K., & Leibold, C. (2022). Directional Tuning of Phase Precession Properties in the Hippocampus. *The Journal of Neuroscience*, *42*(11), 2282–2297. https://doi.org/10.1523/JNEUROSCI.1569-21.2021

Author contributions

Manuscript I - Directional Tuning of Phase Precession Properties in the Hippocampus

The manuscript was published as:

Yiu, Y.-H., Leutgeb, J. K., & Leibold, C. (2022). Directional Tuning of Phase Precession Properties in the Hippocampus. *The Journal of Neuroscience, 42*(11), 2282–2297. https://doi.org/10.1523/JNEUROSCI.1569-21.2021

Author contributions: **Y.-H.Y.**, J.K.L., and C.L. designed research; C.L. conceived the project and supervised the research; J.K.L. provided data; **Y.-H.Y.** and C.L. performed research; **Y.-H.Y.** implemented data analysis; **Y.-H.Y.**, J.K.L., and C.L. wrote the manuscript.

Manuscript II - A theory of hippocampal theta correlations accounting for extrinsic and intrinsic sequences

The manuscript was published as:

Yiu, Y.-H., & Leibold, C. (2023). A theory of hippocampal theta correlations accounting for extrinsic and intrinsic sequences. *eLife, 12*, RP86837. https://doi.org/10.7554/eLife.86837.4

Author contributions: C.L. conceived the project, supervised the simulation and analysis; **Y.-H.Y.** did the modelling, wrote software, and implemented the simulation and analysis; C.L. and **Y.-H.Y.** wrote the manuscript.

We assert that aforementioned author contributions are correct and accurate:

München/ Munich
October 16, 2023
(Datum/ Date)

Yuk Hoi Yiu
(Author)

Christian Leibold
(Supervisor)